Sedimentology and Depositional Environment of a Marine Target, Southern Namibia: 3D Stratigraphic Architecture and Diamond Mineralisation Potential

Megan Jean Runds

B.Sc. (Hons.) – University of Cape Town

Dissertation presented for the degree of Master of Science in Geology in the Department of Geological Sciences, University of Cape Town

2017

Supervisor: Dr Emese M. Bordy

ABSTRACT

The world's largest diamond placer lies on the southwestern coast of Namibia, within the restricted area known as the *Sperrgebiet*, and comprises, amongst others, a series of Plio-Pleistocene to Holocene littoral deposits preserved onshore for >120 km northwards from the Orange River mouth. Through comprehensive seismic and sedimentological analysis, this study provides the first attempt at linking the well-documented onshore diamondiferous deposits of the *Sperrgebiet* with the submerged landscape of a diamondiferous marine target, called the Purple Target Area (PTA), situated beneath up to 70 m of seawater, some 3.5 km offshore of the onshore deposits.

Four seismic units (A – D) have been identified on 2D seismic reflection profiles, and calibrated to lithological data from several boreholes. These have then been integrated into a detailed landscape evolution model for the PTA. The principal controls on the stratigraphic development of the PTA are rate of sediment input and relative sea-level (RSL) fluctuations. The latter is defined as the interplay of vertical tectonic changes in accommodation space and eustatic sea-level (ESL) fluctuations. The most noteworthy phase of deposition within the PTA basin is the normal regressive coarse gravel beaches trending shore parallel, with the primary gravel barrier and its preserved coeval back-barrier deposits exceeding 7 km in length. The approximate age of the PTA gravel beaches, due to a lack of absolute age constrains, are estimated with reference to their correlated water depths (palaeo-bathymetry) in relation to the ESL curve. Based on this approximation, the PTA gravel beaches have survived the transgression and erosive wave-ravinement processes associated with the Late Pleistocene-Holocene, which occurred between 19 and 7 ka before present.

The preservation of the primary gravel barrier beach complex is linked here to a rapid RSL rise during the last transgression, namely Meltwater Pulse 1B. The smaller gravel beaches that are landward of the main barrier were partially preserved through overstepping, but endured more intense ravinement associated with the rapid RSL rise. The primary gravel barrier complex preserved the same cross-beach variability in clast shape sorting (disc/blades and spherical clasts consistent with the middle section and seaward section of the gravel beach, respectively) and back-barrier lagoonal facies identified laterally across the locally known ED barrier beach complex, preserved onshore 65 km south of the PTA.

The sedimentary facies correspondence between the onshore and offshore deposits presents a rare opportunity to study the emplacement and preservation processes of gravel beach deposits on a high energy shelf. In addition, the diamond mineralisation potential of the offshore gravel beaches can be assessed with respect to the well-documented onshore diamondiferous beaches.

PLAGIARISM DECLARATION

I know that plagiarism is wrong. Plagiarism is to use another's work and pretend that it is one's own. Each significant contribution to, and quotation in this dissertation is from the work of other people has been attributed and has been cited and referenced. I have not allowed, and will not allow anyone to copy my work with the intention of passing it off as his or her own work. I therefore further declare that the material presented in this dissertation is a result of my independent research and has not been presented to any other universtity for the purpose of a higher degree.

Signed by candidate

Signature removed

Megan Jean Runds

24 January 2018

Date

TABLE OF CONTENTS

LIST OF FIGURES

LIST OF TABLES

ACKNOWLEDGMENTS

The guidance and advice from my supervisor, Emese Bordy, is greatly appreciated.

Funding for the project was provided by Namdeb Diamond Corporation (Pty) Limited, and Charlie August and Jürgen Jacob are thanked for organising this support.

Thank you to Johann Conradie, Jana Jacob and Jürgen Jacob for taking the time to review various drafts of the project.

A humongous thank you goes out to John Pether and Pepler Head for reviewing the dissertation from cover to cover, providing valuable and thought-provoking comments.

I would especially like to thank Lynette Kirkpatrick for taking the time out of her own thesis to discuss the project at hand and vastly improve the dissertation as she read through countless draft versions of it.

John Ward is thanked for taking an interest in the project from the start and reviewing the geological background chapter.

John Pether and Michael Williamson are thanked for the lively discussions on the mv The Explorer and their guidance in putting the geological puzzle pieces of the target area together. You both ignited the spark that allowed me to pursue this project.

An extra special gratitude goes out for all the encouragement and support to my mom, my dad and my Neil.

CHAPTER 1 – INTRODUCTION

1.1 Context of the Research

Marine diamond placers are scarce; the only occurrence of economic importance exists along the west coast of South Africa (370 km in length) extending into Namibia, along its coastline, for a distance in excess of 1 400 km (Spaggiari, 2011). The largest and most complex diamond mega-placer deposits can be found on the south-west coast of Namibia within the *Sperrgebiet* - "The Forbidden Area" (**Figure 1.1**). Namdeb Diamond Corporation (Pty) Limited, a diamond consortium co-owned by De Beers and the Namibian government, currently holds the mining licences (ML) which span from the onshore some 10 km offshore between the towns of Oranjemund to the south and Lüderitz to the north (**Figure 1.1**).

The term diamond mega-placer is used for deposits in excess of 50 million carats at ≥95 % gem quality. Aside from the quality and quantity, the mega-placer must also originate from a drainage system that has undergone continuous transport and deposition to, at best, a single focused sink (Bluck *et al.,* 2005). The Namibian mega-placer has yielded more than twice the necessary quantity requirements to date (Bluck *et al*., 2005).

The development of the diamond mega-placer offshore of Namibia is attributed to a combination of processes. The source and conduit for the supply of diamonds to the Atlantic Ocean sink was from and across the southern African hinterland (i.e. Kaapvaal Craton) via an ancestral drainage of the Orange-Vaal River system (e.g. Hallam, 1964; Apollus, 1995; Jacob, 2001; Spaggiari *et al.,* 2002; Jacob, 2005; Bluck *et al.,* 2005; Spaggiari *et al.,* 2006; Grobbelaar *et al.,* 2008; Spaggiari, 2011). From the primary sink, near the mouth of the palaeo-Orange River, a powerful northward directed longshore drift, driven by a strong unidirectional southerly wind regime, fractioned, redistributed and concentrated the diamondiferous sediment load of the Orange River into various trap sites along the coast (e.g. de Decker, 1988; Bluck *et al.,* 2005; Jacob *et al*., 2006; Grobbelaar *et al.,* 2008; Spaggiari, 2011). The Cainozoic diamond mega-placer encompasses several different sediment trap sites from the palaeo-Orange River mouth northward in the form of linear beaches, pocket beaches and aeolian deposits (**Figure 1.1**; e.g. Corbett, 1989; Spaggiari *et al.,* 2006; Jacob *et al*., 2006). A northward decrease in diamond size and gravel accumulation is recorded within these various sediment trapsites (e.g. Hallam, 1964; Apollus, 1995; Spaggiari *et al*., 2006).

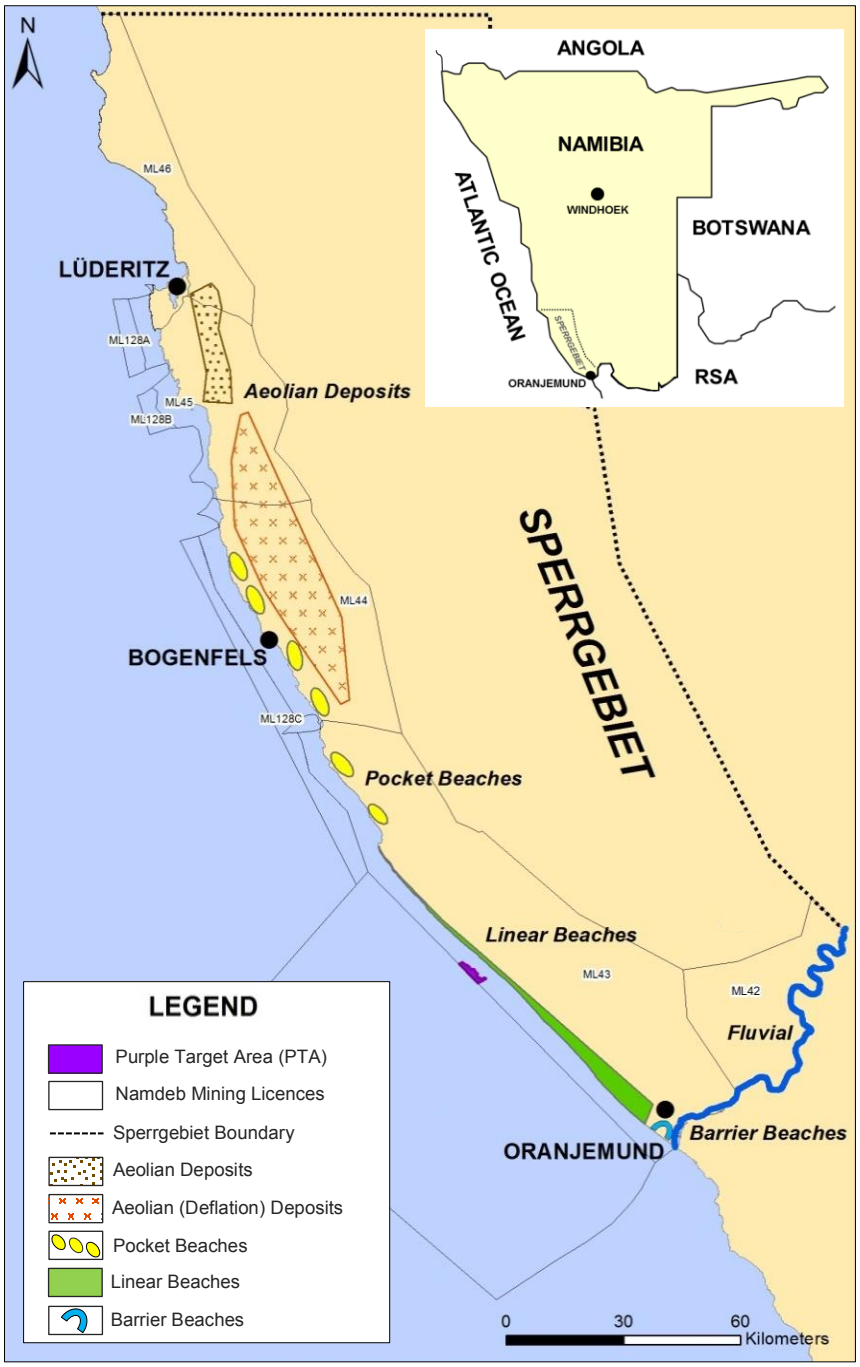

Figure 1.1. Locality map of the *Sperrgebiet*, South-West Namibia showing the extent of the Namdeb mining licences (ML) and varying sedimentary settings preserved onshore. The Purple Target Area is located between Oranjemund and Bogenfels, adjacent to the onshore linear beaches of Mining Area 1 (ML 43).

Diamond mining operations have taken place in Namibia for more than a century since the initial discovery of diamonds in 1908 (Corbett and Burrell, 2001). Approximately 85 million carats have been mined from various sedimentary settings onshore since their discovery (R.J. Jacob, pers. comm., October 2017; **Table 1.1**). Several attempts have been made since the early 1960s to exploit the diamonds within the marine setting after suggestions were made that the onshore deposits might extend offshore (Williams, 1996). So far, approximately 24 million carats have been produced from various mining licences in the offshore setting (**Table 1.1**).

Table 1.1. Subdivision of the total amount of carats produced from the Namibian mega-placer as per end of 2016 production data (R.J. Jacob, pers. comm., October 2017 adapted from de Wit *et al*., 2016).

	Namibian Mega-placer Areas	Carats
Onshore	Lower Orange River	3 989 813
	Mining Area No. 1	62 585 797
	Aeolian Deposits	16 528 214
	Saddle Hill and Conception Bay	447 769
	Skeleton Coast	30 777
Offshore	Midwater and Shallow Water	2 963 838
	Atlantic 1	19 201 724
	Offshore Production (Other Licences)	1 780 383

1.2 Study Area

The Purple Target Area (PTA), roughly 9.25 km² in size, is situated in the offshore portion of ML43, approximately 3.5 km west of the current shoreline within a water depth range of 55 to 70 metres below mean sea-level (**Figure 1.1**). The target area trends parallel to the prolific, locally known, onshore Mining Area 1 (MA1), which is Namdeb's main mining hub. The *in situ* linear beach deposits in MA1, which have produced more than 60 million carats (**Table 1.1**), are slowly becoming depleted (Prins and Jacob, 2014). Therefore, determining the extent and productivity of untapped offshore deposits, such as the PTA, could assist with increasing the life of mine for Namdeb.

Pre-2000, the geometry and genetics of the diamond-bearing sediments in the offshore sink were largely understudied, and therefore a rudimentary sampling and mining approach was used. In the last 15 years, geological models based on geophysical surveys, swath bathymetry and geological drilling were initiated to better understand the nature of the marine deposits and decipher their economic potential (C. August, pers. comm., July 2015).

1.3 Aim of the Research

The aim of the project is to determine the stratigraphic architecture of the Late Cainozoic sediments and depositional dynamics within the PTA. In particular, this research aims to compare the submerged landscape and sediment bodies with those preserved onshore.

The objectives and datasets for this project are:

1. Analysis and sequence stratigraphic interpretation of a regional Topas geophysical dataset in conjunction with borehole data, to identify key geological events (e.g. relative sea-level changes), vertical stacking and lateral variations in sedimentary facies. This will aid in modelling the changes in the ancient sedimentary environment and deduce, at least, the relative age of deposition.

2. Determination of particle composition and clast sizes variation in the submerged successions, which would aid in identifying the depositional processes. Based on the correlation between rounded cobble-to-boulder sized fractions and diamond accumulation – diamonds concentrate within the gravel pore spaces – oversized samples can be used to decipher the sedimentary controls (Jacob *et al.,* 1999). This approach will also allow the isolation of potential diamond bearing gravels that would have been prone to reworking and upgrading their diamond content.
3. Assessment of local onshore deposits that possibly formed under similar depositional conditions to that of the PTA through the assessment of clast assemblages, spatial distribution of the bed geometries and structures. This will aid in constraining the depositional environments of the submerged successions.

CHAPTER 2 – GEOLOGICAL BACKGROUND

2.1 Geological Setting

The Purple Target Area (PTA) is underlain by the local basement rocks that formed during the Late Proterozoic to Early Palaeozoic crustal events in south-western Africa (e.g. Apollus, 1995; Frimmel *et al.,* 1996; Frimmel and Frank, 1998; Frimmel, 2008). The Gariep Fold Belt comprises two major tectonostratigraphic zones (**Figure 2.1**); namely the predominantly oceanic Marmora Terrane to the west and the continental Port Nolloth Zone to the east (**Figure 2.2**; Apollus, 1995, Basei *et al.,* 2005; Frimmel, 2008).

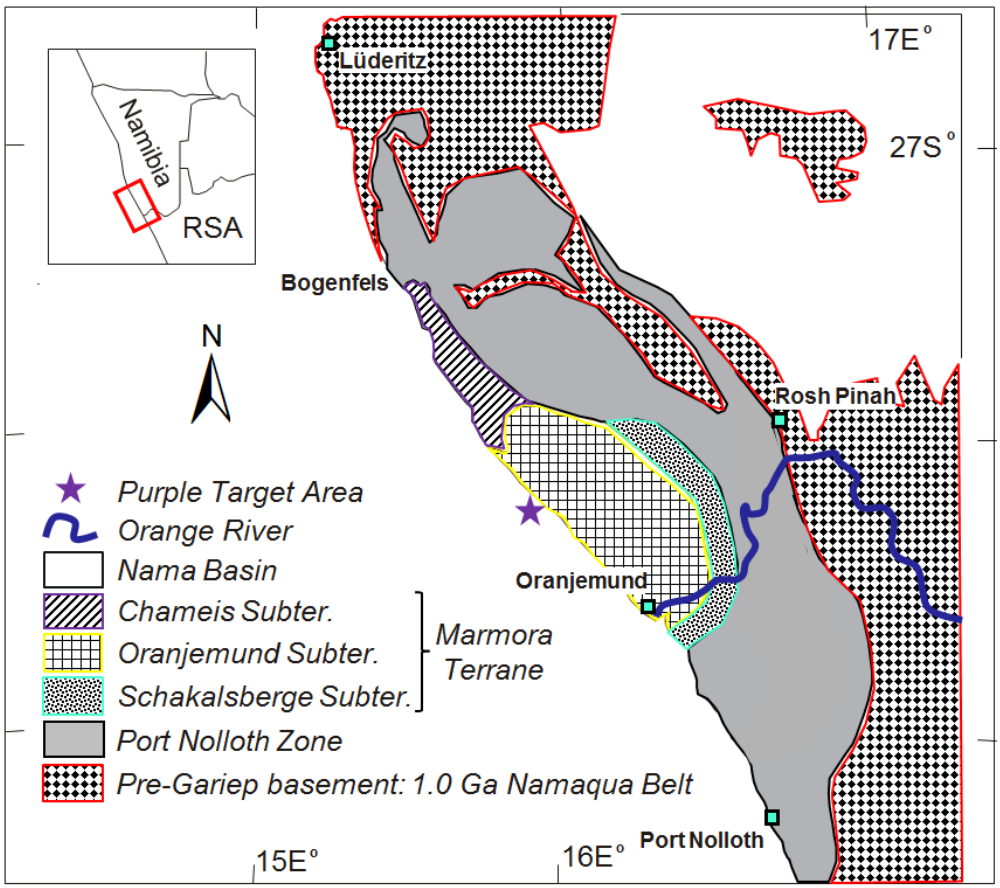

Figure 2.1. Gariep Belt subdivided into tectonic terranes (adapted from Frimmel *et al*., 1996).

The PTA falls within the Marmora Terrane, which is subsequently subdivided into three tectono-stratigraphic units interpreted to have formed in contiguous environments (Frimmel and Frank, 1998; Frimmel, 2008). These tectonic sub-units comprise, from north-west to south-east, the Chameis, Oranjemund and Schakalsberge Subterranes (**Figure 2.2**).

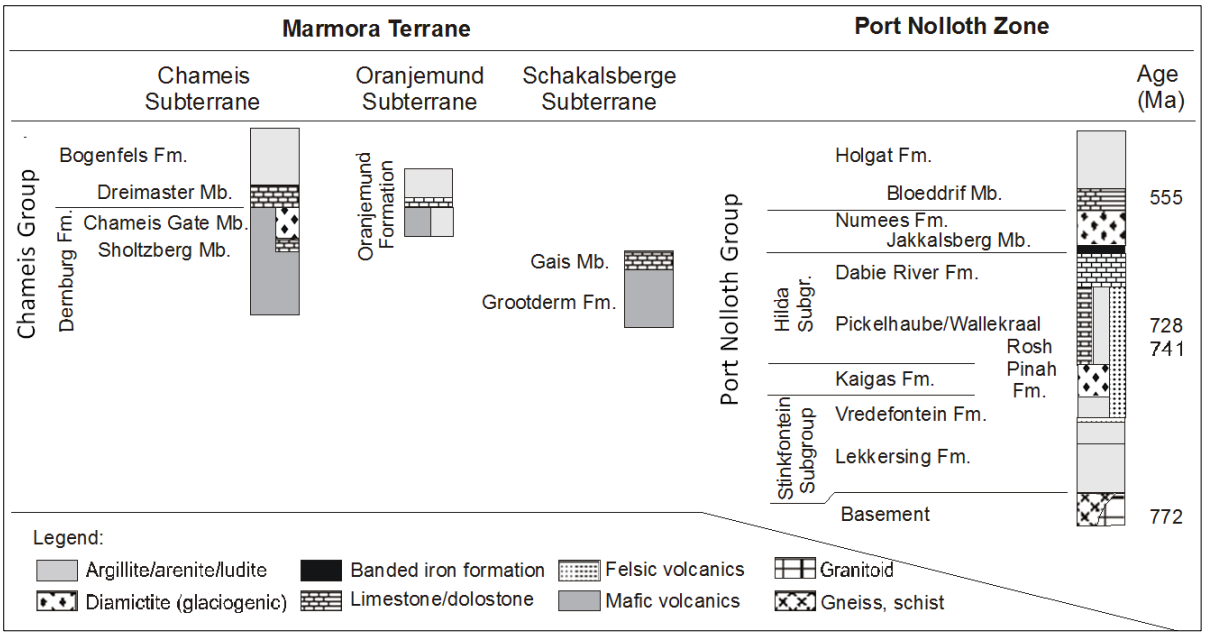

Figure 2.2. Stratigraphic sub-division of the Gariep Supergroup, with suggested correlations between the Port Nolloth Zone and Marmora Terrane (Frimmel, 2000).

Based on petrological and geochemical analyses on the Chameis and Schakalsberge Subterranes, both units indicate an oceanic signature categorised by an aseismic ridge or oceanic seamounts (Frimmel *et al.,* 1996; Jacob, 2001). The Oranjemund Subterrane is stratigraphically more complex and the units that form therein comprise the Oranjemund Group, which is of interest here (SACS, 1980). The outcrops of the Oranjemund Group can be traced along a 120 km long narrow coastal strip trending northward of the current Orange River mouth (**Figure 2.1**; Jacob, 2001). In comparison to the other subterranes, the Oranjemund Group lacks the typical large quantity of intrusive and mafic volcanic rocks (Frimmel, 2008). The predominant phyllites/schists found at the base of the Oranjemund Group are similar to the Chameis and Schakalsberge Subterranes mafic rocks, and is therefore believed to have originated from the debris of the adjacent oceanic seamounts (Frimmel, 2008). The mafic component is in turn locally overlain by meter and decimetre thick dolomite and chert beds, respectively (Frimmel, 2008). The upper part of the group comprises, amongst others, turbidites (Basei *et al.,* 2005; Frimmel, 2008).

2.2 Regional Setting

2.2.1 Southern African Hinterland Source and Orange-Vaal River System Conduit

The breakup of West Gondwana and formation of the western margin of southern Africa were initiated during the continental rifting phase in the Late Jurassic (e.g. Dingle *et al.,* 1983; Apollus, 1995; de Wit, 1999; Aizawa *et al.,* 2000; Jacob, 2005; Bluck *et al.,* 2007). Following the breakup of Gondwana, the interior of southern Africa experienced rapid erosion with extensive Late Cretaceous denudation (Jacob, 2005; Hanson *et al.,* 2009; Spaggiari, 2011). By this time, the bedrock topography of the west coast was also developed as a result of intense erosion of the continental margin (Apollus, 1995). The estimated amount of sediment stripped during this humid period (de Wit, 1999; Frimmel, 2008) ranges from ~1.35 km (Hanson *et al.,* 2009), ~1.9 km (Hawthorne, 1975), to controversially as much as 2 – 5 km (Brown *et al.,* 1998; Brown *et al.,* 2000; Gallagher and Brown, 1999); however, recent findings suggested reduced denudation rates of <1 km (e.g. Wildman *et al.,* 2017). The majority of the Cretaceous (80 – 140 Ma) diamond-bearing kimberlites, which are confined to the Kaapvaal Craton within southern Africa (Gurney *et al.,* 1991; Brown *et al*., 1998), would have been extensively eroded during this period. The diamonds were retained in colluvial and alluvial deposits within the regional drainage system awaiting further transportation by an evolving Orange-Vaal River System (**Figure 2.3**; e.g. Hallam, 1964; de Wit, 1999; Bluck *et al.,* 2005; 2007; Hanson *et al.,* 2009; Spaggiari, 2011). The latter, draining the interior of southern Africa, developed sometime between the Jurassic (Apollus, 1995) and Middle-Late Cretaceous (de Wit, 1999).

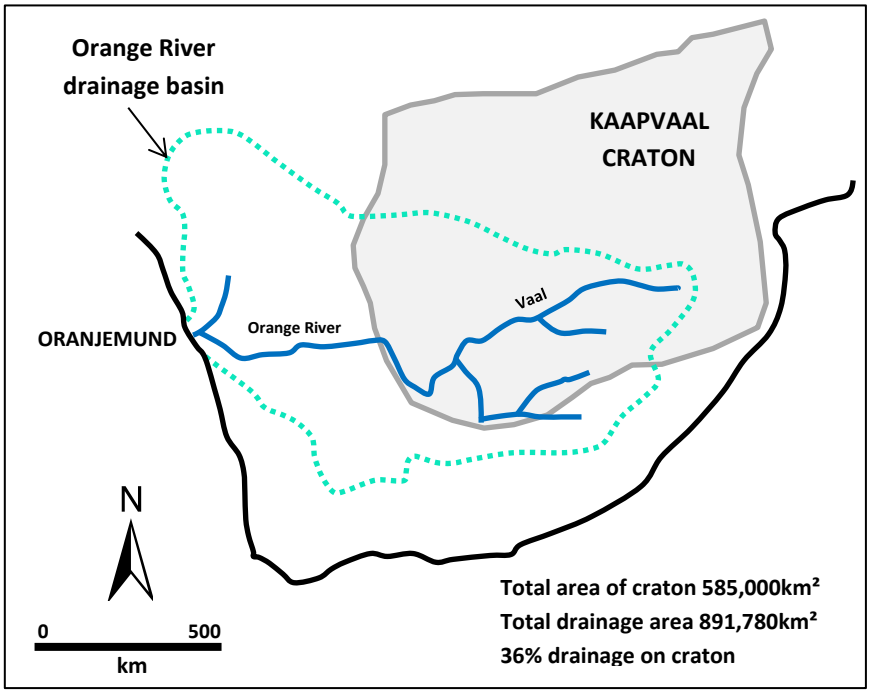

Figure 2.3. Roughly one third of the drainage area of the Orange-Vaal River System is over the part of the Kaapvaal Craton that contains diamondiferous kimberlites (adapted from Bluck *et al*., 2005).

It is suggested that during the Late Cretaceous, approximately 93 – 70 Ma ago, the ancestral or forerunner Orange River (or Kalahari River of de Wit, 1999) was a suspended-load fluvial system dominated by fine-grained sediment outfall that formed the Orange River Delta (Kudu Delta; Aizawa *et al.,* 2000; Bluck *et al.,* 2005; Spaggiari, 2011). Geophysical surveys and borehole data show that the Orange River Delta comprises fine-grained deposits (e.g. clay and silt) and more than 90 % of it can be attributed to the suspended-load Orange River during that time (Aizawa *et al.,* 2000; Bluck *et al.,* 2005; Bluck *et al.,* 2007; Spaggiari, 2011).

The changeover from suspended-load to bed-load dominated, bedrock incised fluvial system was established by Middle Eocene, roughly 43 Ma ago, as a result of regional sub-continental uplift that entrenched the ancestral, meandering Orange-Vaal River System into the basement rock types through the pre-Cretaceous (e.g. Karoo Supergroup) sediment cover of southern Africa (e.g. Stocken, 1978; Partridge and Maud, 1987; de Wit, 1999; Jacob *et al.,* 1999; Bluck *et al.,* 2005; Spaggiari *et al.,* 2006; Spaggiari, 2011). An approximate uplift of 1 km during the Late Cretaceous/Early Cainozoic has been estimated (Aizawa *et al.,* 2000), supported by borehole drilling roughly 250 km south-west of the current Orange River mouth (i.e. K-B1 and K-A2 wells; Miller, 2008). The borehole data indicates a ~7 km thick Cretaceous package in the offshore Orange Basin, bounded by the Gondwana breakup unconformity at the base and a partial sub-Cainozoic unconformity at the top (Frimmel, 2008).

The major uplift during the Late Cretaceous/Early Cainozoic is the most important event of the Orange-Vaal River System evolution, not only because it increased the catchment area to approximately 900 000 km^2 (Compton *et al.,* 2002; Jacob, 2005; Bluck *et al.,* 2007; Spaggiari, 2011), but also because it promoted erosion of the primary and secondary diamond sources within the Early Cainozoic Orange-Vaal catchment (Aizawa *et al.,* 2000; Bluck *et al.,* 2005). The increase in slope allowed the transportation of pebble to cobble sized sediments, including diamonds, from the interior to the Atlantic Ocean westward (Jacob, 2005; Bluck *et al.,* 2005; Spaggiari, 2011). The changeover in facies is shown by the Eocene clast assemblages recovered in the river mouth as well as possibly Paleocene/lower Eocene clasts and upper Eocene clasts found roughly 150 km north of Oranjemund at Buntfeldschuh (Siesser and Salmon, 1979) and Bogenfels (Siesser, 1977b), respectively. The gravels comprise yellow chalcedony and agates with reduced amounts of quartz and jasper that are similar to the Mahura Muthla gravels found on the Ghaap Plateau in the interior of South Africa and prominent in the Vaal River gravels, e.g. Lichtenburg and Parys areas (Bluck *et al.,* 2005; Jacob, 2005; Spaggiari, 2011). Agates with diameters of up to 10 cm have also been discovered in the Bogenfels deposits (Jacob, 2005; Bluck *et al.,* 2005; Spaggiari, 2011). Finer grained

exotic fragments found in the lower Orange River yield vital provenance information, such as the banded ironstones (including riebeckite, a distinctive blue variety) sourced from the Transvaal Supergroup (SACS, 1980) and Orange and Vaal River agates, distinguished by their colour, being sourced from the Drakensberg Group and possibly sources long-since eroded, respectively (Jacob, 2005). Small white zeolite pebbles, liberated from the Drakensburg Group basalt host rock, are evident in the Orange River which drains the Drakensburg, but not observed in the older and modern Vaal River deposits (Jacob, 2005). Makwassie porphyry, a distinctive purple/red quartz porphyry, is primarily observed in the younger marine deposits (Jacob, 2005).

The Early Cainozoic is associated with reduced rates of erosion compared to the Cretaceous period (Apollus, 1995; de Wit, 1999; Spaggiari, 2011). This is supported by reduced Cainozoic depositional rates in the offshore (Dingle, 1993; Spaggiari, 2011) and apatite fission track (AFT) analysis (Aizawa *et al*., 2000; Wildman *et al.,* 2015). More specifically, the latter suggests that the Cainozoic is associated with average erosion rates of approximately 5 – 10 m/Ma (<1 km of erosion), which consequently indicates a decline in the stripping of the diamondiferous kimberlites during the Cainozoic (e.g. de Wit, 1999, 2007; Spaggiari, 2011; Wildman *et al.,* 2015). Post-Eocene changes in diamond supply by the Orange River to the Atlantic Ocean are linked to two additional uplift events of about 100 – 200 m in the Early-Middle Miocene and about 100 – 900 m in the Plio-Pleistocene (Partridge and Maud, 1987; Apollus, 1995; Jacob, 2005).

In contrast to previous workers, Burke (1996) and Burke and Gunnel (2008) proposed that by the early Oligocene, Africa, including southern Africa, was a low-elevation and low relief land surface that was covered by a major weathered surface (the African Surface) which formed between approximately 130 – 30 Ma. This period of relative tectonic inactivity was followed by surface uplift at approximately 30 Ma (e.g. Burke, 1996; Burke and Gunnel, 2008; Paul *et al*., 2014), preserving the weathered surface in sedimentary basins at the continental margins and in the continental interior. However, large deposits of Oligocene age are not documented offshore (Jacob, 2005), a fact credited to the start of desertification in southwestern Africa (Burke, 1996). In addition, based on the length scale at this time, approximately 4 – 5 km of denudation across the coastal plain, with much deeper erosional trends than what are calculated for the interior, would be required to overcome isostatic compensation (Wildman *et al*., 2015; 2017). This does not oppose surface uplift across southern Africa during the Cainozoic, but based on AFT analysis it does restrict the total amount of erosion to <1 km (Wildman *et al*., 2015).

Mining operations and associated geological investigations (Fowler, 1976; 1982; Jacob, 2005) on the Lower Orange River (approximately 100 km upstream of the river mouth) have provided vital

information on the diamond concentration, i.e. grade and size, within the palaeo-Orange River deposits (terraces) that were responsible for trapping diamonds through time (Spaggiari, 2011). In general, a decrease in grade and increase in stone size is recorded from older to younger Lower Orange River terraces (**Figure 2.4**; van Wyk and Pienaar, 1986; Bluck *et al.,* 2005). The Proto Suite of terraces, comprising the locally termed Pre-Proto and Proto-Orange River deposits (Arriesdrift Gravel Formation; SACS, 1980), are assigned an Eocene/Oligocene and Early-Middle Miocene age (Corvinus and Hendey, 1978; Jacob *et al.,* 1999; Jacob, 2005; Spaggiari, 2011). The Meso Suite of terraces, comprising the locally termed Meso-Orange deposits and four other discreet deposits, has not been sufficiently dated, but are tentatively assigned a Plio-Pleistocene age (Ward *et al.,* 1998; Jacob *et al.,* 1999; Jacob, 2005; Spaggiari, 2011). The older Pre-Proto gravels, trapped in deep scours cut into the bedrock strata, represent the best grade diamonds found within the Orange River terrace system. Although these diamonds are high grade, they have small average stone sizes in contrast to the Proto gravels that contain larger stones of lower grade (Jacob *et al.,* 1999; Bluck *et al*., 2005). High diamond concentrations are directly proportional to the occurrence of fixed bedrock trap sites within the Orange River bed (Jacob *et al.,* 1999). The demise of the main flush of diamonds is heralded by the younger Meso-Orange deposits, which comprise large-average stone sizes, but lower grade (Jacob *et al.,* 1999; Jacob, 2005).

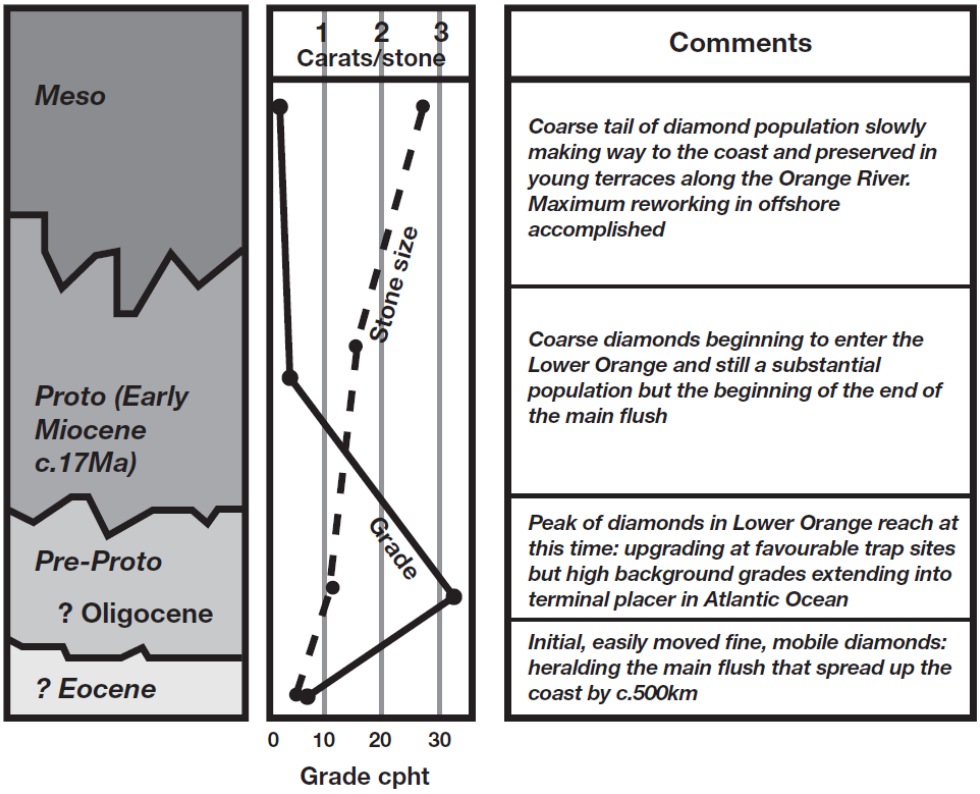

Figure 2.4. Variations in the grade and diamond size through the Lower Orange River terraces. Cpht = carats per hundred tonnes of gravel (Bluck *et al.,* 2005).

2.2.2 Atlantic Ocean Sink

2.2.2.1 Present Coastal System and Climate

The persistent South Atlantic sub-tropical anti-cyclone offshore, pushing cold air from the south-west Atlantic Ocean landward (Goudie and Viles, 2014), controls the strong onshore directed southerly to south-westerly winds (30 – 80 km/hour) experienced along the south-west coast of Namibia since at least the Eocene (e.g. Jacob, 2001; Frimmel, 2008; Spaggiari, 2011). The anti-cyclone is not only responsible for the consistent high winds in the region, but also for the high-energy, short period waves experienced along the coast (de Decker, 1988; Frimmel, 2008). The wave heights of approximately 90 % of the waves along the offshore of the Orange River fall within the range of 0.75 – 3.25 m, averaging to 1.5 m in summer and 1.75 m in winter (de Decker, 1988; Spaggiari, 2011). The wave base is estimated to be at a depth of approximately 40 m, but suggestions have been made of a deeper storm wave base, at approximately 110 m, that has been documented during semi-submersible dives, based on the presence of wave-generated water movements strong enough to agitate sediments (de Decker, 1988; Bluck *et al.,* 2005). The tidal range experienced off the Orange River mouth is only ~1.8 m, typical of micro-tidal coasts (de Decker, 1988; Bluck *et al.,* 2005; Spaggiari, 2011). The oblique nature of the south-westerly swell and locally produced wave orthogonals along the coast allow for an energy conversion into a northward directed longshore drift (Bluck *et al.,* 2005; Frimmel, 2008; Spaggiari, 2011). The Benguela Ocean Current, flowing in a northward direction at 88 mm/sec, is a major contributor to the movement of the water masses on the shelf (Bluck *et al.,* 2005; Frimmel, 2008).

2.2.2.2 Cainozoic Relative Sea-level Changes

Relative sea-level (RSL) changes are the combined manifestation of changes in the local tectonics (i.e. uplift and subsidence) and eustatic sea-level (ESL). The changes in RSL, in conjunction with the amount of sediment supply from the land, determine the shoreline trajectory through time (Catuneanu, 2006). The sedimentation patterns along the south-west coast of Africa has been repeatedly impacted, in conjunction with intense wave energies and a northward longshore drift system, by numerous oscillations in RSL, particularly since the Miocene (Jacob, 2001; Bluck *et al.,* 2005; 2007; Spaggiari, 2011). Drilling and seismic surveying in the offshore reveal that the shelf area, particularly to the immediate north and south of the Orange River, has accumulated little sediment since the Late Cretaceous/Early Cainozoic uplift and that little, if any, subsidence has occurred during that time (e.g. Aizawa *et al.,* 2000; Bluck *et al.,* 2005; Spaggiari, 2011). Therefore, in this region, the main driving force behind the RSL changes is not local tectonics, but ESL changes. Furthermore, this data also implies that the position of the shoreline relative to the land (i.e.

transgressions, regressions) is mainly driven by RSL changes and less importantly by the sediment supply from the land.

The wave-cut platforms, bevelled across the bedrock, are the product of wave erosion during slow RSL rise in the Late Cainozoic (Jacob, 2006). The bedrock platforms comprise abundant fixed diamond trap sites which are classified as potholes, cylindrical depression formed by the grinding action of gravel and sand through wave turbulence as well as gullies, which are longitudinal furrows that results from the erosional coalescence of multiple adjoining potholes (Wright, 1964; Apollus, 1995; Jacob, 2001). The ruggedness of the bedrock terrain (i.e. relief of the potholed and gullied substrate) has been linked to rheological heterogeneity of the Gariep Group (i.e. competence difference between meta-arenites vs. schistose units; Murray *et al*., 1970; Miller *et al*., 2000; Jacob *et al*., 2006).

As suggested by geomorphological evidence and the similarity of the clast assemblage to that of dated localities (Stocken, 1978), the highest standing RSL along the west coast of southern Africa was at approximately 170 metres above mean sea-level (m amsl) and occurred during the Eocene; i.e. Buntfeldschuh in the *Sperrgebiet*, which pre-dates the onset of terrestrial glaciation in Antarctica (**Figure 2.5**; e.g. SACS, 1980; Siesser and Dingle, 1981; Francis and Hambrey, 2008; Bluck *et al.,* 2005; 2007; Frimmel, 2008). The Buntfeldschuh region hosts evidence of a wave-cut platform beneath Eocene sediments, which is related to the major Eocene transgression (Jacob, 2001). Dingle (1971b) recognised a major Oligocene aged unconformity on the west African continental shelf through seismic analysis and estimated a potentially global regression of 120 metres below mean sea-level (m bmsl; Dingle *et al.,* 1983; Frimmel, 2008; Bluck *et al.,* 2007; Spaggiari, 2011). The global regression during the Oligocene is associated with a combination of ice-sheet build-up (Francis and Hambrey, 2008) and tectonics: isolation of Antarctica and the opening of the Drake Passage, which allowed the restructuring of the ocean circulation and subsequent development of bottom currents (Kennett and Stott, 1990; Séranne and Anka, 2005). Following the major ice cap build-up of Antarctica during the Oligocene, the subsequent waxing and waning of this major ice sheet has largely driven RSL changes in the Neogene of southern Africa (Bluck *et al.,* 2007). Although the Eocene high stand has not been reached since, the Oligocene low stand scenario has reoccurred during glacial maxima in the Neogene, with the Last Glacial Maximum between 22 and 19 ka before present, dropping the ESL to 120 – 130 m bmsl (**Figure 2.6**; e.g. Compton *et al*., 2002; Bluck *et al.,* 2005; 2007; Spaggiari, 2011; J. Ward, pers. comm., April 2016).

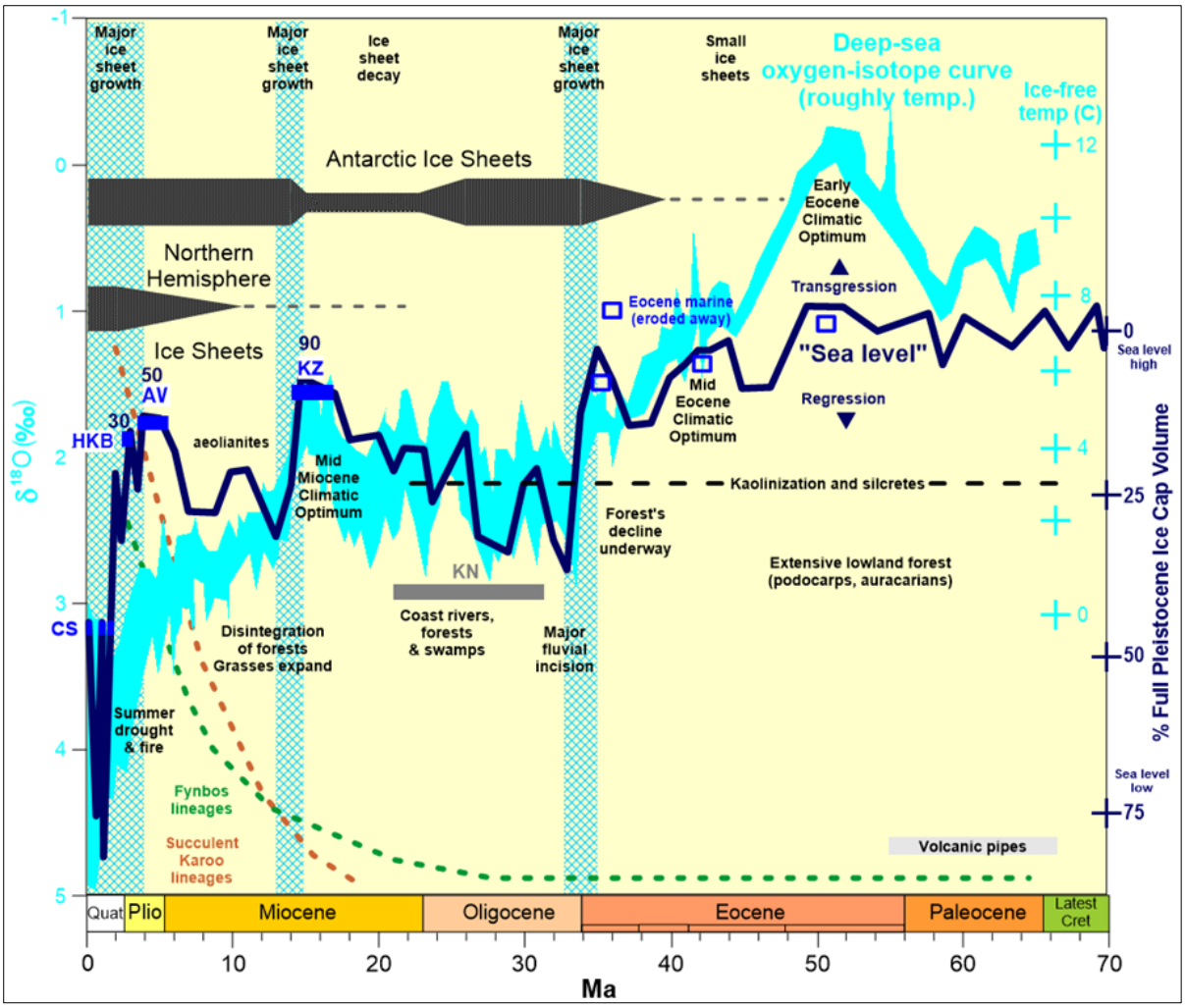

Figure 2.5. Changes in global palaeo-climate proxies, phases of regional vegetation occurrences and the setting of marine formations of the West Coast Group, Alexander Bay Subgroup from the Late Cretaceous to Quaternary period (Pether, 2017). Cyan curve indicates history of deep-ocean temperatures in °C adapted from Lear *et al*. (2000). Global ice volumes approximately indicate eustatic sea-level history caused by seawater stored on land as ice. The increase of Fynbos and Karoo vegetation is adapted from Verboom *et al*. (2009). AV = Avontuur Formation, CS = Curlew Strand Formation, HK = Hondeklipbaai Formation, KN = Koingnass Formation and KZ = Kleinzee Formation.

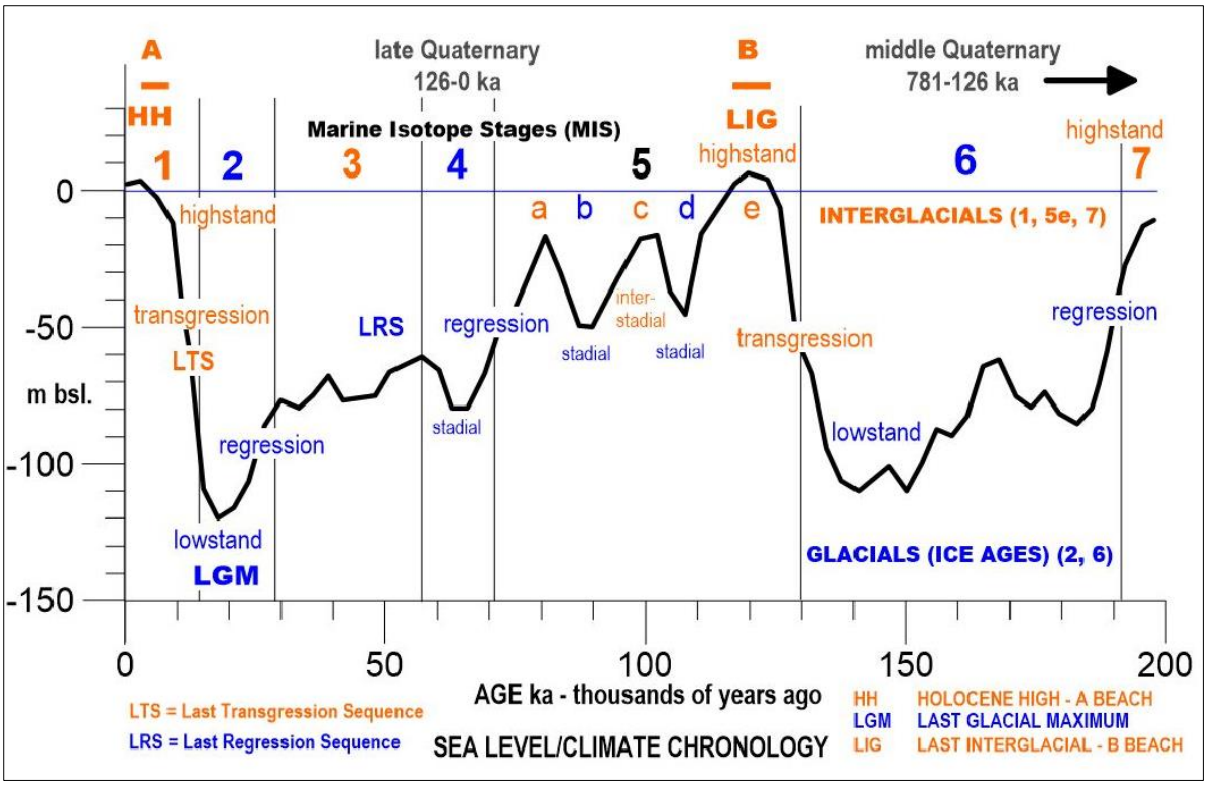

Figure 2.6. Estimated eustatic sea-level changes during the last 200 ka. LRS = Last Regression Sequence, LTS = Last Transgression Sequence and LGM = Last Glacial Maximum (Pether, 2013 adapted from Siddall *et al.,* 2007).

2.2.2.3 Sediment Dispersal and Trapping

The continental shelf edge off Oranjemund is at an approximate depth of 500 m bmsl and the shelf break is situated approximately 70 – 150 km offshore (Stevenson and McMillan, 2004). Since the Late Cretaceous/Early Cainozoic uplift phase, the shelf offshore southwestern Africa has remained remarkably buoyant and shallow (e.g. Siesser and Dingle, 1981; Aizawa *et al.,* 2000; Bluck *et al.,* 2005; 2007). Consequently, the depositional environment for the majority of the Cainozoic sediments would have shifted beyond the Late Cretaceous shelf edge due to the reduction of accommodation space available over the shelf, with the inner shelf having been an area of sediment bypass (**Figure 2.7**; Aizawa *et al.,* 2000; Bluck *et al.,* 2007; Miller, 2008).

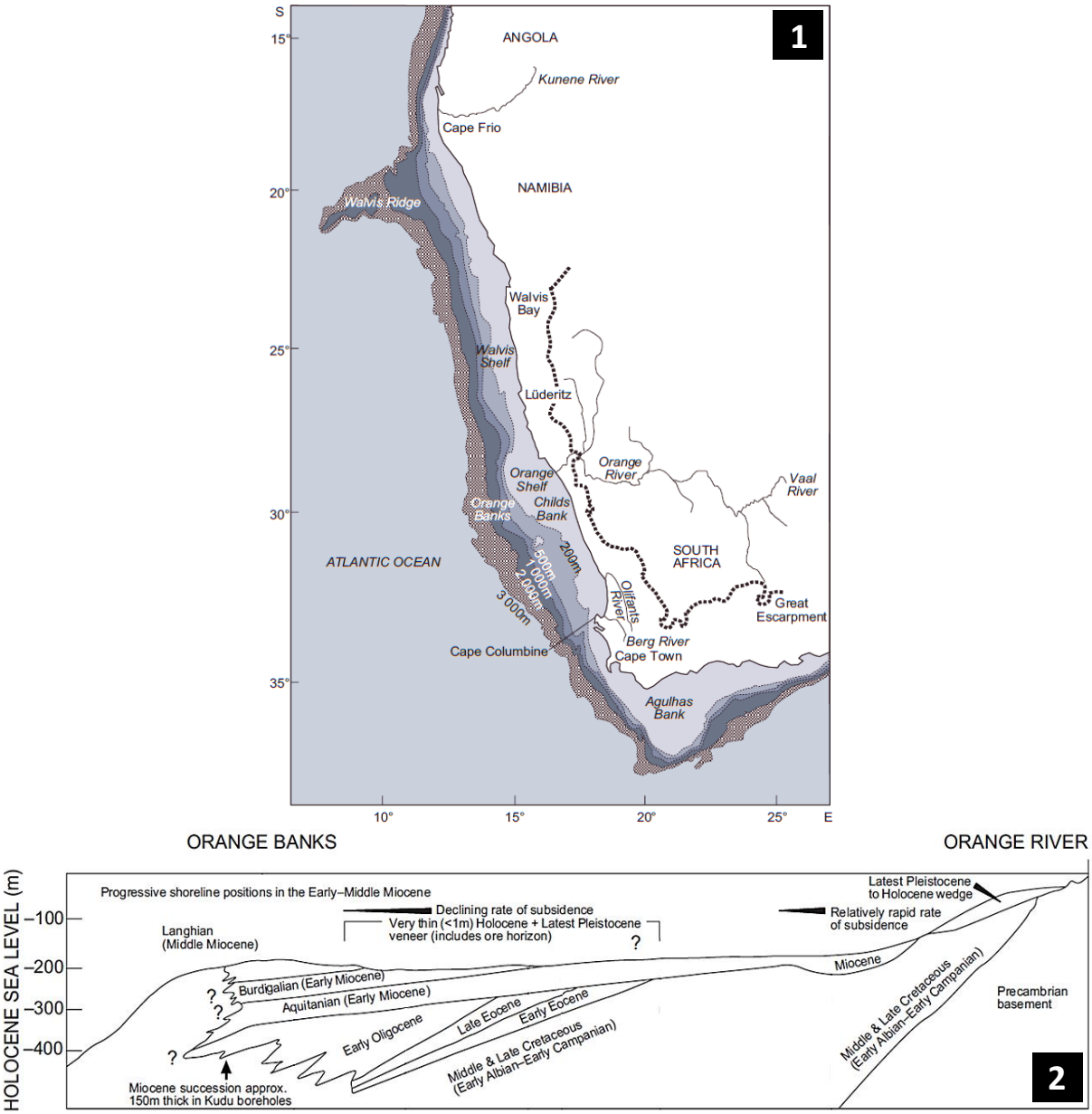

Figure 2.7. 1) Bathymetric map of the continental margin off south-western Africa (Rogers and Rau, 2006 adapted from Rogers and Bremner, 1991). 2) The stratigraphy of the Orange River shelf varies from steeply dipping Precambrian bedrock and Cretaceous sediments in the inner shelf to broad, gently dipping Palaeogene and Neogene sediments in the middle and outer shelf (Rogers and Rau, 2006 adapted from Corbett *et al*., 1995 and Corbett, 1996).

During the Cretaceous, the Orange River Delta was largely fluvially dominated; however, by the Eocene, with the onset of a unidirectional southerly wind regime, the sediment dispersal systems transitioned into a wave-dominated delta and then to a forceful wave-aeolian system (Bluck *et al.,* 2007). The change in sediment dispersal systems is a combination of sediment supply, accommodation space as well as climate and wind regime in the region (Bluck *et al.,* 2007). The actions of a high energy wave regime on a neutrally buoyant shelf aggressively redistributed the sediment outfall from the river since at least the Eocene (Siesser and Dingle, 1981; Aizawa *et al.,* 2000; Spaggiari, 2011). The strong longshore drift has been migrating nearshore deposits from the Orange River Delta northward (Bluck and Ward, 2000; Frimmel, 2008). The gravel, sand and mud

(silt and clay) fractions are redistributed into discrete zones of accumulation along the coast. Sand and gravel are carried as far as 1200 and 350 km north of the Orange River mouth, respectively (Hallam, 1964; Bluck *et al.,* 2007; Frimmel, 2008), whereas the silt and mud are dispersed over a larger area and deposited on the shelf edge and further offshore (**Figure 2.8**; Aizawa *et al.,* 2000; Bluck *et al.,* 2007). The highly energetic coastal system distributes the gravel fractions within the intertidal to subtidal zones in the form of spit/barrier beaches, linear beaches and pocket beaches (**Figure 1.1**; e.g. Corbett, 1989; Spaggiari *et al.,* 2006; Jacob *et al*., 2006). The PTA lies adjacent to the linear beaches of Mining Area 1 (MA1). The majority of the diamonds mined in MA1 are from a narrow thin strip of Late Cainozoic beach and related marine deposits (Bluck *et al.,* 2005). This 120 km long marine platform, hosting the diamondiferous deposits, varies in width from 3000 m at the Orange River mouth to less than 500 m near Chameis Bay (**Figures 2.1 and 2.7**; Jacob, 2001). The sand fractions are blown further inshore by strong onshore winds (**Figures 1.1 and 2.7**) after accumulating in J-shaped bays along the coast (Bluck *et al.,* 2005; 2007). The offshore to onshore supply of fine-grained sediments into desert sand seas (Sossus Sand Formation; SACS, 1980) has occurred since at least the Middle Cainozoic (Ward, 1988; Pickford, 2000).

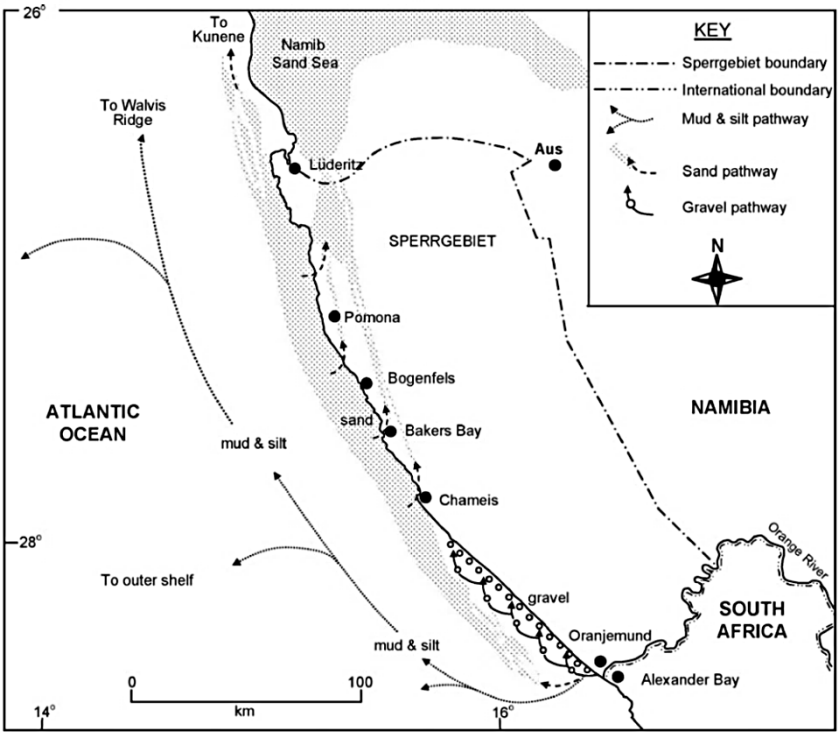

Figure 2.8. Sediment dispersal paths of gravel, sand and mud along the high energy coastline of the southwestern Africa (Spaggiari *et al.,* 2006).

CHAPTER 3 – METHODOLOGY

To define the diamondiferous resources in the offshore setting, three technical datasets were acquired: 1) surface geophysical via bathymetry and side scan sonar, 2) sub-surface/sub-bottom geophysical via seismic surveys and 3) geological/sedimentological via exploration borehole drilling and resource borehole sampling. The compilation and analysis of the Purple Target Area (PTA) datasets permitted the investigation of the stratigraphy, determination of the depositional environments and ultimately delineation of geological zones laterally and vertically across the study area for resource estimation purposes.

3.1 Surface Geophysical Surveys

3.1.1 Bathymetry

The target area is covered by RESON 8101 multi-beam bathymetry survey with approximately 5 x 5 m binned horizontal resolution (X and Y) and approximately 1 m vertical resolution (Z). The bathymetry data, which visualises the topographic highs and sedimentary characteristics of the seafloor, has been extensively referred to for borehole site selection during exploration drilling and resource sampling campaigns. **Figure 3.1** shows the current multi-beam bathymetry dataset that stretches from the offshore mining licences adjacent to onshore No. 2 Plant in the south to Lüderitz in the north.

The data are suitable to distinguish between the Precambrian bedrock and sediment cover, and to delineate topographic features such as bedforms, scours and bedrock structures, i.e. gullies and potholes (Green, 2009). For drilling purposes, only the sediment-covered areas will be targeted and defined. This does not mean that diamondiferous gravel cannot be found within the vast areas of exposed bedrock depressions; however, these areas are mostly shallower than 30 metres below mean sea-level (m bmsl) and inaccessible due to the operating depth constraints of the sampling vessel.

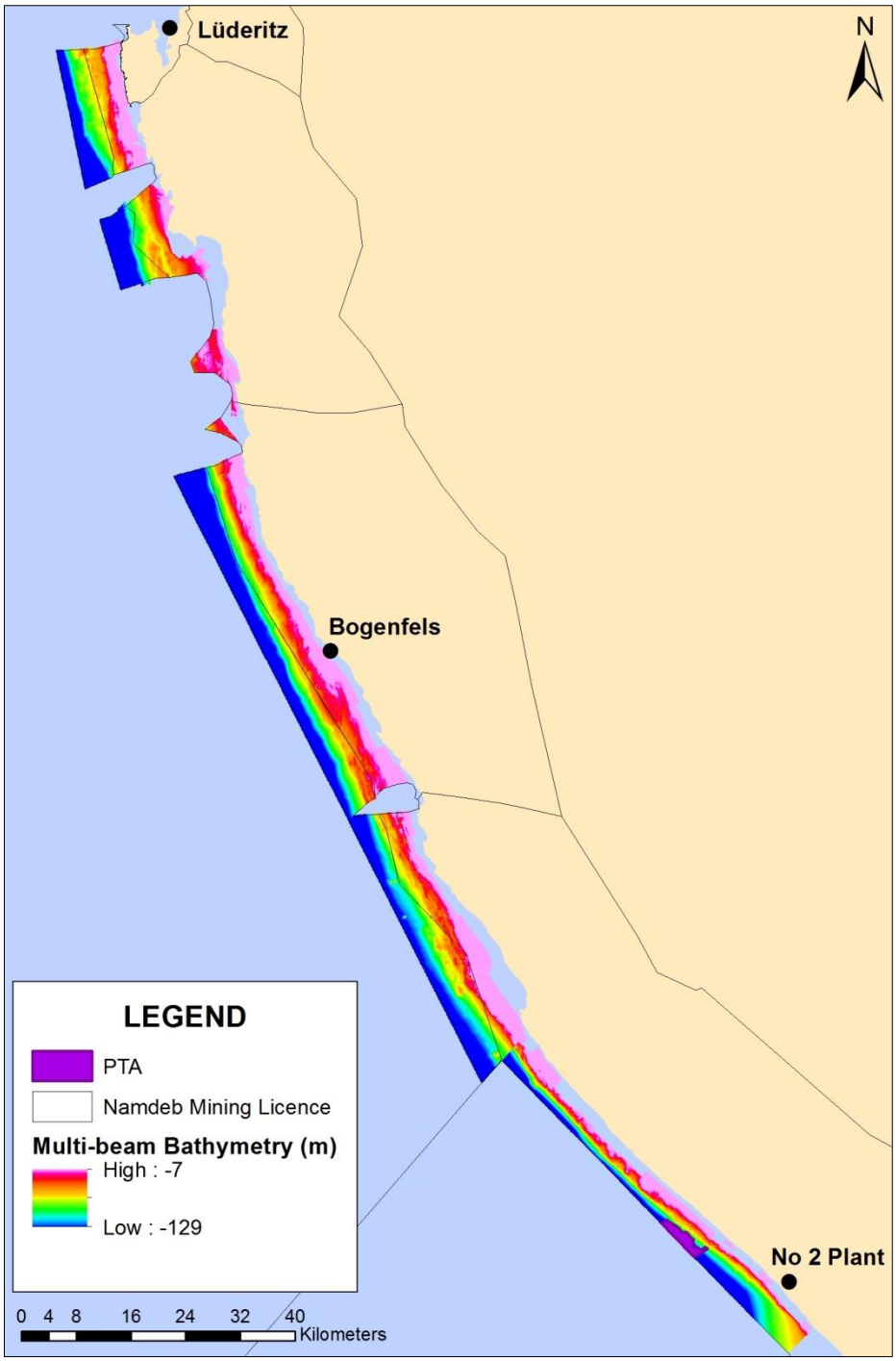

Figure 3.1. Multi-beam bathymetry coverage within the offshore Namdeb mining licence extends from No. 2 Plant in the south to Lüderitz in the north. The warm colours represent bathymetric highs and the cool colours bathymetric lows, with relative water depths ranging from ~7 m bmsl and ~129 m bmsl for the onshore and offshore of the bathymetric dataset, respectively.

3.1.2 Side Scan Sonar

The 100 kiloHertz (kHz) side scan sonar mosaics, covering a 14.13 km² area of bedrock/footwall exposure and sediment cover, are an additional sonar imaging tool that provides data from which information about the surface texture and composition can be derived. In conjunction with the accurate positioning of the multi-beam bathymetry dataset, up to decimetre resolution seafloor interpretation can be achieved (**Figure 3.2**).

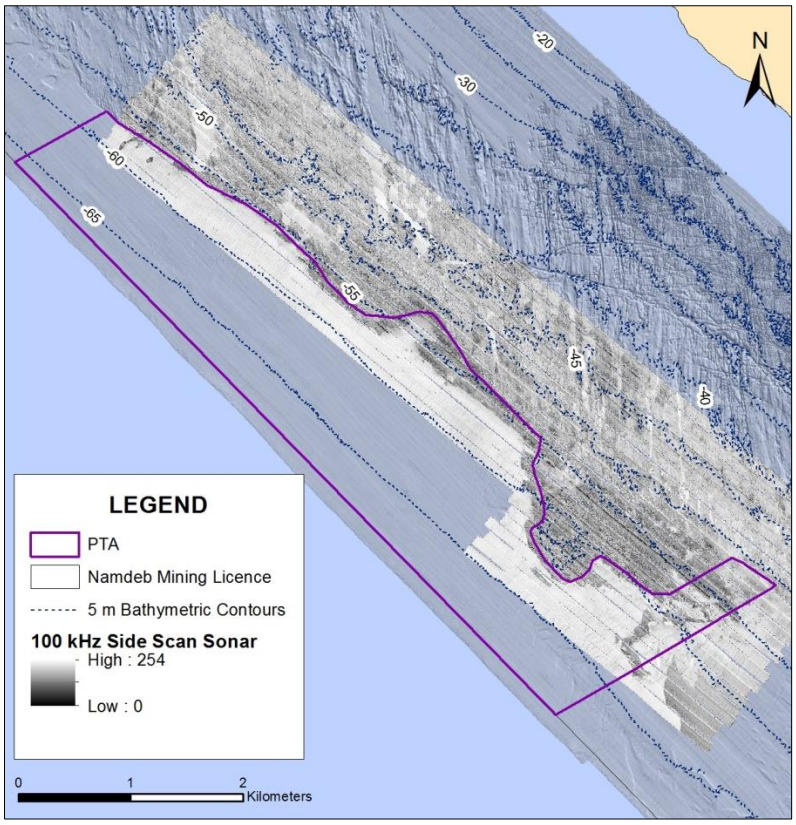

Figure 3.2. Side scan sonar coverage superimposed onto the multi-beam bathymetry (displayed in greyscale) over the shallow inner shelf portion of the PTA.

3.2 Sub-bottom Geophysics/Seismic Surveys

The PTA data collection field survey comprises a total of 17 profiles of single-channel high-resolution seismic Topas data. The seismic survey lines were arranged coast-perpendicular on an evenly spaced grid of 400 m (**Table 3.1; Figure 3.3**).

Table 3.1. Topas geophysical dataset used for the PTA and its survey parameters

Survey	Frequency	Line Spacing	Orientation	Line kms
17 Topas lines, 2011	~3500 Hz	400 m	NE – SW	74

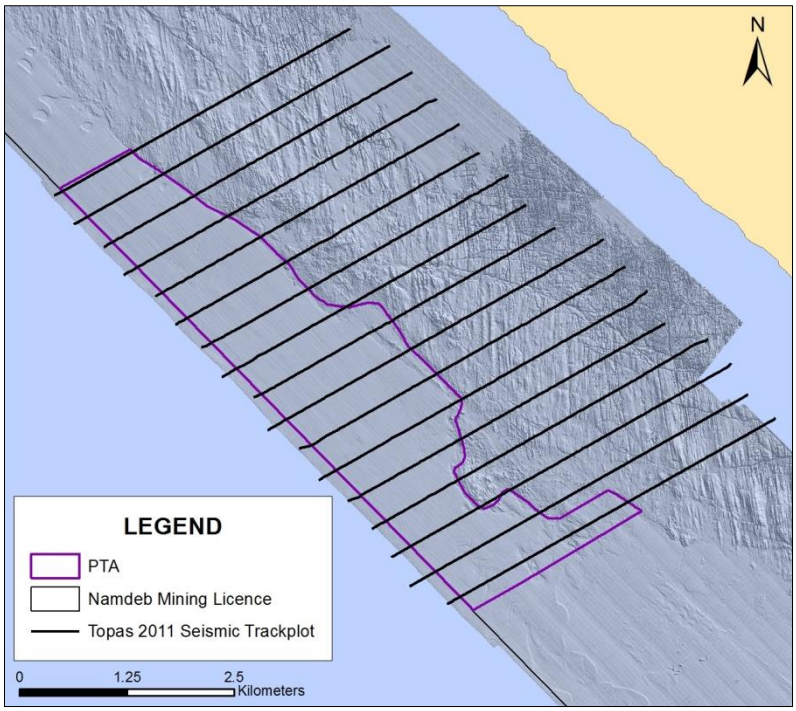

Figure 3.3. NE – SW orientated geophysical dataset comprising a 400 m spaced Topas seismic dataset over the PTA.

Three coast-perpendicular Topas seismic profiles were selected that best represented the change in seismic stratigraphic patterns laterally across the sediment-covered portion of the target area (**Figure 3.4**).

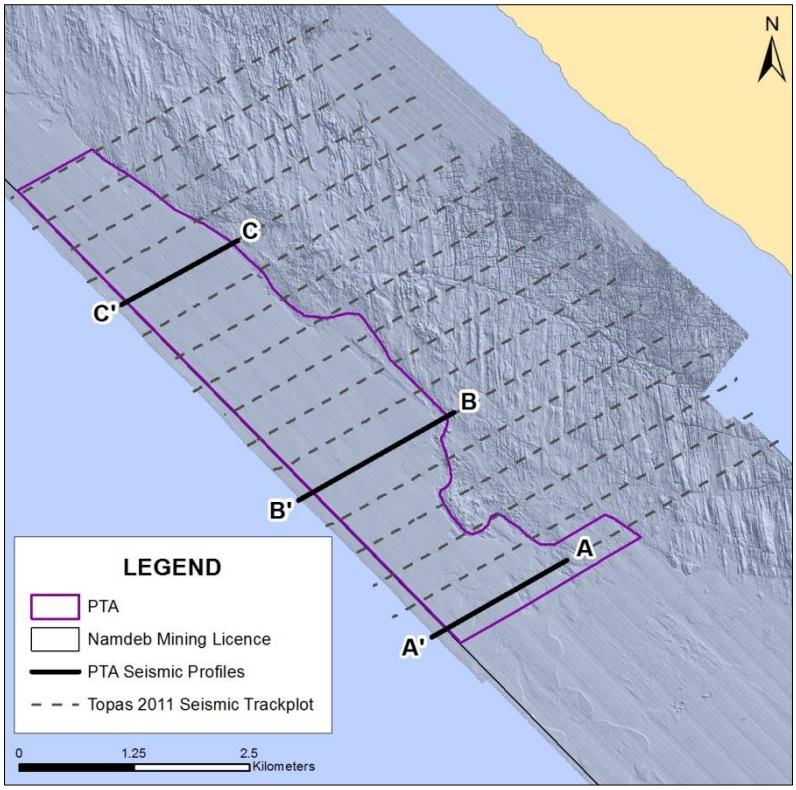

Figure 3.4. Topas seismic profiles, A – A', B – B' and C – C', best represent the change in seismic stratigraphic patterns across the sediment-covered PTA.

The seismic lines were interpreted using Geosuite Allworks© software (versions 2.5.5277.22331 Beta and 2.6.5947.28111) in SEGY-Y format. Seismic sequence boundaries were picked by delineating visible high-amplitude reflectors or variations in seismic facies using the same software. To validate the seismic reflection interpretation, borehole data from drilling and sampling campaigns were correlated to the seismic profiles. To approximate the thickness of the subsurface sediment from two-way time (TWT) in milliseconds (ms) to metres, a simple equation was used to convert the time to depth (Conradie, 2014):

$$Z = \frac{V \times 10^{-3}}{2} \times T$$

Where Z is the depth (m), V is the velocity (m/s) and T is the TWT (ms). The velocity and travel time was divided by 2 because this is TWT. Based on velocity analysis, and considering a change in velocity with depth, a velocity of 1500 m/sec and 1720 m/sec was applied for seawater and solids, respectively.

Following detailed seismic reflection interpretation of the geophysical datasets and their validation, similar geological terrains were identified using the geophysical characteristics determined in the seismic analysis. One of the workflow phases was the extrapolation of the manually picked/interpreted line data to (continuous) surfaces, by applying gridding techniques in, for example, Geosoft© or ArcGIS© software.

3.3 Geological Drilling and Sampling

3.3.1 Vessel

The mv The Explorer (mv TE) sampling vessel, owned by International Mining and Dredging Holding Limited (IMDH) and operated by Namibian Underwater Technology and Mining (Pty) Limited (NUTAM), was contracted to undertake the geological drilling and resource sampling campaigns in the Namdeb offshore concessions. Phase 1 of drilling entailed a geological drilling or exploration campaign that comprised borehole site selection based on interpreted seismic lines to decipher the regional geology within a target; whereas phase 2 resource sampling was based on grid spaced borehole site selection to further define diamondiferous gravel bearing features discovered during phase 1.

The vessel has an overall length of 114 m and is capable of operating in water depths between 30 to 180 m bmsl (International Mining and Dredging Holding [IMDH], 2016). The vessel is equipped with modern survey and navigational systems, i.e. differential global positioning (DGPS), gyrocompass

and motion reference units, all interfaced with a computer running the HYPACK© 2015 navigation/positioning software (E. Nel, pers. comm., April 2016). This allows the vessel to accurately place the sampling tool on a predetermined position on the seabed as well as collect positioning data at a high rate (1 – 2 Hz) during sampling and when moving between boreholes. This data is stored for quality control and auditing of the borehole positions.

The average seismic velocity for the geological units in the study area, in absence of specific seismic velocity, was estimated from generic values obtained from the literature (e.g. Brown, 1999; Stevenson, 1999). The drill depths accuracy, which initially only takes into consideration the amount that the drill moves through the drill frame, is influenced by the fact that the seabed competency varies. The seabed competency determines the amount that the drill frame sinks into the seabed, and this has to be factored into total drill depth measurement(s). To correct for the frame sink, one or more "altimeters" or single beam echo sounders measure and record the vertical position of the drill frame with regards to the seabed at 2 second intervals for the entire duration of the borehole drilling (**Figure 3.5**). These readings are post processed to correct for any spurious values, calculate the amount of frame sink and correct the drill depths, but there is still some degree of uncertainty of the data.

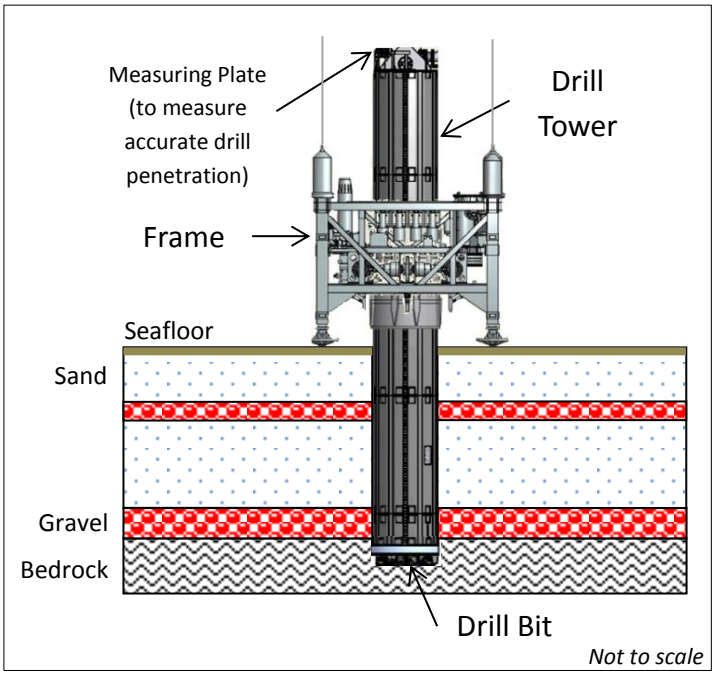

Figure 3.5. Graphics of the mv TE drill tower, frame and drill bit lowered from the vessel onto the seafloor. The drill bit protrudes from the drill tower into the seafloor (This picture has been kindly provided by the owner of the drill tower concept, Namibian Underwater Technology and Mining (Pty) Limited ("NUTAM"), an entity within the IMDH Group of companies).

3.3.2 Sampling Tools

The vessel is equipped with a reverse-circulation (RC) drill bit attached to a frame that is lowered through the moonpool of the vessel and rests on the seabed (**Figures 3.5 and 3.6**). The drill bit protrudes from the base of the drill tower and is capable of drilling into hard competent bedrock/footwall. The diameter of the RC boreholes cannot be disclosed due to a confidentiality agreement between Namdeb Diamond Corporation (Pty) Limited and NUTAM.

In the past 4 years, exploration and sampling campaigns (with the mv TE) have utilised multiple sampling tools to ultimately develop the "Swiss army knife" that delivers a sampling rate of at least 12 holes per day and is robust enough to drill in any type of terrain, whilst maintaining a good sample integrity and delivering accurate geological information.

The enhancements made to the tool over the years have seen major improvement in the sampling campaigns; however, unfortunately the tool did not always succeed in penetrating the bedrock/footwall because of some technical limitation (e.g. drill depth, penetration capability). The success/integrity of a RC drilled borehole is determined by the amount of contamination (sediment collapse during drilling) in the borehole, drilling parameters (penetration rates, torque, pitch and roll of the vessel) and good evidence of bedrock/footwall intersection.

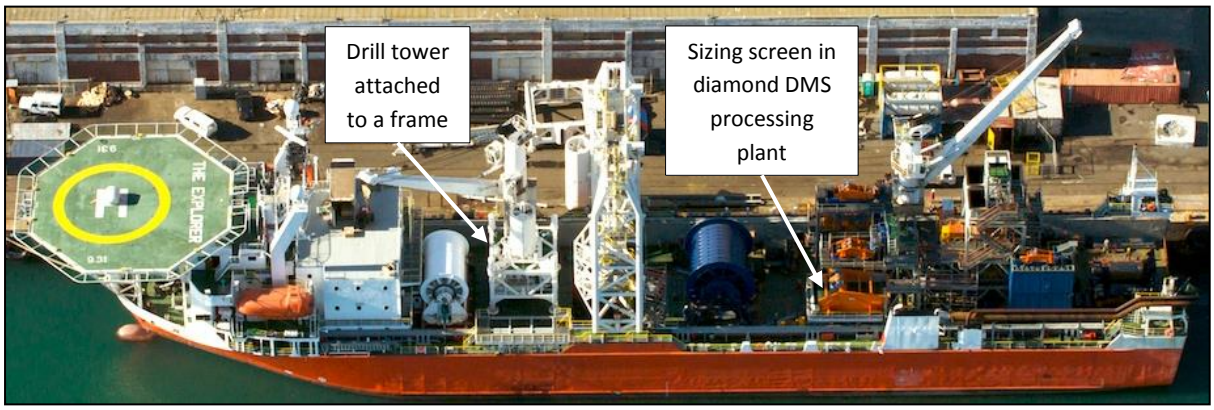

Figure 3.6. The mv TE (IMDH) with her reverse-circulation (RC) drill bit attached to a frame and sizing screens in the diamond dense medium separator (DMS) processing plant (IMDH, 2016).

3.3.3 Geological Drilling and Resource Sampling

The spacing in the borehole grid, which is a function of the size of the target area as well as the assumed cross feature variability, was 200 m (X) in the north-south direction (or multiples of 200 m) and 50 m (Y) in an east-west direction.

The first campaign (phase 1) with the mv TE (in 2013) was to establish a reconnaissance geological framework. The boreholes were widely spaced on predetermined positions along seismic lines (2011 Topas data).

Phases 2 and 3 of the drilling/resource sampling locations in the PTA were predetermined on the following, denser sampling grids:

- Phase 2 in 2014 – 1600 m x 50 m sampling as well as one infill line at 800 m x 50 m in the southern portion of the PTA,
- Phase 3 in 2016 – 800 m x 50 m infill lines within the southern extent of the PTA, followed by infill sampling at 400 m x 50 m and finally, at 200 m x 50 m (**Figure 3.7**). The latter were planned for resource estimation purposes. Phase 3 sampling planned for thinner sediment packages (preferably max. 4 m from top of seabed to top of bedrock/footwall) to accommodate current mining vessel capabilities and desirable mining rates.

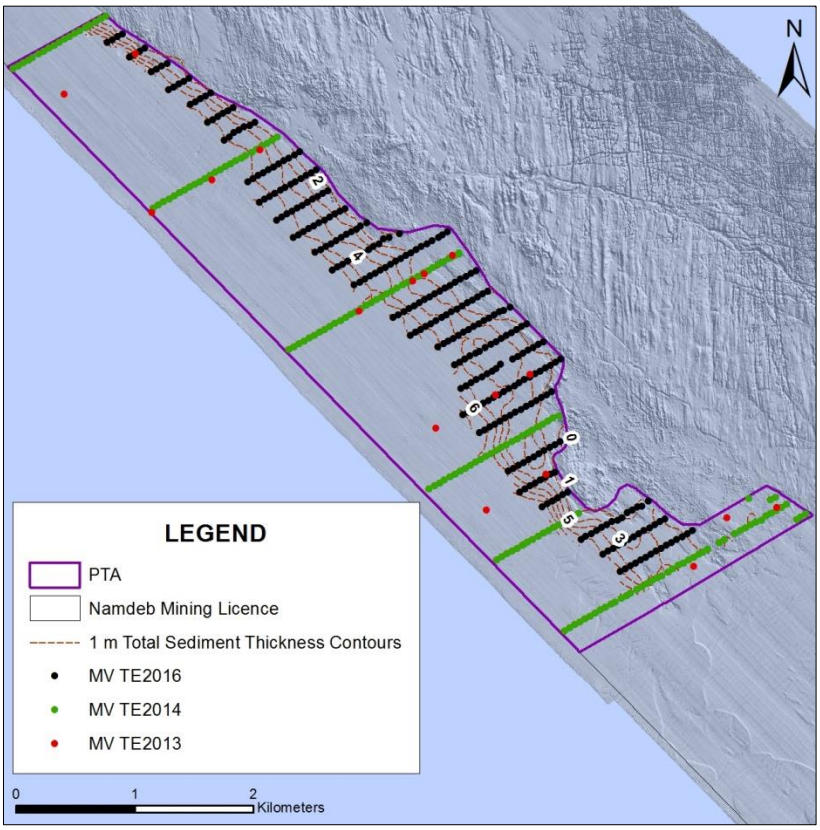

Figure 3.7. Distribution of boreholes drilled within the PTA with the mv TE in 2013, 2014 and 2016.

3.3.4 Geological Data Collection

NUTAM and De Beers Marine Namibia geologists were contracted by Namdeb to undertake the screen logging and data collection for all the geological drilling and resource sampling campaigns held within the Namdeb offshore concessions on the mv TE.

Data gained from the geological drilling and sampling campaigns comprise comprehensive geological logsheets (including vertical sedimentological logs at 1:20 scale), stratigraphical logs and cross-sections using Strater© 4 software, as well as digital logs in the form of photographs and videos.

3.3.4.1 Geological Logsheets

Logging of a borehole is designed to compile a record of the stratigraphic column. The logging procedure used on-board the mv TE was adapted from the "Manual of Standard Logging Procedures" for De Beers West Coast Mines. The logging procedure generated two logsheets:

1. Drill Hole Log Sheet that describes the change in stratigraphy with depth, depicts the stratigraphic succession intersected in the borehole, geographical coordinates and borehole drill data, i.e. borehole ID, geologist's summary of the lithologies encountered in the borehole as well as start and end drill date/time.

2. Drill Hole Tick List Sheet records the proportion of major petrological constituents of the stratigraphic units (e.g. conglomerate, sandstone, quartzite, schist, etc.), exotics (agate, jasper, riebeckite, chalcedony, etc.), composition of bioclasts (bivalve and gastropod shell fragments), sand and clay content as well as the bedrock/footwall composition. The textural features of the clasts, i.e. size, sorting, surface features, roundness and particle shape are visually estimated (Pettijohn *et al.,* 1987; Tucker, 1988) and can provide vital information on the transport processes, degree of erosion and depositional environments (Boggs, 2010).

3.3.4.2 Geological Samples

Geological samples of coarser material (max. diameter >19 mm) and finer material (max. diameter <1.4 mm) were collected in sample bins (LinBins) whenever a change in lithology was observed with depth. During the 2013, 2014 and 2016 PTA campaigns a total of roughly 200 samples were handpicked from the LinBins for further analysis onshore. Photographs were taken of each individual LinBin (**Figure 3.8**), whereas video footage was limited to unexpected variations in lithology only.

Figure 3.8. Geological sample collected from a borehole comprising 1) coarse clastic material and 2) its corresponding finer fragments. Scale represents 15 cm.

CHAPTER 4 – RESULTS

Delineation and interpretation of seismic units yields important information on the properties of the sediments, depositional environment and rate of deposition within a sedimentary basin (Mitchum *et al.,* 1977; Mellet *et al.,* 2012). Reflection configurations, stratal terminations and systems tracts, deduced when possible, are identified based on the principles and standardised sequence stratigraphic terminology of Catuneanu (2006) and Catuneanu *et al.* (2009; **Appendix A**). A systems tract refers to the sediments deposited at a particular stage within a sequence, differing in geometry, and where applicable, in vertical grain size trends from other adjacent systems tracts and bounded by distinct horizons, which are key stratigraphic surfaces. Four systems tracts are identified in a complete stratigraphic sequence: the Falling Stage Systems Tract (FSST), the Low Stand Systems Tract (LST), the Transgressive Systems Tract (TST) and the High Stand Systems Tract (HST).

Three coast-perpendicular Topas seismic profiles (**Figures 4.1 – 4.3**), which best represent the change in stratigraphic patterns laterally across the target area, are shown in **Figure 3.4**. The seismic profiles are displayed in order from south to north. The interpretation of selected seismic profiles from the Purple Target Area (PTA) revealed 4 major seismic units (units A – D) and seismic horizons (H1 – H4) in the region (**Table 4.1**).

The seismic profiles show primarily the sediment-covered areas. Each seismic profile is represented twice: 1) an uninterpreted seismic section and 2) an interpretation of the seismic stratigraphic patterns in Geosuite Allworks© format (**Figures 4.1 – 4.3**). The vertical scale of the seismic profiles is presented in depth in metres below mean sea-level (m bmsl) and the horizontal distance is shown by a scale bar expressed in metres.

The relationship between the seismically interpreted units and facies data from borehole samples are shown on the seismic profiles. Correlating lithological data from borehole samples with seismic units can support interpretations and allow for a more thorough reconstruction of the palaeo-depositional environment and landscape evolution (Mellett *et al.,* 2012). The description of the seismic units and their corresponding facies is not in stratigraphic order, but described in spatial order from the distal to the proximal portions of the basin.

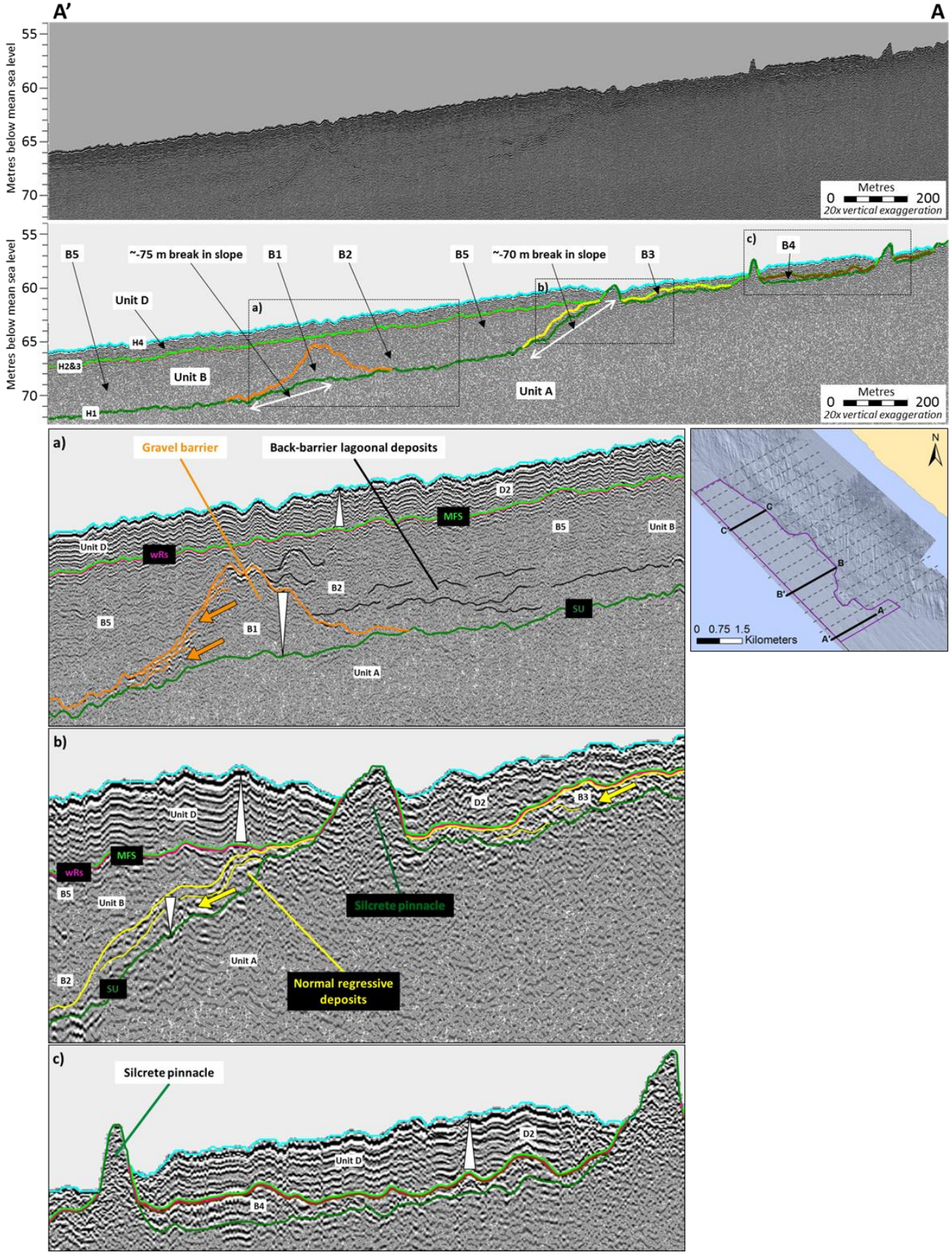

Figure 4.1. Topas seismic section and interpretation showing two high-amplitude surfaces across the profile. Expanded areas show: a) seismic architecture of sub-unit B1 comprising prograding tangential oblique high-amplitude reflectors in the distal portion of the feature, with onlapping back-barrier lagoonal deposits toward the proximal basin; b) Note the segregation of sub-unit B3 into two packages by an outcropping silcrete (unit A) pinnacle. Sub-unit B3 displays seaward dipping prograding tangential reflectors in the downdip direction, seaward of the silcrete pinnacle, and straddles the ~70 m bmsl break in slope. Sub-unit B3 is truncated by H2 in the proximal portions of the basin; c) Sub-unit B4 comprises low-medium-amplitude reflectors aggradationally stacked above the acoustic basement (unit A), truncated by H2 at the surface. Note the upward coarsening and upward fining annotations displayed in the various seismic sub-units. Note the white arrows showing the approximate width of the H1 breaks in slope.

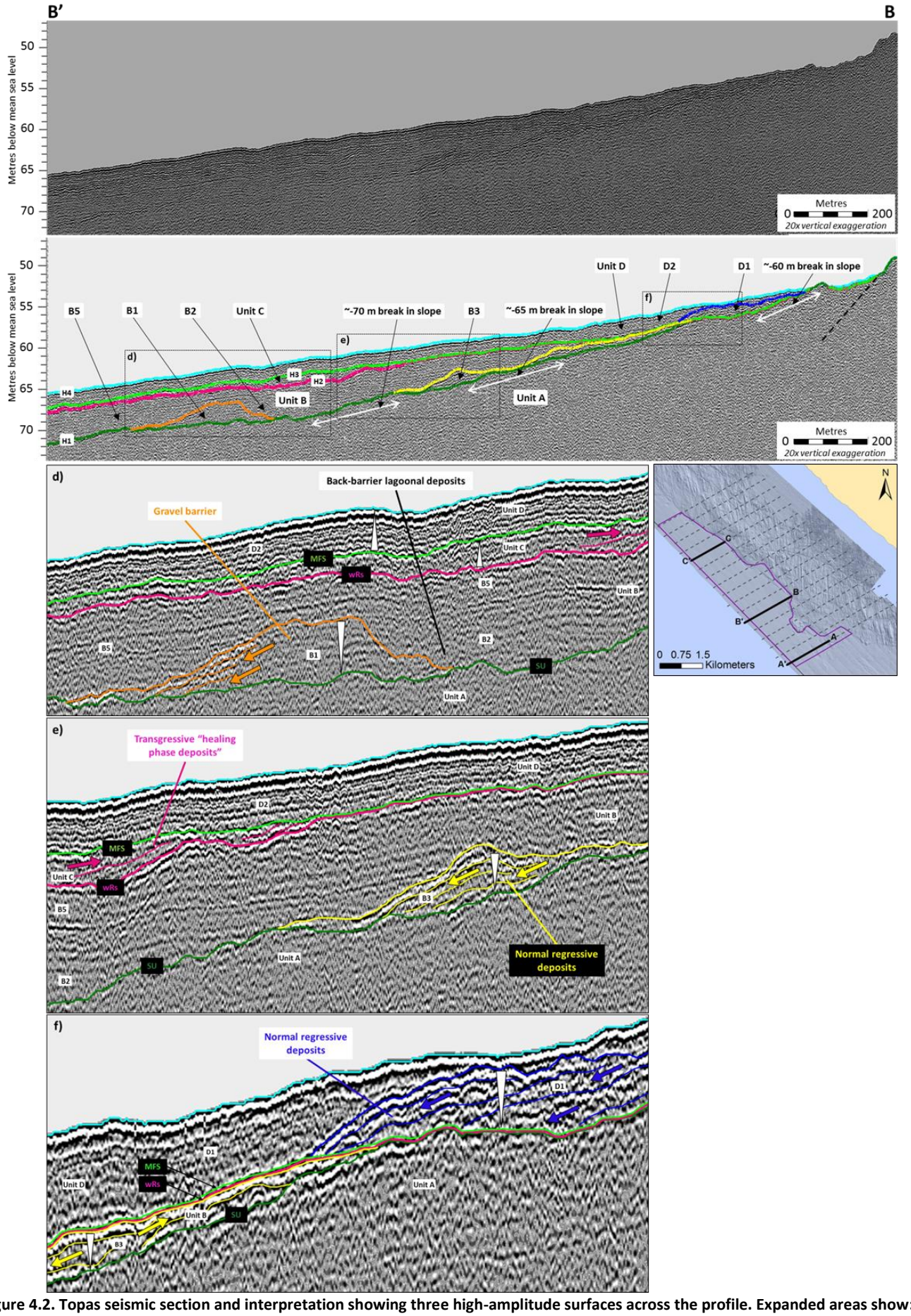

Figure 4.2. Topas seismic section and interpretation showing three high-amplitude surfaces across the profile. Expanded areas show: d) Unit C bound by H2 (wave-ravinement surface, wRs) and H3 (maximum flooding surface, MFS) at its base and surface, respectively; e) Unit C comprising low-medium-amplitude reflectors onlappping H2 toward the onshore. Sub-unit B3s preservation becomes more apparent in an offshore direction; f) Sub-unit D1 is only traced northward of the silcrete headland and exhibits high-amplitude prograding tangential oblique reflectors that downlap H3. Note the white arrows showing the approximate width of the H1 breaks in slope.

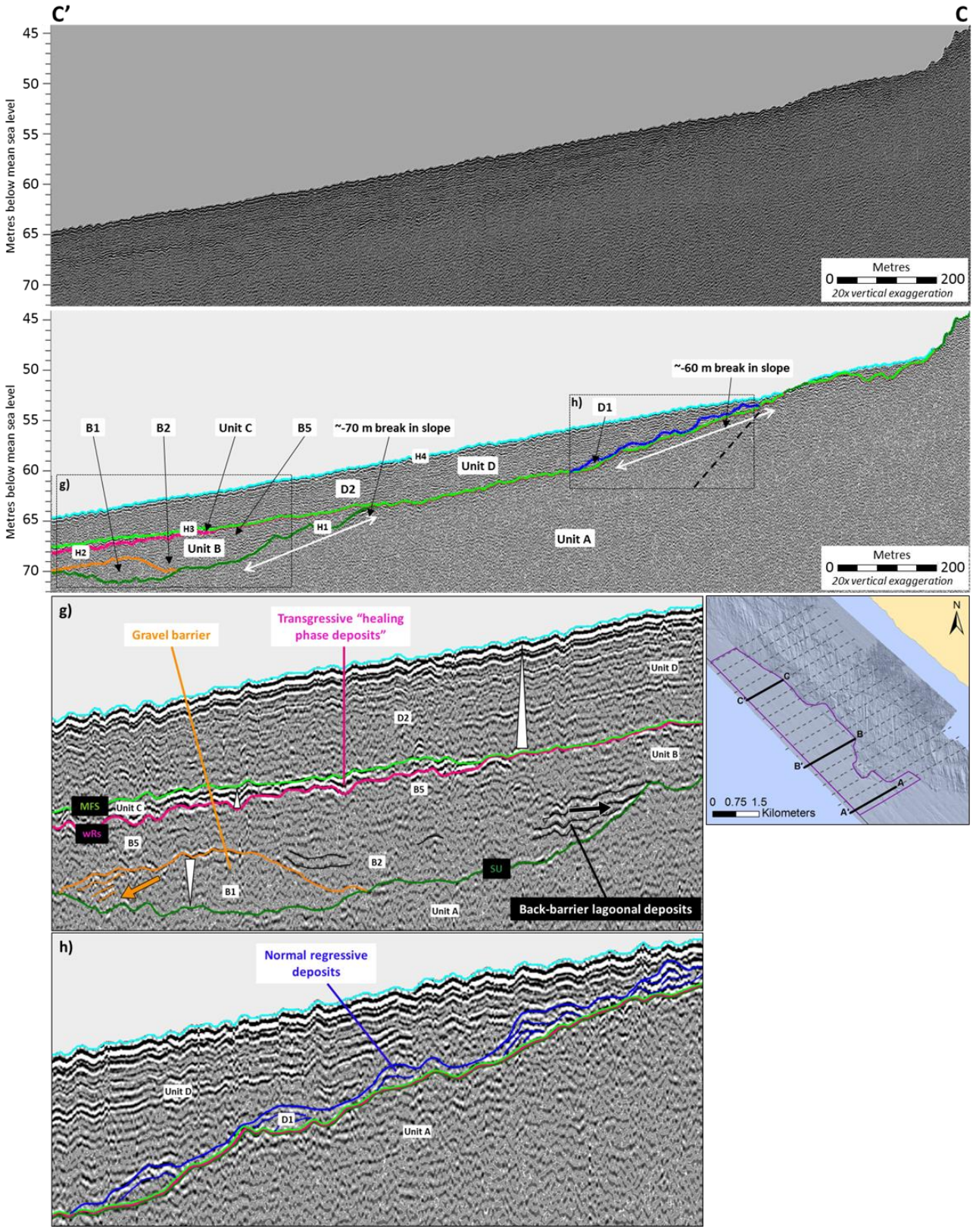

Figure 4.3. Topas seismic section and interpretation showing three high-amplitude surfaces stratigraphically lower within the profile. Expanded areas show: g) The surface horizon (H3) and basal horizon (H2), encompassing unit C, amalgamate to form one discernible surface toward the proximal portion of the basin; h) Sub-unit D1 progressively thins in a northward direction to beyond the seismic resolution of the dataset. Note the white arrows showing the approximate width of the H1 breaks in slope.

Table 4.1. Seismic stratigraphy describing internal reflector configuration, bounding surface relationships and interpretation of seismic units.

Unit	Sub-unit	Horizon	Reflection Configuration	Reflection Continuity	Reflection Amplitude	Stratal characteristics	Interpreted Depositional Environment	Thickness
		H4				Continuous, high-amplitude basin wide horizon	Present seafloor	
D	D2		Sub-parallel to divergent	Continuous to semi-continous	Low-amplitude	Low-amplitude sub-parallel to divergent reflectors that exhibit an aggradation stacking pattern, separated from the underlying unit C by H3 and truncated at the surface by H4.	Sediment wedge	≤4 m
	D1		Tangential oblique	Continuous	High-amplitude	Continuous high-amplitude, prograding tangential oblique reflectors that downlap H3.	Foreshore gravel beach	≤2 m
		H3				Medium- to high-amplitude bounding horizon	Maximum flooding surface	
C			Convex up	Semi-continuous	Low- to medium-amplitude	Convex up low- to medium-amplitude semi-continuous reflectors onlapping H2 toward the onshore and capped by H3.	Transgressive "healing phase deposits"	≤2 m
		H2				Medium- to high-amplitude bounding horizon	Wave-ravinement surface	
B	B5		Parallel to sub-parallel	Continuous	Low-amplitude	Semi-continuous sub-parallel to parallel oblique reflectors aggradationally stacked above B1 and B2 toward the distal portion of the basin and onlaps B3 toward the proximal portion.	Sediment wedge	≤4.5 m
	B4		Sub-parallel	Discontinuous	Low- to medium-amplitude	Discontinous, low to medium-amplitude reflectors aggradationally stacked above unit A.	Foreshore gravel beach	≤1.5 m
	B3		Parallel to sub-parallel toward the onshore and tangential-oblique toward the offshore	Continuous	Low- to high-amplitude	Low amplitude, sub-parallel to parallel retrogradational to weakly aggradational reflectors toward the onshore that onlap and downlap the underlying H1. Continuous, medium- to high-amplitude progradational reflectors that downlap the H1 surface.	Foreshore gravel beach	≤2 m
	B2		Parallel to sub-parallel	Discontinuous	Medium-amplitude	Laterally discontinuous medium-amplitude reflectors that onlap B1 in a seaward direction and B3 in a landward direction. Where B3 is not developed, B2 reflectors directly onlap H1.	Back-barrier lagoonal deposits	≤1 m
	B1		Parallel to tangential oblique	Semi-contiuous to continuous	Low- to high-amplitude	Low-amplitude aggradational reflectors toward the onshore and high-amplitude prograding to tangential oblique reflectors that downlap H1 toward the offshore.	Gravel barrier beach	≤4 m
		H1				Continuous, high-amplitude basin wide horizon	Subaerial unconformity	
A						Acoustically impenetrable	Acoustic basement	N/A

4.1 Unit A

4.1.1 Observations

4.1.1.1 Seismic Stratigraphy

Unit A represents the lowermost unit in the PTA and forms the acoustic basement (**Figures 4.1 – 4.3; Table 4.1**). Unit A is identified on all the seismic profiles; however, no prominent seismic features have been observed within it.

Horizon 1 (H1) can be traced as a prominent surface capping unit A. H1 is highly irregular horizon forming gullies, pinnacles and ridges across the southern outcropping headland (**Figures 4.1, 4.5 and 4.6**). Mapping of H1 indicates a seaward dipping slope (~0.4 – 0.6°) that shallows to <0.25° at the offshore edge of the study area (**Figures 4.1 – 4.3 and 4.7**).

4.1.1.2 Lithostratigraphy

Unit A consists of Precambrian basement rock, Albian – Cenomanian (Cretaceous) formation and a thin silcrete (~0.15 m) that caps the Cretaceous succession. The crystalline basement rocks, varying from fresh to weathered, comprise Neoproterozoic schists, phyllites and saprolites. An abrupt change in facies to the Middle Albian/Lower Cenomanian (112 – 90 Ma) strata offshore, achieved through ground-truthing of geophysical data (Stevenson, 1999; Stevenson and McMillan, 2004), is easily identified during sampling. The Cretaceous succession comprises a mixture of unconsolidated white angular vein quartz rubble, hard subangular-subrounded vein quartz bearing conglomerate, white friable to very porous quartzose sandstones and white to grey-green hued non-marine kaolinitic clays (**Figure 4.4;** Stevenson and McMillan, 2004)**.** A yellow-cream to pale grey hard silcrete caprock is restricted to the Cretaceous succession. The silcrete varies from a fine-grained clay matrix through to silicified conglomerates containing angular vein quartz clasts in a fine-grained, classic type silcrete matrix (**Figure 4.4**; Pether and Williamson, 2016). The dominantly vein quartz clast content and texture of the silcrete reflects the host Cretaceous deposits. Like the Cretaceous formations, the prominent pale grey silcretes are associated with advanced kaolinitic weathering.

Figure 4.4. Samples of the major footwall encountered in the PTA: 1) Precambrian schist, 2) Cretaceous vein quartz rubble, 3) Cretaceous conglomerate, 4) Cretaceous clay, 5) Cretaceous sandstone and 6) classic type of silcrete footwall. Scale represents 15 cm.

The Precambrian rocks are exposed in the landward portions of the PTA with the majority of unit A comprising Cretaceous deposits (**Figure 4.5**). The best exposure of the silcrete caprock is toward the inshore of the Cretaceous strata in the south of PTA where it forms a prominent headland that straddles a water depth of 50 – 65 m bmsl (**Figure 4.5**). The silcrete is more resistant than the surrounding Cretaceous strata and therefore erodes to form positive relief features. These acoustically reflective ridges crop out at roughly 58 – 68 m bmsl (**Figure 4.1**).

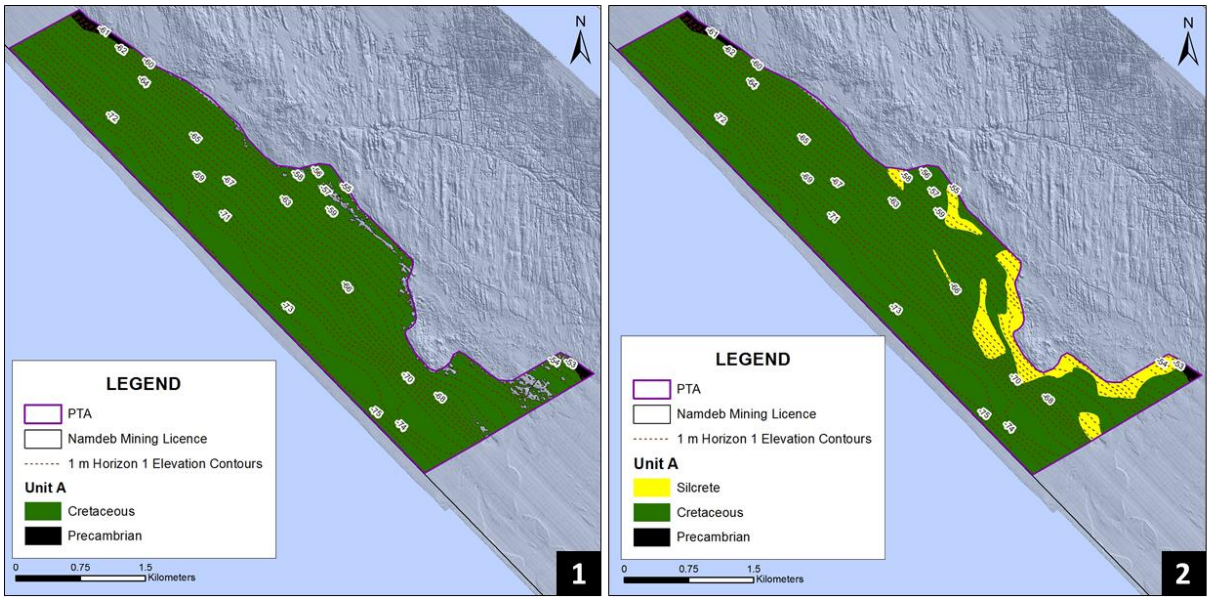

Figure 4.5. Sampling data, sub-bottom and surface geophysical data combined to generate 1) Precambrian bedrock vs. Cretaceous footwall map and 2) Precambrian bedrock vs. Cretaceous and silcrete caprock footwall map.

4.1.2 Interpretation

Based on seismic reflection geometries and lithological data, the Albian-Cenomanian succession (Cretaceous) has been interpreted as an aggradational fluvial system building upwards and outwards of the Precambrian bedrock (Stevenson, 1999; Stevenson and McMillan, 2004). The silcrete deposits are interpreted as equal or younger age, only discernible from its host Cretaceous deposits through borehole data. Wave erosion along the exposed silcrete headland, combined with the silcretes resistance to weathering, has resulted in gullies and ridges (Davis and Fitzgerald, 2004). The precise contact between the Precambrian and Cretaceous/silcrete deposits (black dashed line in **Figures 4.1 – 4.3**) is interpreted and based on sampling data due to the limited resolution of the seismic datasets.

Based on the surface geophysical dataset, the outcropping exposures of Precambrian bedrock (water depth of 20 – 55 m bmsl) are rugged, consisting of a series of parallel ridges and gullies with a prominent strike close to 0° (**Figure 4.6**). The flat, even-toned appearance on the bathymetry and the low-amplitude, light texture on the side scan sonar image, also with the same noticeable trends, correspond to low-lying areas between the ridges, and are interpreted as sediment–filled gullies (**Figure 4.6**). On a regional scale, the presence of the outcropping Cretaceous deposits is noted by a darker/coarser texture in the side scan sonar image and a shaded relief image of the bathymetry data in the same position shows that the topography is "pitted" and uneven.

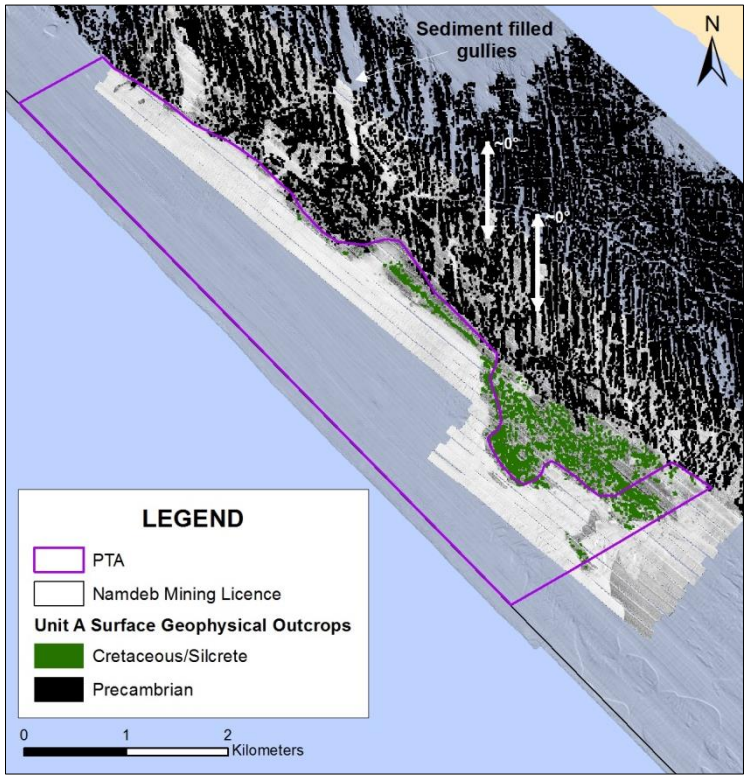

Figure 4.6. Surface geological map generated using mainly the bathymetry and to a lesser degree supported by the side scan sonar.

4.1.2.1 Horizon 1 (H1)

The lowermost boundary, horizon 1 (H1), is interpreted as a subaerial unconformity capping Unit A (**Appendix B**). H1 is interpreted as a regional sequence boundary. **Figure 4.7** shows the elevation of the interpreted seismic surface, H1. The subaerial unconformity, H1, is interpreted as part of a FSST, which formed during a shallow marine erosional event associated with the Late Cretaceous/Early Cainozoic uplift and possibly the Oligocene forced regression (**Chapter 2**; **Appendix A**). The upper Cretaceous sediments on the inner continental shelf were subsequently eroded during the Pleistocene by numerous oscillations in relative sea-levels (RSL; Compton *et al.,* 2002).

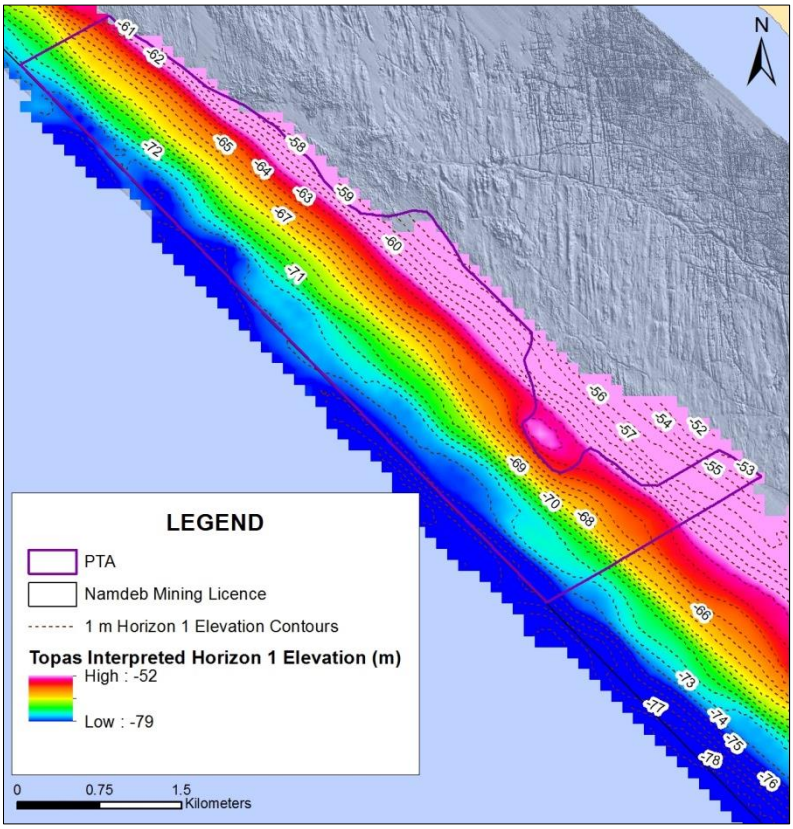

Figure 4.7. 1 m elevation map of Horizon 1 generated through Topas seismic interpretation. The warm colours represent bedrock highs and the cool colours bedrock lows, with relative water depths ranging from ~52 m bmsl to ~79 m bmsl for the onshore and offshore of the interpreted Topas seismic dataset, respectively.

<u>H1 cliff lines</u>

Through seismic interpretation, four breaks in slope are identified on H1: three minor breaks at approximately 59 – 61 (~1.50°), 64 – 66 (~1.55°) and 73 – 76 m bmsl (~1.20°), and a primary break traced across the entire length of the PTA at roughly 68 – 71 m bmsl (~1.70°; **Figure 4.8**).

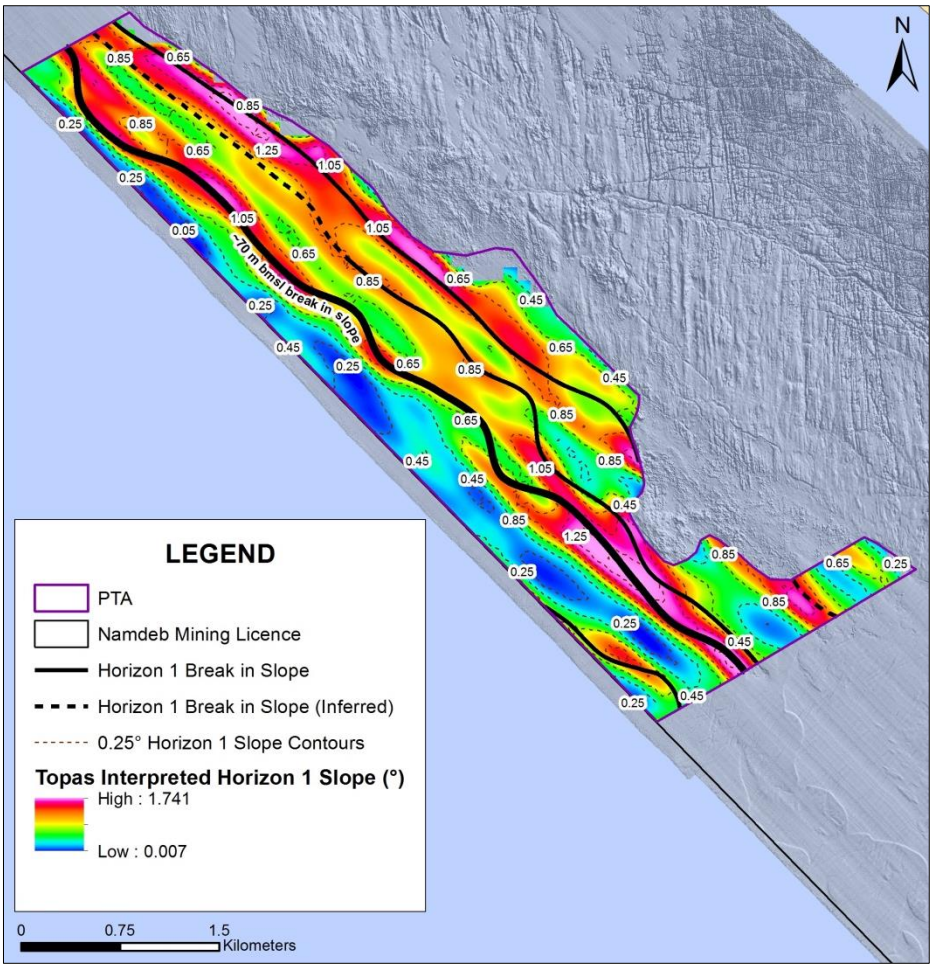

Figure 4.8. Aerial image showing the minor (~60, ~65 and ~75 m bmsl) and primary (~70 m bmsl) breaks in slope on Horizon 1 digitised using the interpreted Topas seismic data. The warm and cool colours represent steeper and shallower breaks in slope, respectively.

These breaks in slope are interpreted as palaeo-cliff lines that mark the most seaward extend of a shoreline during rapid RSL rise and ensuing transgression to form a wave-cut platform (**Figures 4.1 – 4.3**; **Appendix A**; Jacob, 2001; Zecchin *et al.,* 2011; Schulmeister, 2016). Based on onshore wave-cut platforms in MA1, the extent of the platform is not easily identifiable due to the irregular nature of its surface; therefore a cliff or break in slope toward its landward edge assists with determining its extent (**Figure 4.9;** Murray *et al.,* 1970).

The lateral variability in preservation of cliff lines during rapid RSL rise and ensuing transgression depends on factors such as bedrock composition, wave energy, local physiography, bathymetry and, rates of RSL rise and sediment input (Zecchin, 2007; Zecchin *et al.,* 2011). The onshore cliff lines generally trend in a northwest direction and parallel to the coastline, controlled by the direction of foliation and jointing of the Precambrian bedrock (Murray *et al.,* 1970; Jacob, 2001). The highest wave energy experienced on a wave-cut platform is toward its seaward extent, breaker zone, where waves carrying abrasive clastic material break and induce the deepest incision (**Figure 4.9**; Jacob, 2001). The wave-cut platforms within the PTA are better preserved due to the soft nature of the

underlying Cretaceous footwall, which was more susceptible to erosion by wave action during transgression (when the RSL rapidly rose).

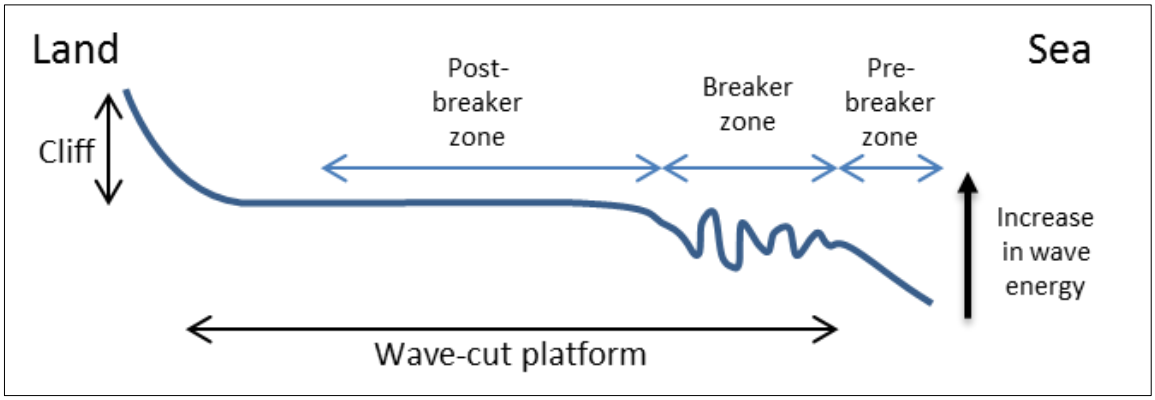

Figure 4.9. Bedrock/footwall topography formed on the wave-cut platform during transgression where the wave base incises the basal strata as the RSL rises rapidly and the shoreline advances landward (adapted from Jacob, 2001).

4.2 Seismically Undefined Basal Deposits

The deposits documented within the PTA are not always preserved laterally across the study area and thus the stratigraphy is fragmented (Spaggiari, 2011). This inconsistent preservation is partly promoted by the precursor topography controlling deposition, post-depositional geomorphological processes and, more significantly, RSL fluctuations partially or completely removing earlier deposits (Pether, 1994; Spaggiari, 2011). Five poorly preserved facies have been defined, unconformably overlying H1, based exclusively on borehole data (**Appendix B**).

4.2.1 Observations

4.2.1.1 Seismic Stratigraphy

The five basal deposits, limited to small wedges (<0.5 m), are too thin to be seismically defined and are therefore completely absent in the seismic sections.

4.2.1.2 Lithostratigraphy

Basal_Sandstone 1 (SST1)

Basal_SST1 unconformably overlies unit A and represents the oldest sandstone in the PTA. *In situ* Basal_SST1, <0.2 m thick, is documented in <3 % of the ±500 boreholes drilled in the PTA, commonly observed toward the proximal portion of the basin and within the vicinity of the headland (**Figure 4.5**; Pether and Williamson, 2016). It is supported by the presence of fresh sandstone chips on the observation screen, a lack of tool penetration and high tool force during drilling. Basal_SST1 is predominantly observed as sub-angular to rounded cobble sized clasts and broken angular clasts within the younger overlying units. It is dominated by hard, well-lithified reworked yellow-brown to dark brown medium sandstone and analogous mudstones, siltstones and conglomerates. The

sandstone comprises well-sorted, fine-grained sands either laminated or massive as well as “cherty” mud interbeds and laminae (**Figure 4.10**). Coarse shelly sandstone and minor amounts of sandstone clasts, bored by marine organisms with supporting carbonate cement, are observed; however, a coarser matrix of well-sorted felspathic sands is also present. Some clasts comprise small-pebble paraconglomerates dominated by quartz, quartzite and zeolites with minor amounts of Orange River Suite (ORS) exotics (e.g. agates and jaspers) in a matrix of muddy sand. Although the majority of the sandstone samples are structureless, there are some clasts exhibiting ripple and planar laminations, and burrow trace fossils. Fossil shells are mainly dissolved away and represented by moulds, other than pieces of thick-shelled, calcitic oysters (Pether and Williamson, 2014; 2016).

Figure 4.10. Slabby laminated, massive and paraconglomeritic Basal_SST1 samples.

Basal_Gravel (GVL)

Only 5 % of the ±500 boreholes drilled in the PTA intersected the ~0.5 m thick Basal_GVL layer laterally preserved in a semi-continuous coast-parallel direction in water depths between 55 and 65 m bmsl. Approximately 25 % of the boreholes intersecting Basal_GVL toward the base correlated with the ~70 m bmsl break in slope (**Figure 4.8**). The marine gravels within the PTA have a composition of, in order of predominance: quartzite, Cretaceous vein quartz, limestone, schist, granite, mafic and felsic volcanic rocks (Jacob, 2005; Spaggiari, 2011). Boulder sized fractions are only associated with quartzite and the remaining facies is confined to smaller fractions. The brown hued Basal_GVL comprises sub-rounded to rounded discs and blades of ORS derived material, high proportions of angular to sub-rounded small cobble up to boulder sized clasts of Basal_SST1 with varying amounts of local angular Cretaceous and silcrete footwall. Minor amounts of ORS exotics:

jasper, agates, banded ironstone and trace amounts of riebeckite and Makwassie porphyry are observed (**Figure 4.11**).

Figure 4.11. Brown hued Basal_GVL deposits comprising reworked Basal_SST1, silcrete, Cretaceous footwall clasts and ORS derived material. Scale represents 15 cm.

Basal_Clay (CY)

The coarse-grained gravel (Basal_GVL) is overlain by a ~0.5 m thick compact grey to yellow-brown very fine-grained sand/mud facies (Basal_CY), intersected in approximately 5 % of the PTA boreholes drilled. Basal_CY is laterally preserved in a semi-continuous coast-parallel direction, within the vicinity of the outcropping silcrete, in water depths between 59 and 69 m bmsl. Approximately 25 % of the Basal_CY boreholes correlated with the ~70 m bmsl break in slope (**Figure 4.8**). The deposit is vaguely laminated and bioturbated (**Figure 4.12**). Trace amounts of skeletal carbonate, including benthic foraminifera, are recovered from Basal_CY (Pether, 2013). The fine facies show early diagenetic cementing features varying from the formation of hard nodular lumps to distinct cementing.

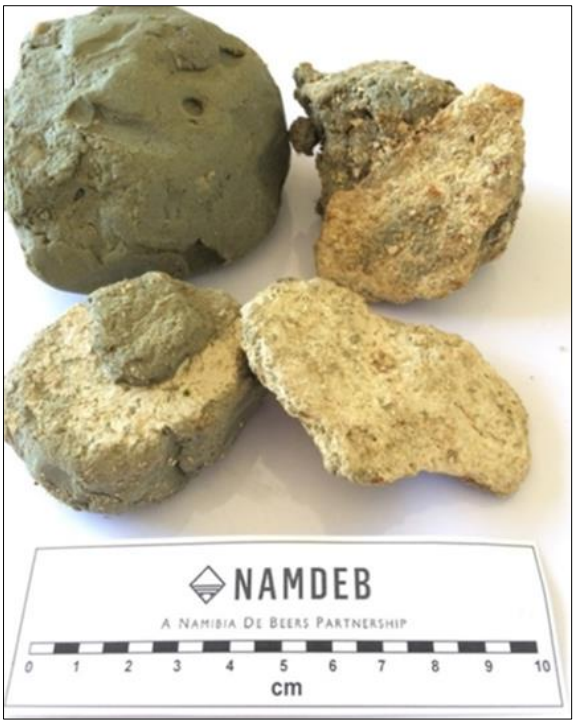

Figure 4.12. Basal_CY comprising mud/fine sand with immature calcrete layer associated with the clay.

Basal_Sandstone 2 (SST2)

The overlying marine sandstone, Basal_SST2, primarily occurs as broken clasts in overlying gravels and gravel-rubbles. *In situ* sandstone, ~0.2 m thick, is documented in <5% of the ±500 boreholes drilled in the PTA, primarily toward the northern section of the basin. The unit comprises angular to sub-rounded clasts of brown-grey, well-sorted medium-grained friable sandstones, coquinas comprising modern shells, coarse shelly sandstones and paraconglomerates comprising small pebbles of mainly Cretaceous vein quartz rubble, quartzite and ORS exotics, primarily zeolites, agates and jaspers (**Figure 4.13**). Modern day shells and black mussels, having retained some of their colour, are observed in the sandstone. The main distinguishing feature of Basal_SST2 is its friability; however, its competency does increase toward the Precambrian/Cretaceous contact (Pether and Williamson, 2016).

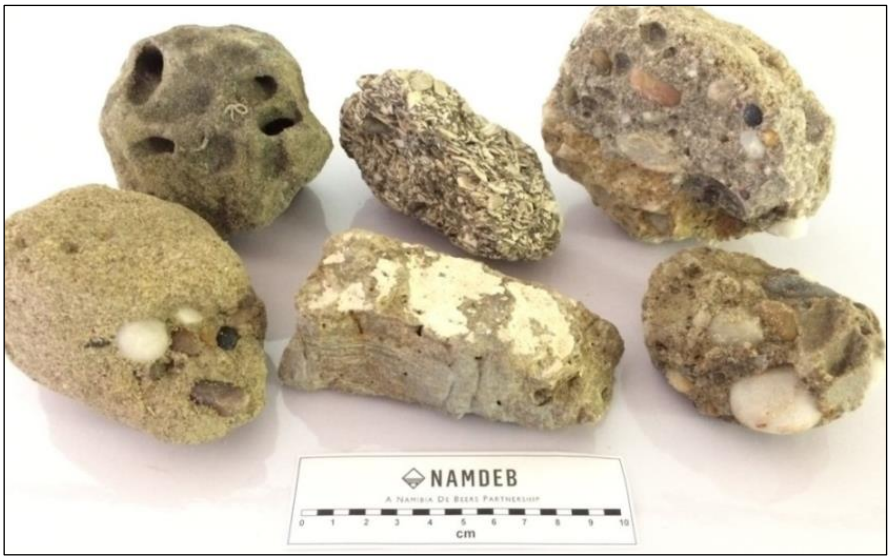

Figure 4.13. Various types of Basal_SST2 ranging from friable and bored to more hard and laminated. Scale represents 15 cm.

Basal_Sandstone 3 (SST3)

Overlying Basal_SST3 is a thin, <0.1 m, *in situ* hard sandstone encountered in only 2 of the ±500 boreholes drilled in the PTA. Basal_SST3 is observed within the vicinity of the silcrete headland between 54 and 60 m bmsl. The yellow-brown well-sorted medium sandstone, with scattered small pebbles, lacks any obvious marine introduction, i.e. bioturbation and skeletal carbonate (**Figure 4.14**).

Figure 4.14. Well-sorted Basal_SST3 deposit lacking marine introduction.

4.2.2 Interpretation

Basal_SST1

The poorly preserved Basal_SST1 deposits, based on sedimentary structures and fossil content, suggest deposition in a shallow shelf and shoreface depositional environment, under conditions of copious sandy sediment supply. Due to the thorough lithification of Basal_SST1, the remaining skeletal carbonate cannot be extracted. Notwithstanding, in addition to recognisable large *Ostrea* species, moulds of large, complete mussel shells can be identified as *Perna perna*. Moulds of a large *Mactra* and a large *Turritella* occur in the sandstones. However, these also occur as whole shells in the Quaternary deposits and have been reworked from the Early Miocene formation further offshore and similarly were reworked into the Basal_SST1. Moulds of the extant bivalve *Venerupis corrugata* are also present, but most shell moulds have ornaments in which familiar modern taxa are not recognisable. A pre-Quaternary age is indicated by the lack of modern taxa and the warm-water *Perna perna* and *Ostrea*. Overall, a Late Cainozoic age for Basal_SST1 is suggested, such as deposition during the Late Miocene or Mid-Pliocene regressions (**Figure 2.5**; Pether and Williamson, 2016).

Basal_GVL

The coarse-grained Basal_GVL facies overlying Basal_SST1 suggests deposition in an environment energetic enough to transport clasts of up to boulder size (Mellett *et al.,* 2012). The Basal_GVL could be remnants of foreshore beaches destroyed during storms or rapid RSL rise ensuing erosive transgressive processes as the shoreline advanced landward (Hallam, 1964). The presence of banded iron stone and riebeckite exotics in the Basal_GVL is indicative of Meso–Orange River inputs (Miller, 2008). The bulk of the marine gravel in the PTA is supplied by the ancestral Meso-Orange River and transported by the northerly longshore drift for a distance exceeding 300 km (Murray *et al.,* 1970; Bluck *et al.,* 2005; 2007). RSL fluctuations would have reworked older gravel bearing beaches that developed off the Orange River mouth back into the system as secondary deposits (Bluck *et al.,* 2005; Spaggiari, 2011).

Basal_CY

A shift in facies and depositional environment is observed above Basal_GVL by the presence of a directly overlying finer grained mud/sand deposit, Basal_CY. The fine-grained mud/sand facies were most likely deposited in a deeper shelf, low energy marine setting and the muddy nature suggests that at least parts of the facies were deposited at significant palaeo-depth (Pether and Williamson, 2016). Subaerial exposure and subsequent pedogenic alteration of Basal_CY is suggested by the

yellow-brown alteration of the facies and the presence of calcrete deposits (Pether and Williamson, 2016).

The preservation of Basal_GVL and Basal_CY in coast-parallel wedges can be attributed to factors such as footwall conditions (e.g. faults and footwall irregularities) and depositional settings (e.g. thick coarse clastic unit or sand unit deposited over the finer facies). Where Basal_GVL deposits were not protected by Basal_CY, the gravel facies were prone to erosional processes during subsequent RSL oscillations and feasibly broken down and incorporated into the younger overlying units, i.e. units A – D (Oelofsen, 2008).

Basal_SST2

A shallowing of the depositional environment is interpreted above the finer facies of Basal_CY, where poorly preserved friable sandstone (Basal_SST2) is observed. Based on its sedimentary structures and fossil content, the interpreted depositional environment of Basal_SST2, like Basal_SST1, was a shallow shelf and shoreface setting. An increase in competency of Basal_SST2 toward the Cretaceous/Precambrian contact could be a result of more advanced cementation along the proximal basin, possibly controlled through groundwater flows off the Precambrian bedrock (Pether and Williamson, 2016). Basal_SST2 deposits not cemented by meteoric groundwater would have been introduced into the younger overlying units as rubble during erosion.

Basal_SST3

The lack of marine introduction in the poorly preserved overlying Basal_SST3 suggests an aeolianite, where regressive conditions allowed terrestrial environments to superimpose themselves upon shallow shelf and shoreface deposits, i.e. Basal_SST2. Deflation events experienced in the Namib would have removed upper shoreface and beach deposits of Basal_SST2 and transformed the marine sands in the intertidal zones into aeolian dunes. Thick sequences of cemented aeolianites are more prone to occur in palaeo-drainage areas such as Bogenfels (sub-Langental) and Channel (Kaukasib) to the north of the study area, where the sediments are subjected to cementing in meteoric groundwaters. Minor preservation of the aeolian environment on the shelf suggests that the majority of the aeolian sands were blown further onshore, eroded away or possibly reworked into the shelf sands (Pether and Williamson, 2016).

The poorly preserved basal deposits described above are overlain by sediments of units B, C and D.

4.3 Unit B

4.3.1 Observations

4.3.1.1 Seismic Stratigraphy

Unit B forms a ~6 m landward pinching sedimentary wedge that progressively thins in a northward direction to <3 m. Unit B unconformably overlies unit A and is truncated by a medium to high-amplitude surface, H2. Within unit B, five sub-units (B1 to B5) are defined (**Figure 4.1**; **Appendix B**).

Sub-unit B1

Sub-unit B1 unconformably overlies unit A and is separated from unit A by a high-amplitude basin wide erosional surface, H1. The overall geometry of sub-unit B1 is asymmetric and elongated in nature. Sub-unit B1 has a maximum thickness of 3.5 m in the south and thins in a northward direction where it also flattens out to <1 m thick. Sub-unit B1 forms a feature parallel to the shoreline that straddles a water depth of 71 – 75 m bmsl and can be traced lengthwise across the entire target area (approximately 7 km; **Figure 4.15**). It comprises varying reflector configurations in the proximal and distal portions of the feature, relative to the coastline (**Figures 4.1(a), 4.2(d) and 4.3(g)**). The proximal portion of sub-unit B1 occurs as an aggradational succession of semi-continuous, parallel low-amplitude reflectors that increase in amplitude seaward (**Figure 4.1(a)**). The distal section comprises continuous high-amplitude prograding tangential oblique reflectors. The package has a common downlapping reflector configuration onto the H1 surface.

Sub-unit B1 has its upper boundary at a low relief, medium to high-amplitude surface (H2) that truncates the sub-unit in the northern portions of the basin.

Sub-unit B2

Despite not being clearly imaged in the high-resolution seismic data, sub-unit B2 displays a series of parallel to sub-parallel laterally discontinuous medium-amplitude reflectors that onlap sub-unit B1 in a seaward direction and sub-unit B3 in a landward direction (**Figures 4.1(a) and 4.2(d)**). Where sub-unit B3 is not developed, sub-unit B2 reflectors directly onlaps the basement subaerial unconformity (H1; **Figure 4.3(g)**).

Sub-unit B2 has its upper boundary at a low relief, medium to high-amplitude surface (H2) that truncates the sub-unit in the northern portions of the basin.

Sub-unit B3

Sub-unit B3 shares similar internal reflector architecture to that of the seaward sub-unit B1. Sub-unit B3 occurs as a shoreline parallel feature, landward of the sub-unit B2 deposits (**Figures 4.1 and 4.2**), between water depths of 61 and 71 m bmsl (**Figure 4.15**). Sub-unit B3 thickens offshore, increasing from ~1 m to a maximum thickness of 2 m (**Figure 4.1(b)**). It is well developed through much of the southern portions of the PTA, mapped along strike for ~4 km where it unconformably overlies H1. Sub-unit B3, in the most southern section of the PTA (**Figure 4.1(b)**), occurs as a discontinuous succession segregated into two packages by a local outcropping silcrete (unit A) pinnacle. Seaward of the outcropping pinnacle, sub-unit B3 dips steeply offshore and straddles the primary ~70 m bmsl H1 break in slope, whereas the sub-unit tends to flatten landward where a significantly more gentle profile is observed (**Figures 4.1(b) and 4.15**). The landward section comprises low-amplitude, sub-parallel to parallel retrogradational to weakly aggradational reflectors that onlap and downlap the underlying high-amplitude H1 surface toward the onshore and offshore, respectively. The offshore section comprises continuous, medium- to high-amplitude, tangential oblique (progradational) reflectors that downlap the H1 surface. The northward transition of sub-unit B3 is not clear. Immediately southward of seismic line C – C' it occurs as a thin succession (0.5 m thick) characterised by low-amplitude sub-parallel aggradational reflectors.

Sub-unit B3 has its upper boundary at a low relief, medium to high-amplitude surface (H2) that truncates the sub-unit at the landward portions of the basin (**Figures 4.1 – 4.3**). The preservation and thickness of sub-unit B3 is therefore limited by the overlying surface, H2.

Sub-unit B4

Sub-unit B4 is laterally discontinuous and restricted to one seismic line (A – A'; **Figures 4.1 and 4.15**) in the southern portion of the basin within a water depth of 59 – 63 m bmsl. Sub-unit B4 occurs as a discontinuous succession segregated into two packages by outcropping silcrete (unit A) pinnacles. This sub-unit comprises a succession of low to medium-amplitude sub-parallel reflectors aggradationally stacked above unit A. The unit preferentially accumulates as a thicker deposit (≤1.5 m) on the landward flanks of the silcrete pinnacles, where it aggradationally onlaps the pinnacle.

Sub-unit B4 has its upper boundary at a low relief, medium to high-amplitude surface (H2) that truncates the seismic sub-unit.

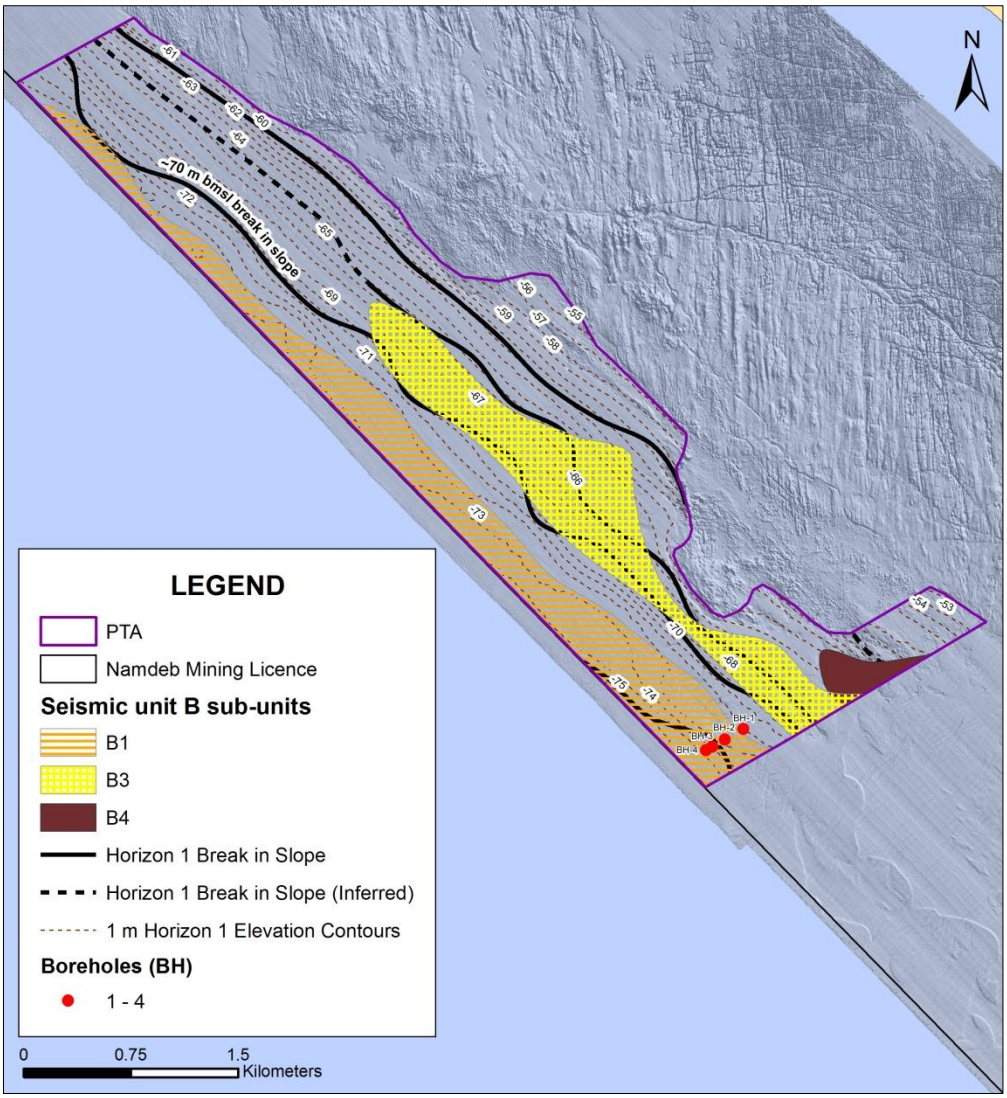

Figure 4.15. Spatial distribution of interpreted seismic sub-units of seismic unit B: B1, B3 and B4. Sub-unit B1 has the most widespread areal distribution, covering the entire offshore extent of the PTA. Sub-unit B2 is spatially located between the seaward positioned sub-unit B1 and landward positioned sub-unit B3. Sub-unit B3 is primarily observed within the vicinity of the silcrete headland and trending parallel to sub-unit B1. Sub-unit B4 is observed in only one seismic line, A – A', in the southern portion of the PTA. Borehole locations indicated for positioning of stratigraphic logs (refer to Figures 4.17 and 4.18).

Sub-unit B5

Sub-unit B5 forms a landward pinching sediment wedge of continuous low-amplitude parallel to sub-parallel reflectors that exhibit an aggradation stacking pattern. Sub-unit B5 is seismically thick in the south of the PTA and thins northward, decreasing from 4.5 m to 1.5 m in thickness. Sub-unit B5 overlies sub-units B1 and B2 toward the distal portion of the basin and onlaps sub-unit B3 toward the proximal portion of the basin (**Figures 4.1 and 4.2**). Where sub-unit B3 deposits are not preserved, sub-unit B5 directly onlaps acoustic basement, Unit A (**Figure 4.3**).

The wedge has its upper boundary at a low relief, medium to high-amplitude surface, H2.

4.3.1.2 Lithostratigraphy

Sub-unit B1

The best development of the upward coarsening marine gravel, B1_GVL, is found south of the silcrete capped headland (**Figure 4.16**). B1_GVL can be divided into two competent gravel units, B1_GVL lower and B1_GVL upper, protecting a ≤ 2.8 m thick medium grey sand core (**Figure 4.17**).

B1_GVL lower (≤1 m) comprises up to triplex gravel layers each with their own defining characteristics (Pether and Williamson, 2016). A complete triplex sequence includes:

1. A basal gravel-rubble dominated by angular to sub-rounded clasts up to boulder size of Basal_SST1, Basal_GVL, minor amounts of reworked Basal_SST2 and varying quantities of reworked Cretaceous rocks (**Figure 4.18**; BH-2(7), BH-3(4) and BH-4(2)). The basal gravel-rubble is generally coarser with varying proportions of rounded ORS gravel (predominantly quartzite and limestone) and minor ORS exotic pebbles (predominantly jasper and agate).
2. The middle gravel-rubble generally comprises black to dark grey hued clasts of sub-angular to rounded large pebbles to boulders of ORS gravel with varying quantities of medium to large ORS exotic pebbles (predominantly jasper, agate, Makwassie porphyry with minor amounts of riebeckite, epidosite and zeolite). The predominating quartzite is commonly observed as well-rounded disc and sphere-shaped cobbles (**Figure 4.18**; BH-1(10) and BH-2(7)). Reworked Cretaceous and Basal_SST2 deposits are sporadically distributed throughout the middle unit. A colour variation between the greyer hued middle gravel-rubble in comparison to the browner hued basal gravel-rubble is an indicator used to separate the two gravel suites (**Figure 4.18**). The colour indicator is due to the middle layer comprising a much higher proportion of reworked Basal_SST2 material (grey hued) compared to the basal layer where reworked Basal_SST1 material (brown hued) predominates.
3. The thin upper layer comprises sub-rounded to rounded medium pebbles to large pebbles, verging on cobbles, of ORS gravel with varying quantities of small ORS exotic pebbles (predominantly jasper, agate and banded ironstone) mixed with shell debris.

B1_GVL upper (≤ 1.5 m) comprises a gravel armouring protecting the medium sand core. It comprises more mature, rounded pebble to large cobbles of mostly grey quartzite and limestone, Cretaceous vein quartz, coquina, lower proportions of reworked Basal_SST2 and a high proportion of ORS exotics frequently up to cobble size (jasper, agates, Makwassie porphyry and minor amounts of riebeckite; **Figure 4.18**; BH-2(5), BH-3(3) and BH-4(1)). Cross-beach variability of the surface B1_GVL (gravels classified according to different clast sizes and shapes; Spaggiari, 2011) are observed; the

crests of sub-unit B1 mostly comprise discs (**Figure 4.18**; BH-2(5)), whilst the offshore slope is dominated by rollers and spheres (**Figure 4.18**; BH-3(3) and BH-4(1)). B1_GVL and the medium to coarse sand core constitute the bulk of sub-unit B1.

Although the borehole data may display varying proportions of the sedimentary facies identified laterally across the sedimentary unit, the type section for sub-unit B1 is seismic profile A – A' (**Figures 4.1(a) and 4.16**). The B1_GVL armoured body and its sand core extend from ~73 to 68.5 m bmsl.

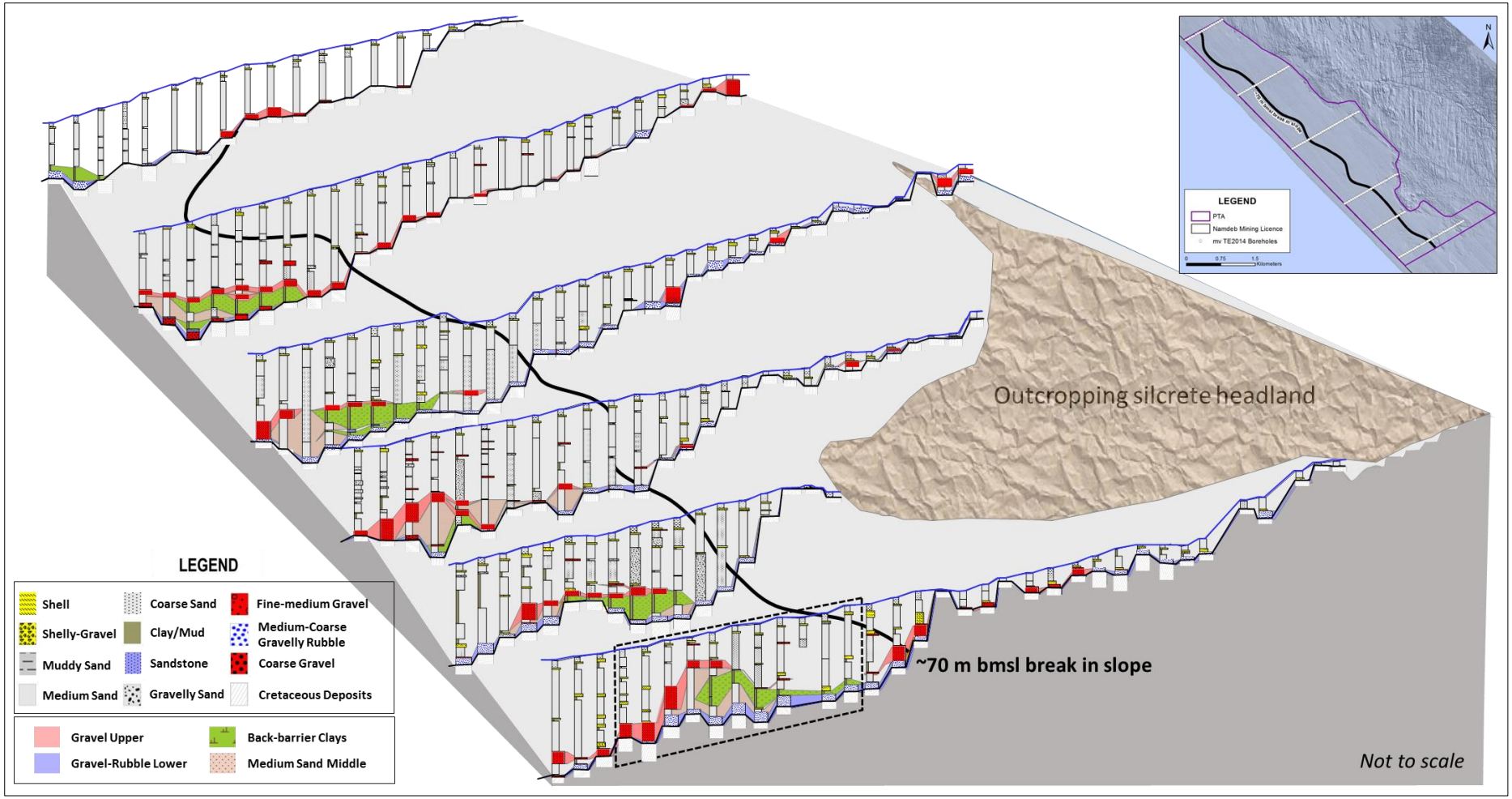

Figure 4.16. The preserved B1_GVL facies and its coeval B2_CY facies trend coast-parallel at elevations between 71 and 75 m bmsl, seaward of the primary ~70 m bmsl break in slope on horizon 1. The local footwall high in the northern distal portion of the basin is assumed to create a topographic obstacle, which forced sub-unit B1 to develop further offshore, outside the bounds of the Namdeb mining licence. Insert in black dashed box is displayed in Figure 4.17.

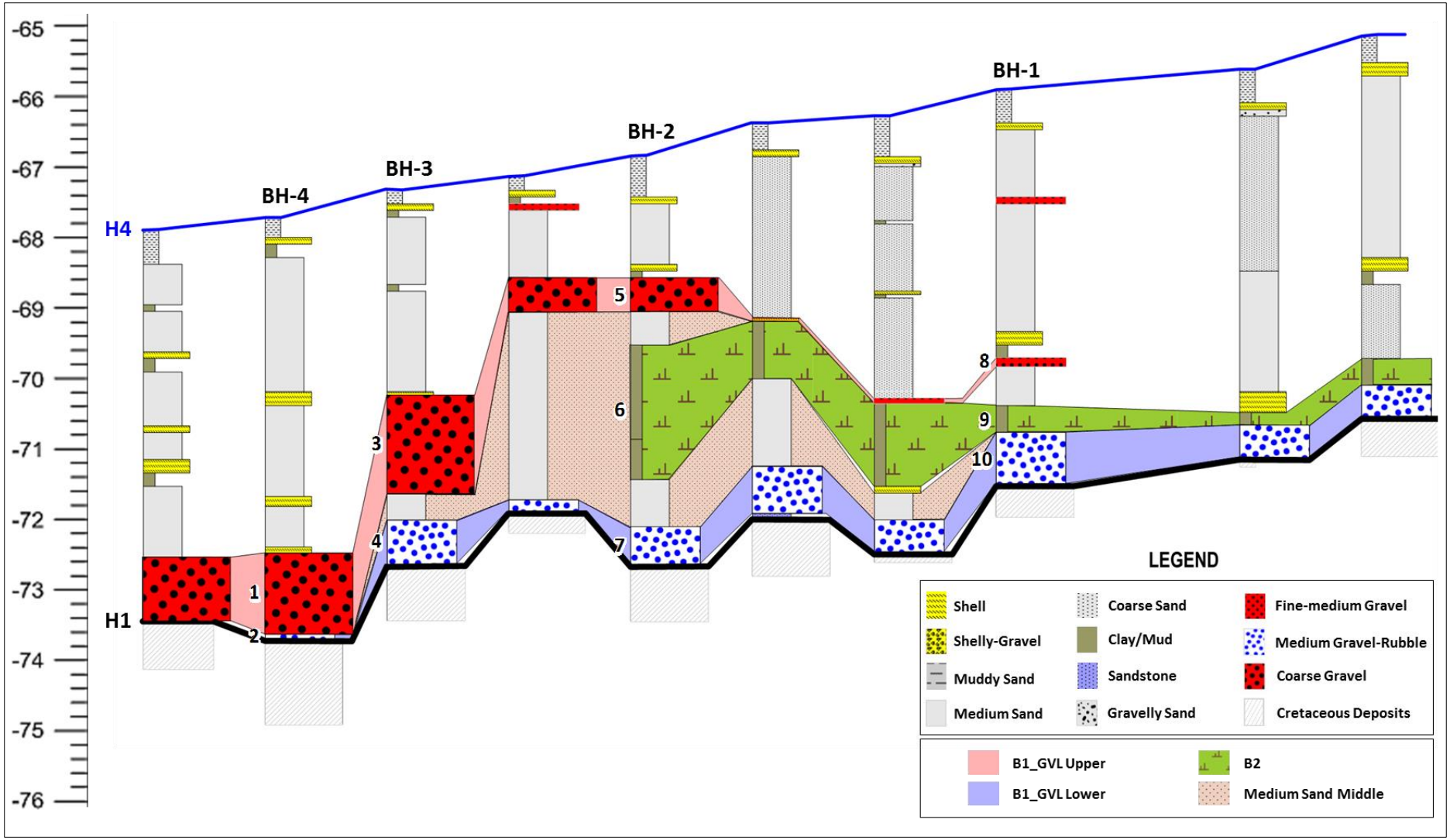

Figure 4.17. Strater© cross-section with corresponding borehole data, 50 m apart, highlighting sub-unit B1 comprising B1_GVL upper (red) and B1_GVL lower (blue) separated by a medium sand middle. B2_CY is located toward the landward side of sub-unit B1. Refer to Figures 4.15 and 4.16 for the positioning of the boreholes and geological samples correlating to the numerical values 1 to 10, respectively. BH = Borehole. Vertical scale is represented in m bmsl.

Figure 4.18. Four borehole samples selected to represent the change in facies across sub-unit B1. The proximally positioned borehole (BH-1) is dominated by fine-grained mud/clay facies, whereas in the distally positioned boreholes (BH-2, -3 and -4) clastic material, primarily sub-rounded to rounded Nama quartzite, limestone and Cretaceous footwall rubble predominate. Refer to Figure 4.15 for the positioning of the correlating geological samples. BH = Borehole. Scale represents 15 cm.

Sub-unit B2

Sub-unit B2 comprises only one lithological facies unit, B2_CY, which is unusually thinly-bedded to partly-laminated, comprising green-grey marine and brown-grey organic bearing muddy sand and mud/clay (**Figure 4.19**). Based on borehole samples only, sub-unit B2 trends parallel to the seaward sub-unit B1 and straddles a water depth of 68 – 74 m bmsl (**Figure 4.16**). The mud/clay ranging in thickness from 0.1 – 1 m landward, grades from sticky and soft at the top to firm and blocky toward the base. Laterally restrictive muddy sands interspersed with white calcareous laminae, beds of peaty material and wood fragments are intersected in the northern portion of the target area. The unit hosts abundant, tiny, corneous-brown mud snails *Assiminea* (cf. A. *globulus*), which is typical of lagoonal tidal flats, and tiny, pointed objects resembling fish teeth, but which on closer inspection proved to be the pointed ends of crustacean nippers, most probably of prawn origin (J. Pether, pers. comm., October 2017). Scattered juvenile black mussels and tiny turritellid *Protomella capensis* are also observed (Pether, 2016).

A thin string of gravel (<0.4 m) comprising well-rounded medium pebble to large cobble quartzites and Cretaceous vein quartz overlie B2_CY, decreasing in thickness and grain size in a landward direction (**Figures 4.17 and 4.18**; BH-1(8)).

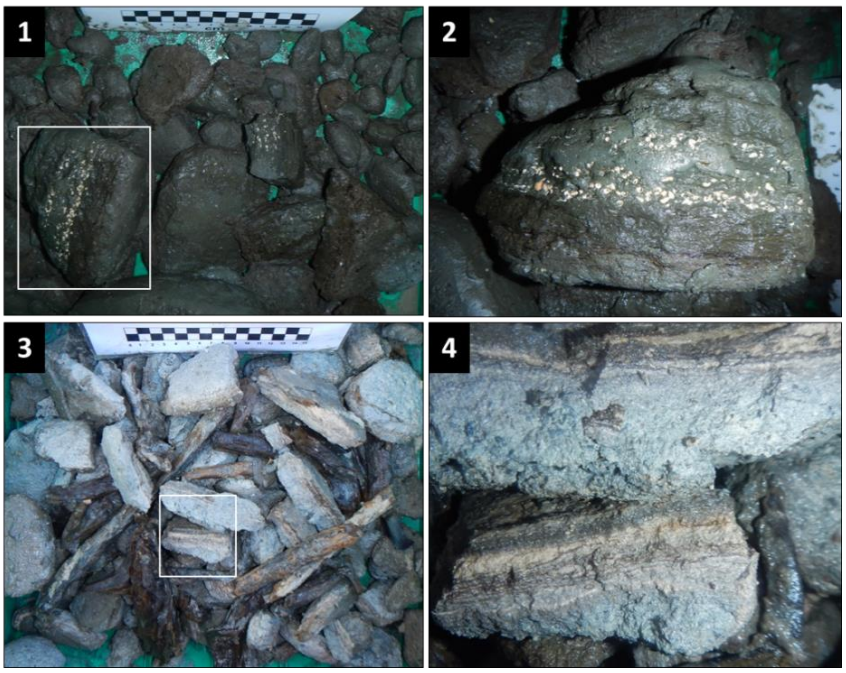

Figure 4.19. 1) B2_CY comprising green-grey marine and grey-brown organic bearing muddy sand and clay/mud. 2) Enlargement of (1) showing the gastropod layers within the dark facies. 3) B2_CY deposits hosting wood fragments, peaty material, shells and crustacean nippers. 4) Enlargement of (3) highlighting the laminations within the sand and clay/mud facies. Scale represents 15 cm.

Sub-unit B3

Sub-unit B3 is dominated by coarse rudaceous gravel, B3_GVL, where resistant clasts such as quartzite and quartz constitute the bulk of the ~2 m thick upward coarsening sub-unit. Similar to B1_GVL lower, in thicker B3_GVL sequences multiple layers of gravel and gravel-rubble can be discerned. The upper layer comprises large pebble to boulder sized black to grey hued clasts of predominantly quartzite, limestone, Cretaceous vein quartz and ORS exotic pebbles (jasper, agate, Makwassie porphyry with minor amounts of riebeckite, epidosite and zeolite; **Figure 4.20(1)**). The rubbliest layer preferably occurs at the base of the thick gravel sequences. The basal gravel-rubble is dominated by sub-angular clasts up to boulder size of Basal_SST1, moderate proportions of sub-angular Basal_SST2 and sub-rounded Basal_GVL cobbles with varying amounts of Cretaceous deposits and exotic pebbles (**Figure 4.20(2)**). A textural maturity in B3_GVL is observed where clast size and shape sorting is noticeable, but not to the same degree of sorting as observed in B1_GVL upper. Sphere and blade-shaped clasts predominate in the upper B3_GVL.

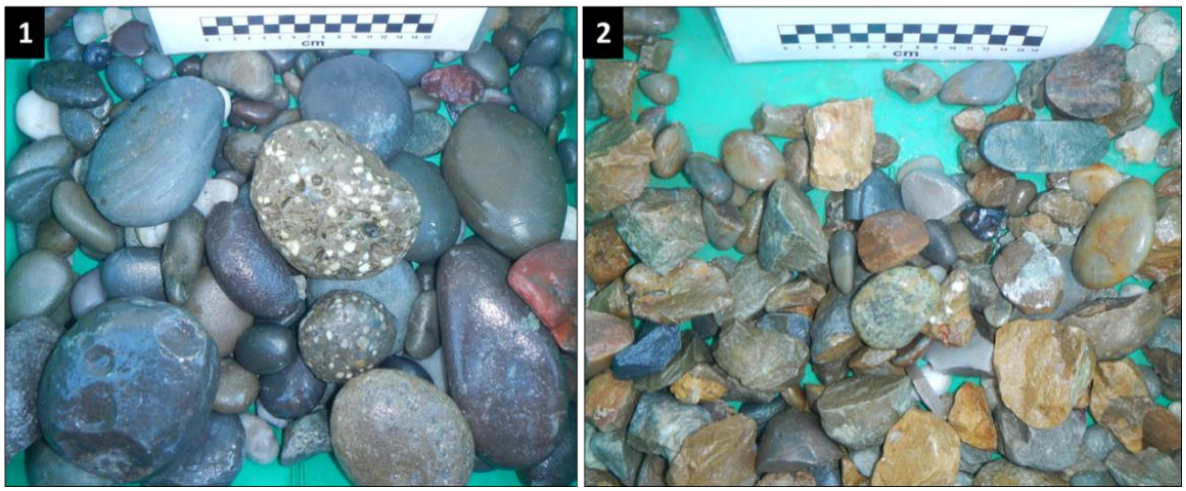

Figure 4.20. 1) Upper B3_GVL dominated by bladed grey quartzites and limestone clasts, reworked Basal_SST2 deposits and rounded small to large pebbles of ORS exotic clasts. 2) Lower B3_GVL dominated by angular Basal_SST1 with varying proportions of ORS gravels and exotics. Scale represents 15 cm.

Sub-unit B4

The bulk of sub-unit B4 comprises a thin (~1 m) layer of gravel material becoming rubblier with depth; comparable to the B3_GVL deposits. B4_GVL deposits show an aggradational to slight upward coarsening profile. The primary facies consists of angular to sub-rounded small pebble up to large cobble sized ORS suite clasts and ORS exotic pebbles: jaspers, agates and Makwassie porphyry. Increasing proportions of reworked Basal_SST1, Basal_SST2, Basal_GVL and Cretaceous deposits are observed toward the base of B4_GVL.

Sub-unit B5

Sub-unit B5 is composed of “birdseed” gravel fining upward into brown to green-brown medium-coarse marine sands, B5_SND. The “birdseed” gravel primarily comprises very well-rounded small pebbles of quartz, quartzite, footwall material and ORS exotics: zeolites, agates and jaspers (**Figure 4.21(1)**). The marine sand is mostly quartzo-feldspathic rich with lower proportions of mica, zeolite, lithic fragments and heavy minerals (Fowler, 1982; Spaggiari, 2011). Occasional lenses of green marine clay, black mussels and large pebble to small pebble gravel are observed within the sand wedge. The gravel comprises angular to sub-rounded quartzite, footwall material and occasional pebbles of rounded ORS exotics (**Figure 4.21(2)**).

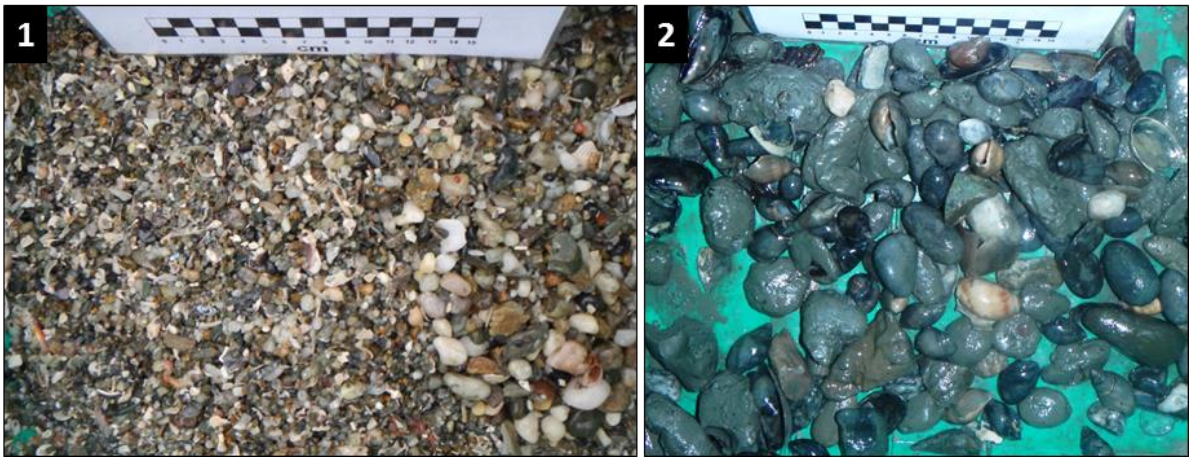

Figure 4.21. 1) “Birdseed” to small pebble gravel fractions observed within the medium to coarse sand in the southern portions of the PTA and 2) sporadic gravel, marine clay and black mussel stringers observed within the sand wedge. Scale represents 15 cm.

4.3.2 Interpretation

Sub-unit B1

Sub-unit B1 was developed through multiple gravel accumulations defined by the change in texture (grain size, sorting and clast shape) and colour of the clastic material with depth.

The B1_GVL lower deposit, comprising a poorly sorted assemblage, records different phases of gravel development, possibly with substantial time gaps between the phases (Bluck, 1999). The lower and middle gravel-rubble could be remnants of either storm deposits, foreshore beaches destroyed during storms or rapid RSL rise ensuing erosive transgressive processes as the shoreline advanced landward (Hallam, 1964). The upper gravel within B1_GVL lower, dominantly comprising spherical pebbles, is interpreted as storm deposits (Bluck, 1999).

The coarse-grained gravel facies, B1_GVL upper, is interpreted to exhibit characteristics of a prograding foreshore gravel beach (e.g. seaward-imbricated discs/blades consistent with the middle portion of the foreshore environment and spherical clasts of up to boulder size accumulated on the most seaward section of the foreshore; Bluck, 1999; Spaggiari, 2011; Mellet *et al.,* 2012). Extreme size and shape sorting of gravel is achieved through high energy wave turbulence and the turbulence generated when swash and backwash interact with large gravel clasts (Bluck, 1999). The presence of large cobbles and boulders provides not only a viable diamond trapsite, but also forms a gravel armouring protecting the gravel body from shallow marine reworking and erosional processes (Oelofsen, 2008).

The medium sand dominated core, protected by the overlying B1_GVL upper facies, is interpreted as a sandy foreshore deposit and possibly linked to the initiation of the barrier beach (Bluck, 1999; Spaggiari *et al.,* 2006).

Sub-unit B2

The presence of a rare laminated deposit with mudflat snails, crustacean remains and wood fragments within B1_CY suggests a marginal coastal environment with both marine and terrestrial deposition (Pether and Williamson, 2014). Sub-unit B2 is interpreted as a lagoonal complex that trends coast-perpendicular across the entire PTA and further southward, outside the bounds of the target area, and potentially further offshore (**Figures 4.1(a), 4.2(d), 4.3(g) and 4.16**).

The geometry and lithological composition of sub-unit B1 are characteristic of a prominent gravel armoured beach and only through its association with B2_CY, a preserved back-barrier lagoonal deposit, can it be classified as a deposit of a gravel barrier (Mellet *et al.,* 2012). A gravel barrier (l = 0 – 100 km+, w = 10 – 100 m+, h = 10 – 20 m) is defined as a landform that separates the open ocean from an enclosed lagoonal environment (Boggs, 2010). The main criterion for the initial development of a barrier beach is sufficient sediment supply to balance the rise in RSL and a wave-dominated coastal setting (Davis and Fitzgerald, 2004; Mellet *et al*., 2012). B1_CY is interpreted as the coeval fine facies developed landward of the coarse gravel sub-unit B1 beach. The poorly preserved peat and wood debris suggest a marsh environment, usually destroyed during a transgression (Compton *et al.,* 2002), that evolved into a lagoonal environment with prawns and mudflats, with further deepening and juxtaposition to the open coast supported by the presence of *Protomella* and marginal colonization by black mussels (Pether, 2016). The marsh environment formed due to rising RSL, succeeded by shallow

lagoon formation during ongoing flooding ahead of the transgression, then by a back-barrier environment landward of the barrier-beach (Pether, 2016).

During RSL rise the influence of strong waves on the barrier feature, sub-unit B1, results in sediment, including coarse clastic material, being transported into the lagoonal environment, sub-unit B2, to form a lobate or sheet-like shaped wash-over fan/delta (**Figures 4.17 and 4.18**; BH1(8); Walker and Noel, 1992; Mellet *et al.,* 2012). Most of the fine-grained clay/mud and marsh facies deposited in the back-barrier environment of sub-unit B2 must have been subsequently covered by the wash-over deposits that buried them and protected them from future erosive processes.

Sub-unit B3

The coarse-grained gravel facies, B3_GVL, is interpreted to exhibit characteristics of a prograding foreshore gravel beach.

Sub-unit B3 exhibits internal reflector patterns and lithological compositions similar to sub-unit B1 (Bluck, 1999; Spaggiari *et al.,* 2006; Spaggiari, 2011).

Although sub-units B3 and B1 comprise similar facies and preservation patterns, their morphology is dissimilar:

1. Sub-unit B3 is positioned landward and at a higher elevation in comparison to sub-unit B1 (**Figure 4.15**).
2. Sub-unit B3 lacks the landward coeval back-barrier facies observed in sub-unit B1, attributing it to a gravel barrier.
3. The sand core observed in sub-unit B1 is absent or poorly documented in sub-unit B3.
4. No distinctive cross-beach shape and size sorting pattern is recorded for sub-unit B3, and this could be attributed to either extensive reworking or high sediment input to prevent such sorting (Carter *et al.,* 1990; Spaggiari, 2011).

Sub-unit B3 is interpreted as a prograding gravel beach with high volumes of coarse sediment input from the alongshore or hinterland (Einsele, 1992; Spaggiari, 2011).

Sub-unit B4

The coarse-grained gravel facies, B4_GVL, making up sub-unit B4 represent remnants of a unit deposited in a high energy environment capable of transporting cobble sized clasts, such as a foreshore beach environment.

The dissimilarity in morphology observed between sub-units B1 and B2 described above is likewise observed between sub-units B3 and B4. No distinctive cross-beach shape sorting patterns (i.e. disc-shaped clasts are absent in the middle of the foreshore environment) are recorded for sub-unit B4 and are attributed to extensive reworking through the emplacement of the overlying H2 that truncates sub-unit B4 in the onshore portions of the basin.

Sub-unit B5

Sub-unit B5 facies, B5_SND, is interpreted as inner shelf sediments delivered to the Atlantic Ocean by an ancestral Meso-Orange River (Bluck *et al.,* 2007) and stored on the continental shelf. Measurements on numerous modern day coasts have shown that in such settings sediment is supplied by mostly longshore current, which are strong enough to transport large volumes of sand (up to several hundred thousands of m^3/year; Einsele, 1992).

Shallow marine and deeper environments, i.e. toward the inner and potentially outer shelf, are influenced and modified by rare storm events. Storms not only create large waves, but are also capable of driving large nett fluxes of water to and from the coast (Einsele, 1992). These result in laterally extensive sheet-like beds of sand and mud referred to as *tempestites*. The development of thin gravel lags or *tempestites* in the marine record is fairly common (Pether and Williamson, 2016). During peak storm flow the base layer lag often comprises mud clasts, broken shells and occasionally gravel and small fragments of bedrock (Einsele, 1992).

4.4 Unit C

4.4.1 Observations

4.4.1.1 Seismic Stratigraphy

Unit C occurs as a wedge-shaped laterally discontinuous deposit, within a water depth of ~65 m bmsl to the offshore licence boundary, pinching out toward the proximal portion of the basin. In the middle of the PTA, where the best exposure of the deposit is observed, unit C has a maximum thickness of ~2 m and thins out laterally across the study area (**Figures 4.1 – 4.3**). Toward the south of the basin, unit C

thins to beyond the resolution of the seismic dataset and cannot be traced as an individual package (seismic line A – A'; **Figure 4.1**). Unit C occurs as a package of convex up low- to medium-amplitude semi-continuous reflectors onlapping the medium to high-amplitude surface, H2, toward the onshore and capped by the medium-amplitude surface H3.

H2 is a fairly continuous, laterally extensive horizon that trends at ~2 m bmsl in the southern portion of the basin and deepens in a northward direction to ~5 m bmsl (**Figures 4.1 – 4.3**). The upper bounding surface (H3) and basal bounding surface (H2) amalgamate into H1 to form one discernible surface toward the proximal and southern portion of the basin (**Figures 4.2(e) and (f)**).

4.4.1.2 Lithostratigraphy

Unit C facies, C_GVL, comprises a thin gravel stringer, with an erosional base, directly overlying H2 and shows a fining upward cycle into marine sand. Toward the onshore, where the wedge of sediment is not discernible, only the thin gravel stringer, with an average thickness of 15 cm, is observed directly overlying H2. The fine gravel comprises sub-angular to well-rounded quartzite, footwall material as well as reworked Basal_SST1 and Basal_SST2 medium pebbles to large cobbles with occasional ORS exotic pebbles (**Figure 4.22**). The overlying sediment wedge facies fine upward into grey-brown coarse to medium marine sand.

Figure 4.22. Sub-angular to rounded scattered pebbles of vein quartz, quartzite, footwall material, exotics and sporadic sandstone material. Scale represents 15 cm.

4.4.2 Interpretation

H2 is interpreted as a wave-ravinement surface (wRs) that is a scour surface cut by high to moderate energy waves in the upper shoreface during rapid RSL rise and ensuing transgression (Cattaneo and Steel, 2003; Catuneanu, 2006; Catuneanu *et al.,* 2011; Bache *et al*., 2014). wRs' are recognisable on seismic profiles by: 1) their smooth, laterally extensive flat surface, 2) erosional truncation of underlying deposits and 3) onlap of overlying deposits (Cattaneo and Steel, 2003; Catuneanu, 2006; Bache *et al.,* 2014). The erosive wRs is commonly marked by a thin surficial coarse lag, comprising coarse sand and gravel (**Figure 4.22**). The wRs is defined as a diachronous surface, because shoreface erosion is restricted to a narrow section of area during transgression and therefore represents a diastem in sedimentation (Cattaneo and Steel, 2003). In order to preserve the concave-up shoreface profile during scouring, the scoured sediments in the upper shoreface are deposited in the lower shoreface at the same rate with the wave energy (Catuneanu, 2006; Catuneanu *et al.,* 2011). These aggrading and retrograding lower shoreface deposits, referred to as transgressive "healing phase deposits", onlap the scour cut in the upper shoreface (Catuneanu, 2006; Catuneanu *et al.,* 2011). Unit C is interpreted as these "healing phase" deposits (**Appendix B**). The transgressive "healing phase" TST wedge is capped by a conformable surface referred to as the maximum flooding surface (MFS), interpreted as H3 (**Figures 4.1(a), 4.2(d) and 4.3(g)**).

Unit C is interpreted as transgressive "healing phase deposits" bound by the wRs (H2) as its base and the MFS (H3) at its surface; **Appendix A;** Catuneanu, 2006; Catuneanu *et al.,* 2011).

4.5 Unit D

4.5.1 Observations

4.5.1.1 Seismic Stratigraphy

Unit D forms a 1.5 m thick unit that progressively thickens in a northward direction to ~4 m (**Figure 4.23**). Unit D unconformably overlies the medium-amplitude erosional surface H3 and is truncated at the surface by H4, a medium to high-amplitude surface. Within unit D, 2 sub-units (D1 and D2) are defined (**Appendix B**). Sub-unit D2 makes up the bulk of unit D.

<u>Sub-unit D1</u>

Sub-unit D1 forms a feature parallel to the shoreline that falls within a water depth of 57 – 64 m bmsl and is traced for 3.5 km until it pinches out in the north. Sub-unit D1 reaches a maximum vertical

thickness of 1.6 m in the south and flattens out to <0.5 m in a northward direction. It is only traced northward of the silcrete headland within the proximal portion of the basin. Sub-unit D1 is a package of continuous high-amplitude, prograding tangential oblique reflectors that downlap H3, expressed as a downlap surface (MFS; **Figures 4.2 and 4.3**). The most northern preservation of sub-unit D1 is just north of seismic line C – C' (**Figure 4.3**), defined by low-amplitude seaward dipping reflectors.

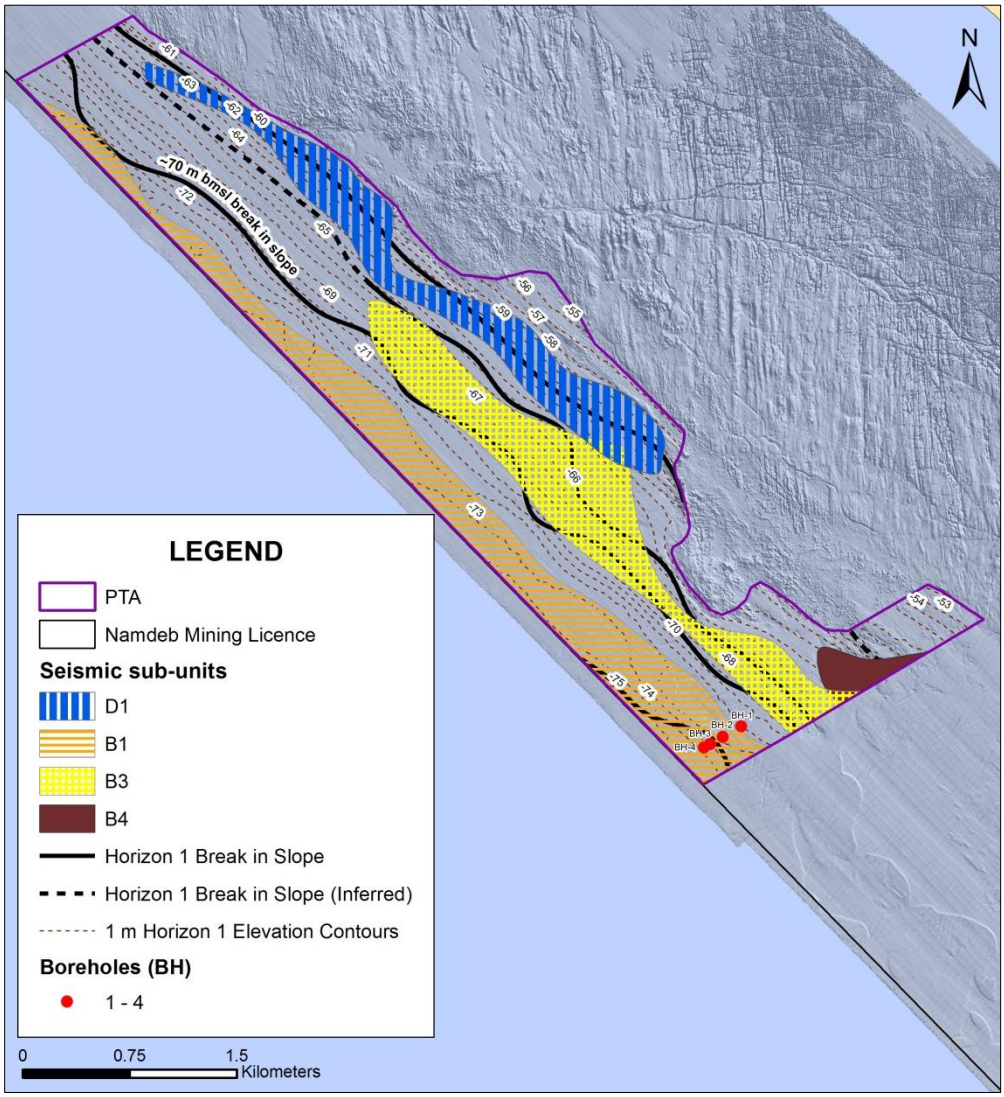

Figure 4.23. Spatial distribution of interpreted seismic sub-units of seismic unit B: B1, B3 and B4, and unit D: D1. Sub-unit D1 is observed northward of the silcrete headland and trends parallel to sub-units B3 and B1. Sub-unit D1 overlaps sub-unit B3 in the central portion of the PST (refer to Figure 4.2(g)). Refer to Figures 4.17 and 4.18 for stratigraphic logs of borehole locations.

Sub-unit D2

Sub-unit D2 laterally covers the entire extent of the PTA and stratigraphically represents the youngest deposit (**Figures 4.1 – 4.3**). Sub-unit D2 is seismically thin in the south of the PTA and thickens susbstantially northward, increasing from 1.5 m to 4 m in thickness. The internal architecture of the sub-unit D2 is generally concealed by large acoustic impedance contrasts and strong water bottom multiples at the seabed, especially toward the onshore where thinner sediment packages accumulate. Sub-unit D2 shares similar seismic characteristics to sub-unit B5. Toward the proximal basin the succession can be delineated and comprises continuous to semi-continuous low-amplitude sub-parallel to divergent reflectors that exhibit an aggradation stacking pattern.

Sub-unit D2 is separated from the underlying unit C by the maximum flooding surface (MFS; H3) and truncated at the surface by modern-day erosional processes associated with the seafloor (H4).

The multi-beam bathymetry and side scan sonar are used to delineate bedform characteristics at the surface of sub-unit D2. Ripples are discernible in the surface geophysical datasets by high-amplitude/dark texture, often with a wavy nature (**Figure 4.24**).

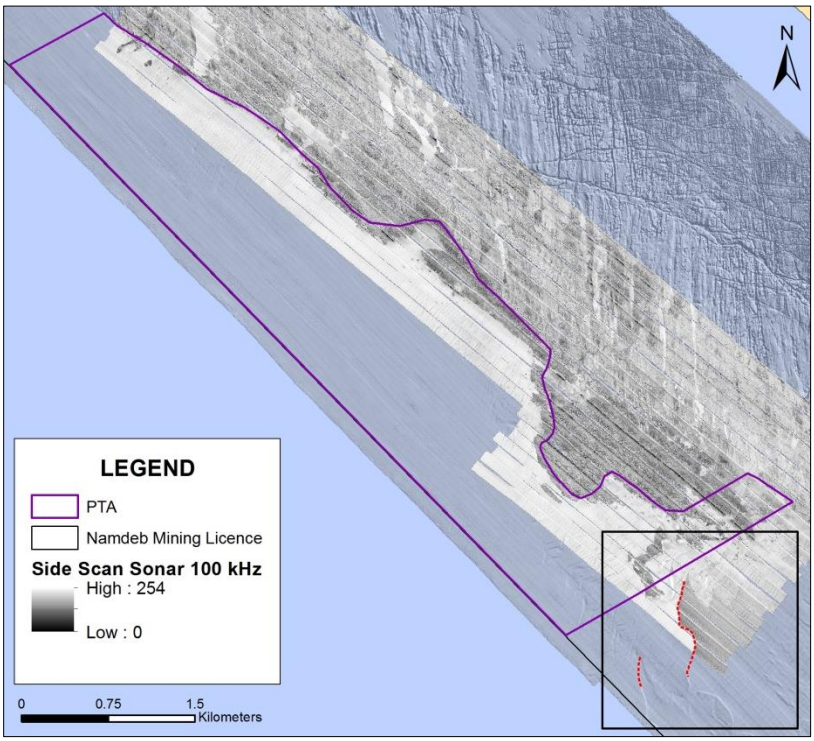

Figure 4.24. Bathymetric and side scan sonar datasets display ripple features (red dashed lines) in the underlying fine-grained sediment of sub-unit D2, preferentially observed in the south of the PTA (black box).

4.5.1.2 Lithostratigraphy

Sub-unit D1

Sub-unit D1 comprises only one lithological facies unit, D1_GVL, consisting of a ≤1.2 m thick layer of gravel material showing an upward coarsening profile. The D1_GVL is comparable to the B3_GVL and B4_GVL deposits, where the textural features of the clasts vary stratigraphically. The basal D1_GVL consists of angular to sub-rounded pebble up to large cobble sized clasts with high proportions of reworked Basal_SST1 and Basal_SST2 facies. The upper D1_GVL comprises more sub-rounded to rounded ORS gravel fractions, of up to boulder size, with varying amounts of ORS exotics (jaspers and agates with rare riebeckite, epidosite and Makwassie porphyry). Minor amounts of reworked Basal_SST1 and Basal_SST2 are observed with depth.

Sub-unit D2

In sub-unit D2 two facies, D2_SND and D2_MD, are resolved that show a general upward fining profile. The basal D2_SND is a sediment wedge comprising brown to green-brown medium to coarse marine sands with occasional lenses of green marine clay, fine gravel and black mussel interspersed. The sands are capped by a succession of strata, generally in the upper 0.5 m of the package, comprising fine-grained olive green to brown muds and shell lags (D2_MD; **Figures 4.1 – 4.3**).

4.5.2 Interpretation

Sub-unit D1

The MFS (H3) separates sub-unit D1 above, displaying progradational strata with downlap terminations onto the MFS, from the retrogradational strata of unit C below (Posamentier *et al.,* 1988; Cattaneo and Steel, 2003; Catuneanu, 2006). The presence of the prograding strata with downlap terminations onto the MFS identifies the MFS as a downlap surface (Catuneanu, 2006). The coarse clastic material making up D1_GVL is interpreted to exhibit characteristics of a foreshore beach environment, emplaced during a RSL high stand (HST). The Cretaceous/silcrete headland could have played a major role in the deposition of the gravel and rubble derived from the ancestral Meso-Orange River. Obliquely directed incoming long period waves intersecting the silcrete headland may have caused the waves to refract. Refraction reduced the energy of the incoming waves in the bay down drift of the headland causing large quantities of sediment being transported northward by the longshore drift to be deposited

northward of the headland (Apollus, 1995). This sediment could possibly have contributed to the accumulation of the normal regressive sub-unit D1 gravel beach.

Sub-unit D2

The marine sand, D2_SND, was ultimately derived from the Orange River. Scattered lenses of gravel, shell and clay in D2_SND, similarly observed in B5_SND, suggest *tempestite* units. D2_MD is the surface phase of sub-unit D2, capping the inner shelf sediment wedge (D2_SND). D2_MD is interpreted as part of the modern high stand sequence (HST) that is still currently being reworked during major storms down to depths of approximately 80 m bmsl (Pether and Williamson, 2016).

Through mining and sampling the bedform features overlying D2_MD have been identified as coarse-grained ripples (CGR). The CGR can easily be traced because the coarser, heavier-grained sediment forms an indentation in the underlying fine-grained sediment, resulting in anomalous patterns in the flat seabed, which dominates the sedimentation area in the south of the PTA (**Figure 4.24**).

CHAPTER 5 – DISCUSSION

5.1 Late Cainozoic Depositional Evolution of the PTA

The formation and preservation of coastal sequences are dependent on several factors; the primary ones being relative sea-level (RSL) fluctuations (including their influence on accommodation space), sediment input and, tidal and wave processes (e.g. Davis and Clifton, 1987; Spaggiari, 2011). The wave regime of the Atlantic Ocean on the west coast of Namibia has remained relatively unchanged since at least the Neogene (de Decker, 1988). Furthermore, the inner shelf offshore southwestern Africa has remained remarkably buoyant and shallow throughout the Cainozoic (e.g. Siesser and Dingle, 1981; Aizawa *et al.,* 2000; Bluck *et al.,* 2005; 2007), apart from two uplifting events of approximately 100 – 200 m and 100 – 900 m in the Early-Middle Miocene and Plio-Pleistocene, respectively (Partridge and Maud, 1987; Apollus, 1995; Jacob, 2005). These results exclude the hypothesis that the present day southern Africa topography formed after the uplift and erosion of an initially low-relief and low elevation land surface over the last ~30 Ma (Burke, 1996; Burke and Gunnel, 2008). Consequently, the principal controls for the development of the Purple Target Area (PTA) stratigraphy are rate of sediment input and RSL fluctuations, which includes changes in the accommodation space driven by local tectonics and eustatic sea-level (ESL) changes (see Catuneanu, 2005; Spaggiari, 2011). Because in this region, tectonic changes were negligible in the post-Cretaceous (Siesser and Dingle, 1981; Aizawa *et al.,* 2000; Bluck *et al.,* 2005; 2007); the RSL changes are equated to the ESL changes.

The lithofacies defined in units B to D (**Figure 5.1**) represent sedimentation within the PTA basin that occurred after the formation of the H1 surface. The precise timing of depositional events is currently unknown due to a lack of absolute age controls in the PTA; making it a challenge to integrate the depositional events and changes in the environment to the established ESL record. Nevertheless, the relative order of depositional events can be estimated based on the analysis of the lithofacies and interpreted water depths (palaeo-bathymetry) relative to the ESL curve (**Figure 5.2**; Compton *et al.,* 2002; Spaggiari, 2011; Mellett *et al.,* 2012).

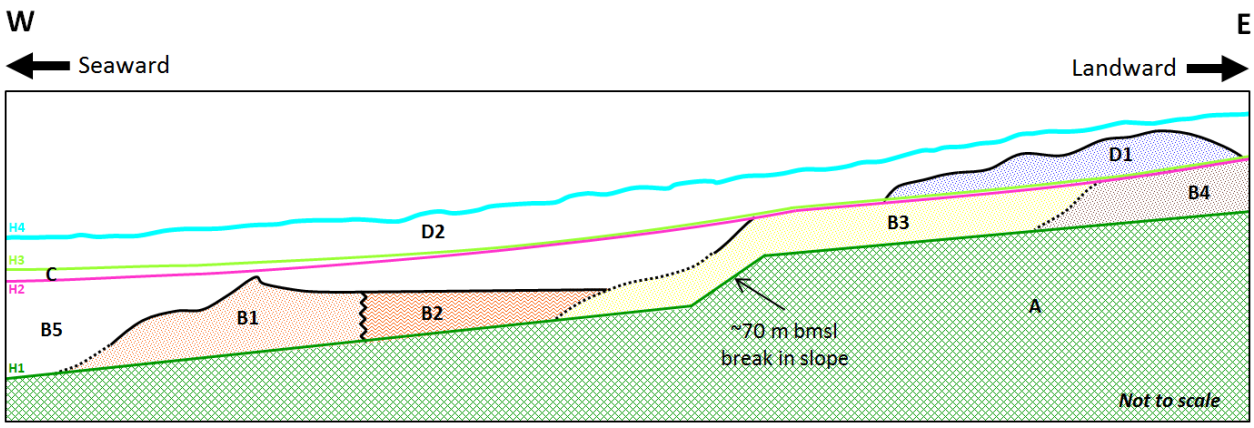

Figure 5.1. Idealised E – W schematic stratigraphic section of the sedimentary successions (units and sub-units) accumulated within the PTA basin during the Late Pleistocene-Holocene transgression. Green hatches indicate basement rocks; other units and surfaces are labelled and explained in the text.

On the basis of their stratigraphic position it is likely that the bulk of the facies identified within the PTA were deposited during the post-Last Glacial Maximum (LGM) transgression (**Figure 5.2**). The melting of the continental ice sheets and subsequent rapid ESL rise of 127 m between 19 and 7 ka before present (BP; e.g. Fairbanks, 1989; Compton *et al.,* 2002; Liu *et al.,* 2004) saw transgressive deposits being emplaced in the PTA. The Plio-Pleistocene basal deposits would have more than likely been exposed and eroded subsequent to the ESL changes associated with the LGM lowstand (120 – 130 m bmsl; Cooper *et al*., 2016). These facies are not observed in the seismic records of the study area due to the limited thickness of the facies that cannot be resolved with the current methods.

Seismic profiles from the PTA reveal several coast-parallel mounded features between 59 and 75 m bmsl that rest unconformably on the major H1 surface (**Figure 5.1**). Based on seismic interpretations and borehole data, the mounded features represent two foreshore gravel beaches (sub-units B3 and B4) preserved toward the proximal portions of the basin and one distally located gravel barrier beach (sub-unit B1) with preserved back-barrier clays (sub-unit B2). Sub-units B3 and B4 did not develop/preserve a back-barrier environment.

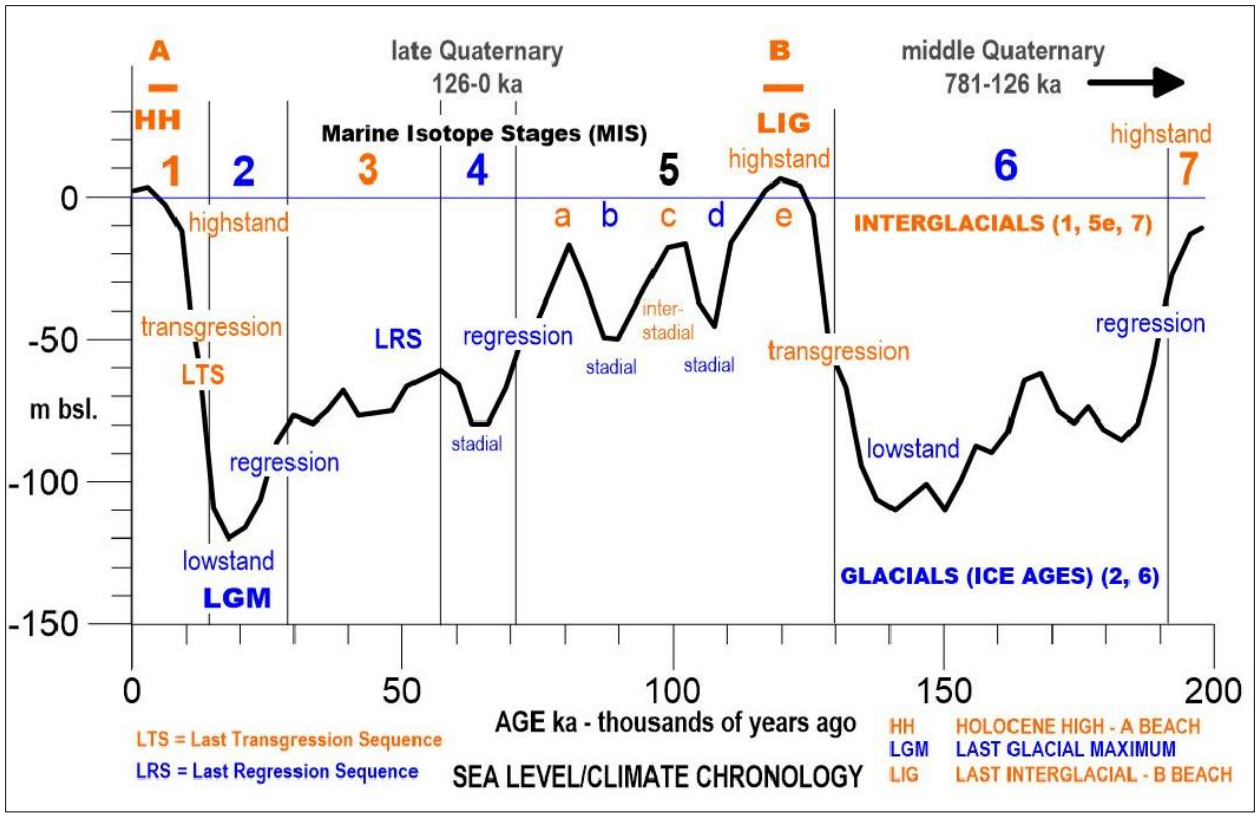

Figure 5.2. Estimated eustatic sea-level changes during the last 200 ka. LRS = Last Regression Sequence, LTS = Last Transgression Sequence and LGM = Last Glacial Maximum (Pether, 2013 adapted from Siddall *et al.,* 2007).

It is proposed that the gravel beaches formed during the transgression following the LGM, but during extended periods of either lower rates of RSL rise, high sediment supply or small-scale regressions (Cattaneo and Steel, 2003; Green and Garlick, 2011). Barrier systems respond to RSL rise in the following ways: breaking down by wave erosion, shifting landward whilst maintaining their volume through rollover or in-place drowning when the RSL oversteps and preserves the entire barrier system offshore (e.g. Orford *et al.,* 1991; Green *et al*., 2013; 2017; Cawthra *et al.,* 2014; Cooper *et al*., 2016). The degree of cross-beach variability (clast size and shape sorting) observed in the upper gravel layers of sub-units B1, B3 and B4 become less preserved in a landward direction. Disc-shaped clasts associated with the middle of the foreshore environment are poorly preserved in sub-unit B3 and completely absent in sub-unit B4. Unlike sub-units B3 and B4, the entire cross-beach sorting pattern of sub-unit B1, including its back-barrier facies (sub-unit B2), have been completely preserved. The preservation of the intact clast assemblage of the barrier feature and the finer facies (lagoonal mud/clay) on a high-energy shelf therefore supports rapid RSL rise and drowning as the preservation mechanism for the entire gravel barrier system, i.e. barrier overstepping (**Figure 5.3**; e.g. Sanders and Kumar, 1975; Rampino and

Sanders, 1980; Cattaneo and Steel, 2003; Spaggiari, 2011; Zecchin *et al.,* 2011; Mellet *et al.,* 2012; Green *et al.,* 2014; 2017; Cooper *et al*., 2016).

The emplacement and preservation model of the foreshore gravel beaches and barrier beach system will be discussed in more detail at a later stage (refer to sub-section 5.3).

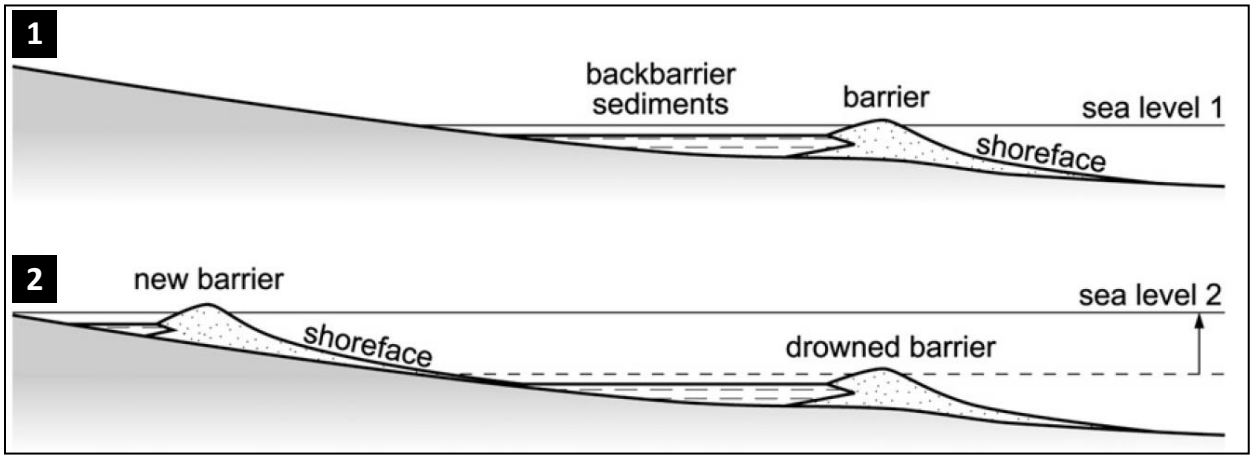

Figure 5.3. Barrier overstepping and in-place drowning model for shallow-gradient shelves by Sanders and Kumar (1975), and Rampino and Sanders (1980). The model proposes 1) gravel barrier development during a slow RSL rise and subsequent drowning and preservation during a rapid RSL rise, and 2) the potential development of a new barrier landward during conditions of slower RSL rise, i.e. shoreface retreat (Zecchin *et al.,* 2011).

As RSL continued to rise during the Late Pleistocene-Holocene transgression, the sand stored on the continental shelf migrated landward with the shoreline (Sloss *et al.,* 2007). As the accommodation space behind sub-unit B1 increased it promoted the development of the thick succession of sub-unit B5 transgressive deposits (**Figure 5.1**; Cattaneo and Steel, 2003). The geometry of transgressive deposits is dependent on the interaction between available accommodation space and sediment supply (Cattaneo and Steel, 2003). Sub-unit B5 displays an aggradational stacking pattern dominated by an upward-fining profile of "birdseed" gravel to medium-coarse marine sand. This sub-unit volumetrically dominates the sediments deposited in the PTA basin and overlies sub-units B1 to B3. Sub-unit B5 is separated from the overlying unit C by a distinct laterally extensive surface, which is labelled here H2 (Cawthra *et al.,* 2014).

Continued RSL rise during the Late Pleistocene-Holocene transgression did not only see facies being deposited with increasing accommodation space, but also erosion during rapid Early Holocene RSL rise. Moderate to high energy waves in the upper shoreface eroded the substrate during rapid RSL rise and ensuing transgression (e.g. Cattaneo and Steel, 2003; Catuneanu, 2006; Catuneanu *et al.,* 2011; Bache *et al*., 2014). This erosive surface correlates to H2 and based on seismic stratigraphic observations and borehole data, it is interpreted as a transgressive wave-ravinement surface (wRs). The wRs develops

within a Transgressive Systems Tract (TST) and thus is not a sequence boundary (Catuneanu, 2006). The wRs truncates unit B in the proximal and northern portions of the basin (**Figure 5.1**). The erosive processes associated with the wRs are held accountable for the lack of cross-beach sorting observed within sub-units B3 and B4. The prominent surface displays a seaward dipping geometry and is commonly marked by a thin surficial coarse lag, comprising local gravel, bedrock material and coarse sand (**Figure 4.22**). The extent of the wRs in a landward direction is dependent on the geometry of the shoreface profile (i.e. steepness of the coastal profile), the rate of RSL rise, and this will ultimately determine how far the shoreline transgressed (Catuneanu, 2006). These transgressive surfaces have been well-documented off the east coast of South Africa (e.g. Green, 2009; Cawthra *et al.,* 2014; Pretorius *et al.,* 2016; 2017; Green *et al*., 2017).

Deposits of unit C are closely associated with the wRs and onlap the prominent wRs toward the distal portions of the basin. These distal aggrading and retrograding lower shoreface deposits are referred to as transgressive "healing phase deposits", and onlap the scour (i.e. wRs) cut in the upper shoreface to maintain the concave-up profile of the shoreface. The "healing phase deposits" preserved as unit C are bound by the wRs at their base and the medium-amplitude surface, labelled here H3, at their tops (**Figure 5.1**).

Unit C is capped by H3, a conformable surface referred to as the maximum flooding surface (MFS). The MFS marks the time of maximum water depth in the PTA and the approximate maximum landward position of the shoreline (**Appendix A**; Cattaneo and Steel, 2003). Toward the proximal and southern portion of the PTA basin, unit C thins to beyond the resolution of the seismic dataset and the "healing phase deposits" cannot be traced. Where unit C is not traceable, its upper bounding surface (labelled here H3) and basal bounding surface (labelled here H2) amalgamate into H1 to form one discernible surface (**Figure 5.1**).

Toward the proximal portion of the basin, within the overlying unit D sediment wedge, the upward-coarsening foreshore beach (sub-unit D1) supports a shift in depositional trends from retrogradation to progradation (i.e. from transgressive to regressive; **Figure 5.1**). A shift from shoreface deposits below (unit C) to overlying beach facies (sub-unit D1) supports the development of a normal regressive succession (Catuneanu, 2006). Similar to the deposition of the unit B beaches, the progradational package within the unit D wedge was formed either during lower rates of RSL rise, higher rates of sediment supply or a small-scale regression within the Holocene (approximately 11.5 ka BP; Cattaneo and Steel, 2003; Green and Garlick, 2011). The deposits comprising this package display a variation in

textural maturity of the clasts with depth. This can be explained by sub-rounded to rounded shoreface deposits accumulating over angular erosive lag deposits ascribed to the wRs.

Sub-unit D2 is stratigraphically the highest unit and represents the youngest phase of deposition within the PTA basin (**Figure 5.1**). Sub-unit D2 comprises a Holocene-age wedge dominated by unconsolidated marine sand, shell debris and occasional gravel lenses fining upward into muds with shell lags. These deposits migrate over the foreshore beach deposits (sub-unit D1) and deposits associated with unit A toward the proximal portions of the basin.

The upper bounding surface of unit D, labelled here H4, forms the present seafloor and is currently still being reworked during major storms (**Figure 5.1**; Pether and Williamson, 2016).

5.2 Onshore Analogues

Bluck *et al.* (2001) recognised four major gravel beach types along the mesotidal coast within Mining Area 1 (MA1) based on the range and combination of bed assemblages: spits and barrier beaches within the palaeo-Orange River mouth, coast-parallel linear beaches for another ~70 km and pocket beaches that represent the northern extreme littoral deposit types (**Figure 1.1**; Spaggiari *et al*., 2006). Coast-perpendicular sampling trenches in MA1 (>1000 m long, 1 – 10 m wide, and in certain areas, >15 m deep) have provided composite cross-section exposures of the preserved gravel beaches (Spaggiari, 2011; Jacob, 2016). The one characteristic that links the various gravel beaches is the degree of shape sorting of the gravel facies. The gravel beaches show clast shape segregation where large spherical or equant clasts, including small discoidal and other shaped clasts, are found at the seaward toe of the beach compared to the beach crest where large discoidal or oblate clasts predominate (Spaggiari *et al.,* 1999; 2006; Spaggiari, 2011). The most landward shore-parallel zone comprises clast supported cobble sized discs, having imbricated disc-shaped pebbles on its seaward side (Bluck, 1967). Large spherical clasts are displaced at the base of the most seaward zone where wave action effortlessly rolls the clasts up the down the steep beach face (>14°; Spaggiari *et al*., 2006; Spaggiari, 2011).

The PTA lies offshore of the linear beaches of Mining Area 1 (MA1) some 65 km north of the point source of sediment supply at the palaeo-Orange River mouth. Estuarine Delta (ED) area barrier beaches are confined to the palaeo-Orange River mouth onshore, but it is proposed that despite the distance from the palaeo-river mouth both beach types (or a form of each) are present in the PTA.

Sections 5.2.1 and 5.2.2 describe the onshore analogues in detail and section 5.3 presents a model for the evolution of the gravel beaches identified in the PTA.

5.2.1 MA1 Gravel Linear Beaches

Marine terraces, rising approximately 30 m above mean sea-level (m amsl) and up to 3 km landward from the current shoreline, are preserved within MA1 between the Orange River mouth and Chameis Bay (**Figures 2.7 and 5.4**). A marine terrace comprises a basal wave-cut platform (i.e. wave-ravinement surface) overlain by marine deposits grading upward into terrestrial deposits (Jacob, 2001; Schulmeister, 2016). Six raised gravel beaches, between 2 and 30 m amsl, have been recognised by Stocken (1962) and Hallam (1964) within MA1. Each of the onshore beaches is made up of a clast supported gravel storm beach (with minimal sand) at the highest elevation, an intertidal beach in the middle and subtidal gravels at the lowest elevation covered by aeolian sands (Hallam, 1964; Miller, 2008). The beaches have been grouped into two marine terraces: A, B and C beaches (younger marine terrace) and D, E and F beaches (older marine terrace; **Figure 5.4**; SACS, 1980; Apollus, 1995; Jacob, 2001; 2016). The gravel beaches associated with the older (upper) terrace host a warm-water marine zone fossil *Donax rogersi*, whereas the younger (lower) terrace is characterised by modern cold-water fauna (e.g. Pether, 2000; Jacob, 2001; Miller, 2008; Jacob, 2016). The gravel beaches comprise a unit of inclined deposits that rest unconformably on, and are backed by, Late Proterozoic bedrock (Frimmel, 2008; **Figure 5.4**). Through progressive mining operations seaward, beaches can be traced offshore to water depths as low as 25 m bmsl; however, the complete sequence of internal gravel beach facies is not observed (Jacob, 2016).

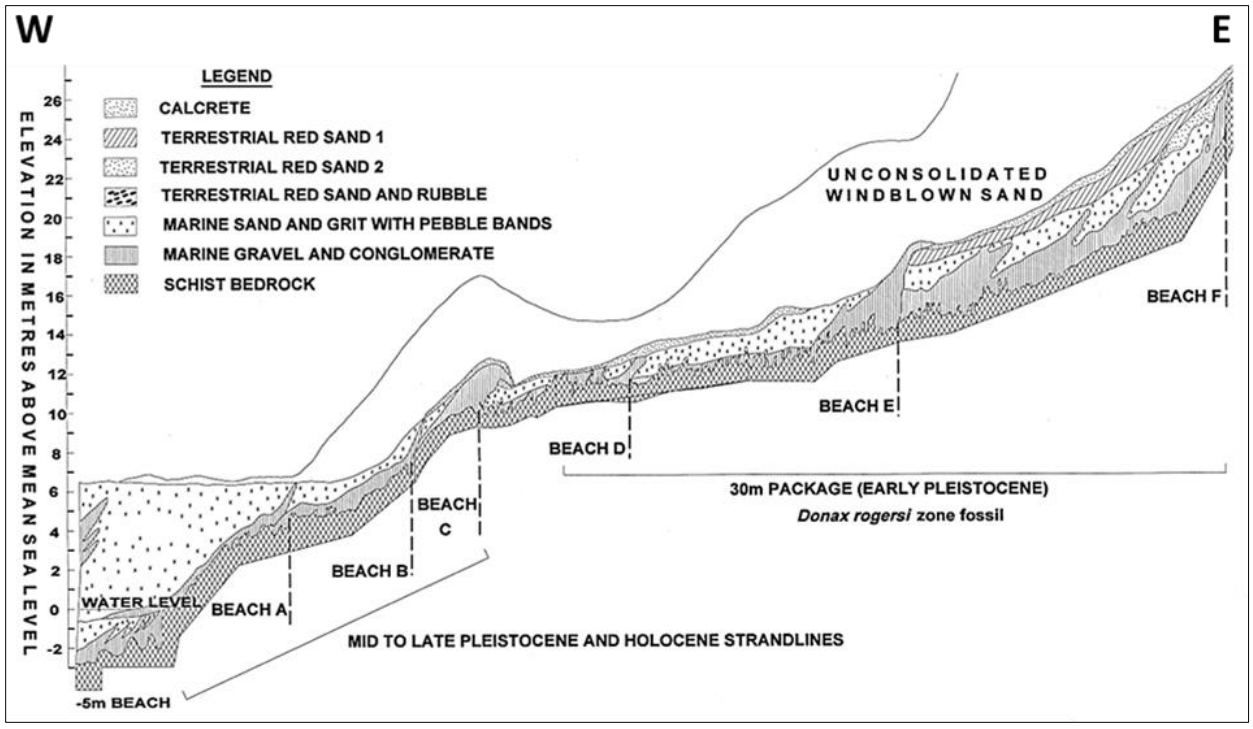

Figure 5.4. E – W cross-section through the onshore linear beach deposits of southern MA1: Sub-10 m (A, B and C beaches) and 30 m Package (D, E and F beaches), and the expected stratigraphy of the respective beaches (after Hallam, 1964; Kalbskopf, 1978; Ward *et al*., 1998; Jacob, 2001).

MA1 marine terraces are undated and therefore their ages of formation are assumed to roughly correlate with the age of the overlying gravel beaches (**Table 5.1**; Jacob, 2001). The gravel beaches are developed at descending elevations with the oldest beach located the furthest landward. The stratigraphic evolution of the MA1 beaches points toward an overall regression; it is suggested that the diamondiferous beach packages were deposited during a transgressive and subsequent regressive cycle, with only the highstand sequence preserved (HST; Pether, 1994; Spaggiari, 2011; J. Ward, pers. comm., April 2016). All six beaches host exotic clasts of riebeckite and banded ironstone, which correlate to the Meso-Orange River deposits (Miller, 2008).

Table 5.1. MA1 hosts six gravel linear beaches developed at descending elevations with the F beach having developed first (J. Pether, pers. comm., October 2017 adapted from Apollus, 1995).

Epoch	Age (BP)	Stratigraphic Unit	Approximate Wave-cut Platform Elevations	Fossils
Holocene	~ 7 – 4 ka	A beach	2 – 3 m amsl	Modern fauna
Late Pleistocene	~125 ka	B beach	4 – 6 m amsl	Modern fauna
Mid Pleistocene	~400 ka	C beach	8 – 10 m amsl	Modern fauna
Late Pliocene	~3 Ma	D, E and F beaches	12 – 30 m amsl	Warm-water fauna with extinct species

5.2.2 Estuarine Delta (ED) Area Barrier Beaches

A local analogue of a barrier beach environment is preserved onshore within the locally known Estuarine Delta (ED) area, confined to the palaeo-Orange River mouth in MA1. The Early Pleistocene coarse gravel spit-barrier comprises vertically stacked sedimentary sequences of marine sediments that form a 4 km long and 0.5 km wide coast-parallel, linear feature approximately 8 – 12 m in height (Spaggiari *et al.,* 1999; **Figure 5.5**). The barrier beach complex is subdivided into three main zones: subtidal zone (shoreface environment), intertidal zone (foreshore environment) and back-barrier zone (lagoonal environment) with various depositional sub-units within each zone (**Figure 5.5**; Bluck *et al.,* 2001; Spaggiari *et al.,* 2006). Coarse clastic materials within the barrier beach are evident in the intertidal zone and wash-over deltas within the back-barrier zone. Behind the wash-over deltas, landward of the gravel barrier, the sediments comprise mainly fine materials of silts and clay (**Figure 5.5**; Spaggiari *et al.,* 1999). The rare presence of *Donax rogersi* links the ED deposits to the Late Pliocene (D, E and F) beaches (**Table 5.1**; Pether, 1994; Spaggiari, 2011). The gravel barrier overlies fluvial sediments of the palaeo-Orange River mouth (Spaggiari *et al.,* 1999).

In addition to the aforementioned transgressive and subsequent normal regressive cycle responsible for the emplacement of the MA1 A – F beaches, a third aspect has been identified within the ED study area. The barrier spit and barrier beach deposits, within the bounds of the Late Pliocene beaches, were not the product of a single cycle of transgression and regression, but based on its facies and stacking pattern, were emplaced and built on cycles of RSL fluctuations within the palaeo-Orange River mouth during the Late Pliocene to Earliest Pleistocene (Spaggiari *et al.,* 2006; Spaggiari, 2011). The ED gravel barrier complex is defined by two principle depositional episodes on an overall transgressive system, these being the accreted spit sequences (emplaced during RSL transgressions) underlying gravel barrier packages (emplaced during RSL high stands; Spaggiari, 2011). The accommodation space within the palaeo-Orange River mouth and rising RSL facilitated the preservation of the gravel-spit barrier. In addition, the calcertisation of the surface gravels and aeolian dune cover assisted with the preservation of the gravel barrier system (Spaggiari, 2011).

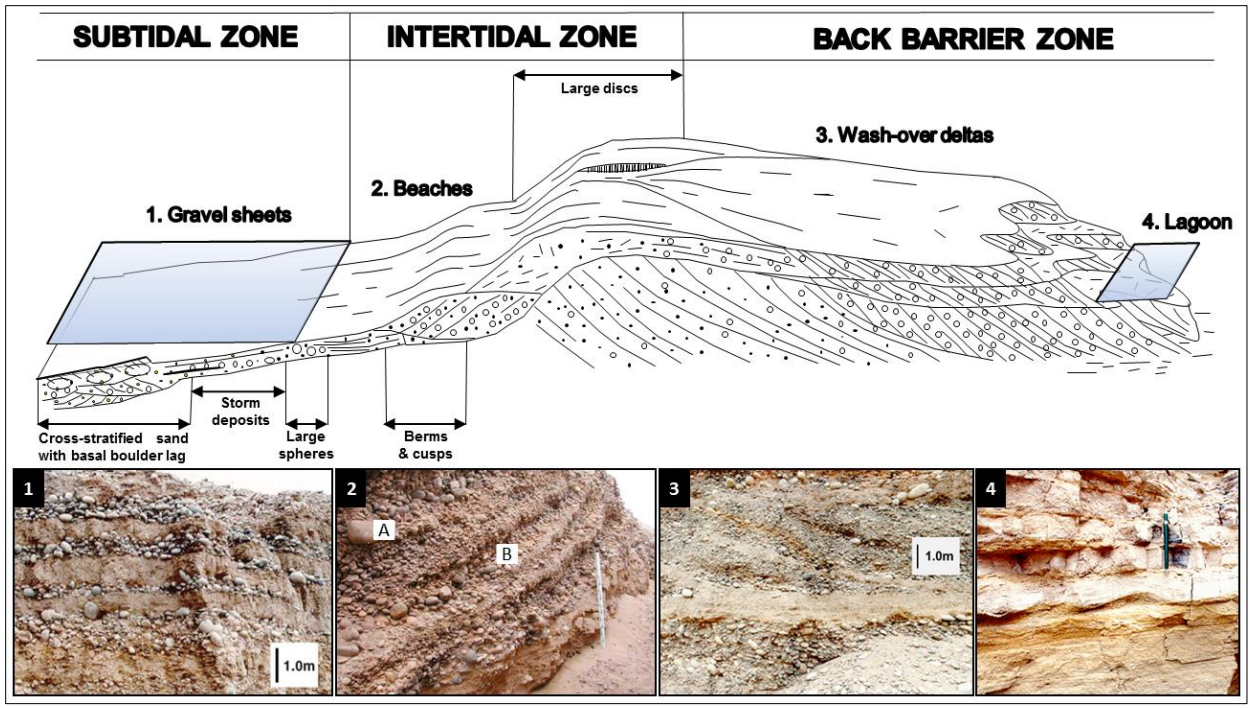

Figure 5.5. Onshore Estuarine Delta (ED) area barrier complex analogue. 1) The subtidal zone, the most seaward section of the ED area, comprises storm generated gravel sheets and post storm, fair weather, shoreface sands. 2) The intertidal zone, structurally complex, comprises a variety of bed assemblages and sub-environment: foreshore deposits and diverse gravel structures. A. Progradational seaward dipping berms in gravel beaches and B. displacement of cobble-sized clasts into finer grained facies. The gravel beaches constitute the majority of the sediments within the ED area and make up a large portion of the barrier complex. 3) The wash-over deltas form part of the most landward section of the ED area, the back-barrier zone, and are deposited on top of 4) fine-grained lagoonal facies when the beach crests are eroded and deposited landward during storms (adapted from Spaggiari *et al*., 1999; 2006; Spaggiari, 2011).

5.3 Shoreline Evolution

The coastal and shallow marine facies of the positive relief gravel beaches are the most noteworthy phases of deposition in the PTA. The deposits record phases of gravel/barrier beach emplacement and partial to complete preservation of the facies. Sub-units B1 and B2 display comparable proportions of sedimentary facies identified laterally across the ED area barrier beach system onshore. The signature of sub-units B3 and B4 have been removed by post-depositional reworking processes and therefore cannot be assigned a definite facies model associated with the local onshore analogues.

The timing of the gravel/barrier beach emplacement and preservation model will be reassessed pending a dating program.

5.3.1 Gravel Beach Emplacement

The main criterion for the initial development of a gravel beach is sufficient sediment supply to balance the rise in RSL (Mellet *et al.*, 2012). The sediment supply to the Cainozoic gravel beaches has been largely determined by the incision and subsequent transport of the Orange River deposits to the Atlantic

Ocean during sub-continental uplift events and forced regressions associated with major ice sheet build-ups (refer to Chapter 2; e.g. Bluck *et al.,* 2007; Dingle *et al.,* 1983; Spaggiari, 2011). A major delivery of coarse clastic material to the Atlantic sink may have been achieved during the LGM, preceding the Late Pleistocene-Holocene transgression, where the shelf was sub-aerially exposed to 120 – 130 m bmsl and thus promoted incision and transport of the locally termed Meso-Orange deposits to the palaeo-shoreline. In addition, older gravel beaches developed off the Orange River mouth would have been available for reworking by the fluctuating RSL during the Late Pleistocene-Holocene transgression and material transported northward by the vigorous longshore drift for secondary emplacement in the PTA (Bluck *et al.,* 2005; 2007).

The gravel beaches, based on their facies and stacking pattern, comprise several gravel layers each with their own defining characteristics, i.e. Pliocene to pre-LGM rudaceous angular rubble at the base followed by a single layer or multiple layers of reworked sub-rounded to rounded Orange River Suite gravel linked to the last transgressive event. The gravel beaches record multiple emplacements of clastic material with substantial time gaps between the phases (Bluck, 1999; Spaggiari, 2011). Similar to the emplacement and growth model associated with the ED area barrier beach, the PTA unit B gravel beaches are likely the result of several regressive and transgressive cycles with the bulk of the facies having been built during the Late Pleistocene-Holocene transgression. During overall transgression, high input of sediment supply or reduced rates of RSL rise can cause the shoreline to be intermittently regressive in character, producing progradational deposits (Cattaneo and Steel, 2003). The formation of the unit B gravel beach complexes correlates well with the slowly rising RSL within the ~70 m bmsl range during the Late Pleistocene-Holocene transgression (between 14 and 11.5 ka BP; **Figure 5.6**; Liu *et al*., 2004).

In addition, sub-units B1, B3 and B4 are mapped on seismic sections ~5 km to the south of the study area and, based on their seismic architecture, it is proposed that they young in a seaward direction. The most distal portion of the landward (and oldest) gravel beach, sub-unit B4, is onlapped by the proximal portion of the subsequent lower elevated gravel beach (sub-unit B3) and so forth (**Figure 5.1**). The PTA progradational beaches thus developed in a setting where they could accumulate over a vertical elevation range of ~15 m (measured from the crest of the landward-most positioned beach to the base of the seaward-most positioned beach). The main criterion for the development of seaward building gravel beaches would be gravel beach abandonment and change in position of sediment delivery seaward (Spaggiari, 2011). This could possibly be explained by the locus of sediment delivery shifting

further offshore as the shoreline displaced seaward during reduced rates of RSL rise or increased rates of sediment input. With sediment now being directed to a younger seaward positioned beach (sub-unit B3), the older landward positioned gravel beach (sub-unit B4) becomes impounded and protected from wave erosion by the seaward growth of the new gravel beach (Spaggiari, 2011). The older beach (sub-unit B4) remains indefinitely cut off from the ocean as the younger beach (sub-unit B3) builds seaward. The same process is envisaged for the development of the youngest PTA gravel beach, sub-unit B1, where the barrier complex built as sediment was directed further offshore and ultimately protected the up-drift gravel beach (sub-unit B3) from marine processes (i.e. wave erosion).

5.3.2 Gravel Beach Breakdown

Gravel beach breakdown results from progressive depletion of the sediment supply (Orford *et al.,* 1991) and/or increase in wave erosion during the rise in RSL (Orford *et al.,* 1995; Mellett *et al.,* 2012). As the shoreface progrades and builds landward, supplied by sediment primarily retained within the breaker zone (Spaggiari, 2011), the water depth decreases locally. This allows high energy waves to interact with the substrate as the shoreline transgresses. The gravel beaches therefore enter a phase of erosion and breakdown (Mellet *et al*., 2012). Angular bedrock facies and rubble facies derived from sub-unit B1 are transported into its back-barrier environment, i.e. wash-over facies. The wash-over facies overlying sub-unit B2 form a gravel armouring protecting the finer grained deposits from further reworking and erosional processes (Mellett *et al.,* 2012).

5.3.3 Gravel Beach Preservation

The complete and partial preservation of the gravel barrier complex (sub-unit B1 and B2) and gravel beaches (sub-units B3 and B4), respectively, suggests overstepping and in-place drowning. This process is well-documented on the barrier shorelines (beachrocks and aeolianites) preserved on the Kwazulu-Natal continental shelf along the east coast of South Africa (e.g. Green, 2009; Salzmann *et al*., 2013; Green *et al*., 2013; 2014; 2017; Cooper and Green, 2016; Pretorius *et al*., 2016). The critical factor proposed for overstepping and preservation of a barrier complex is rapid sea-level rise (e.g. Forbes *et al*., 1995; Storms *et al*., 2008; Green *et al*., 2013). The probability of preservation can be enhanced by additional factors, such as early cementation in sub-tropical settings (e.g. Salzmann *et al*., 2013; Green *et al*., 2013; 2014; Pretorius *et al*., 2016), coarse clastic barriers with long relaxation times (refer to Orford and Carter, 1995; Mellet *et al*., 2012; Green *et al*., 2013), low wave and tide energy (Storms *et al*., 2008), and low-gradient shelves where the shoreline undergoes a stepwise retreat (e.g. Cattaneo and Steel, 2003; Pretorius *et al*., 2016; Green *et al*., 2017). All the conditions documented to encourage

barrier overstepping and preservation are recognised in the PTA, apart from cementation. If the shelf gradient below the gravel barrier complex had been steeper, relative to the primary ~70 m bmsl break in slope area (~1.70°), the higher the likelihood the barrier and its back-barrier deposits would have been reworked by erosive ravinement processes (Davis and Clifton, 1987; Pretorius *et al*., 2016; 2017; Green *et al*., 2017). The wRs (surface H2) associated with the rapid transgression eroded existing sediments, including the surface gravels of the higher elevated sub-units B3 and B4, and the underlying Cretaceous deposits.

The Late Pleistocene-Holocene transgression saw multiple "steps" in ESL rise during minor and major meltwater pulses (mwp and MWP, respectively; **Figure 5.6**) produced from rapid ice sheet melting events (Salzmann *et al*., 2013). MWP-1B, between 11.5 and 11.2 ka BP, was characterised by an ESL rise, which peaked from 58 to 45 m bmsl (e.g. Liu *et al*., 2004; Liu and Milliman, 2004; Zecchin *et al*., 2011; Green *et al*., 2013; Salzmann *et al*., 2013). The existence of MWP-1B is still being debated (Bard *et al*., 1996; 2010; 2016; Carlson and Clark, 2012; Lambeck *et al*., 2014); however, its portrayed rate of ESL rise reached 40 mm/a (Liu and Milliman, 2004; Abdul *et al*., 2016), which exceeds the overstepping modelled rate of 3.3 m/ka (Storms *et al.,* 2002) required to sufficiently encourage overstepping (**Figure 5.6**; Mellet *et al.,* 2012; Green *et al*., 2013). Based on the ESL curve, palaeo-bathymetric level of the PTA gravel beaches and the gravel beaches resistance to dispersion by wRs processes, the beaches were overstepped by the rapid ESL associated with MWP-1B (**Figure 5.6**; Green *et al*., 2013).

Despite the lack of ground-truthing data to the south of the PTA, the preferential preservation of local submerged beaches at specific depths supports high volumes of sediment entrainment northward by the longshore drift, shoreline stability and subsequent overstepping to emplace and preserve gravel beaches/barriers up to ~65 km from the point source.

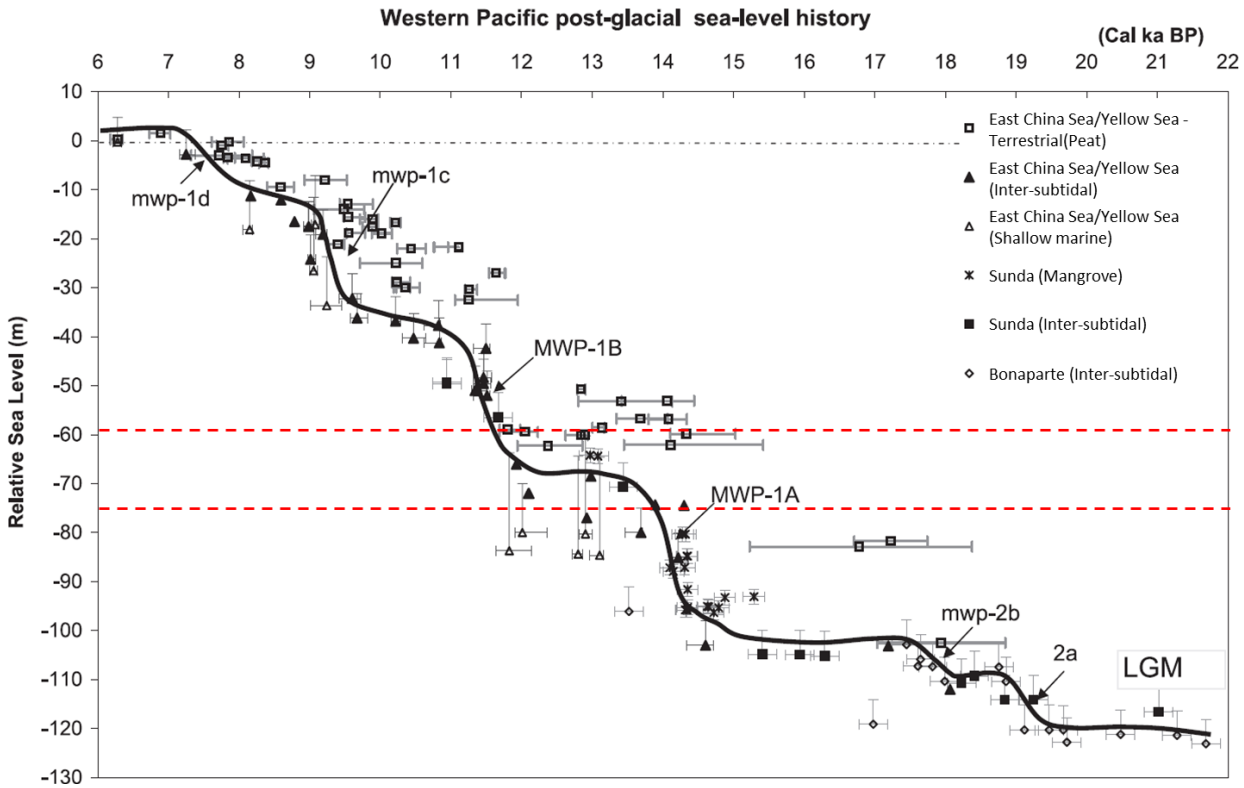

Figure 5.6. The Late Pleistocene/Holocene transgressive curve including major and minor meltwater pulses mostly based on sea-level indicators from the Western Pacific. At the height of the Last Glacial Maximum (LGM), from 22 – 19 ka BP, the ESL was roughly 125 m bmsl (adapted from Liu *et al.*, 2004). The red dashed lines represent the vertical elevation range (~15 m) over which the PTA foreshore gravel beaches and barrier beach were emplaced and developed. The subsequent MWP-1B rapid ESL rise is accountable for the drowning and preservation of the PTA gravel beaches.

5.4 Controls on the Emplacement and Retention of Diamonds

There is general consensus that the palaeo-Orange-Vaal River system supplied coarse gravel and diamonds to the Atlantic Ocean sink (e.g. Stocken, 1978; Partridge and Maud, 1987; de Wit, 1999; Jacob *et al.,* 1999; Jacob *et al.,* 2005; Bluck *et al.,* 2005; 2007; Spaggiari, 2011). Pulses of different characteristic sediment composition (Pre-Proto, Proto- and Meso-Orange River deposits) were delivered to the Atlantic Ocean by the palaeo-Orange River, but not all the diamonds were transported to the coastline, some were trapped in deep scours cut into the bedrock strata along the course of the palaeo-Orange River (Jacob, 2005; Spaggiari, 2011). The phases of diamond pulses not only have diagnostic sediment compositions, but unique diamond characteristics as well (refer to sub-section 2.2.1). Large bodies of sediment were injected into the coastal system with silt and mud dispersed over the largest area offshore, whereas the gravel fraction was distributed within the intertidal to subtidal zone by the intense wave energy and northward bound longshore drift (Bluck *et al.,* 2007; Spaggiari, 2011). The removal of fine sediments during the segregation process, in conjunction with a buoyant shelf that

maintained the sediments within the wave base, was essential to the diamond concentration procedure (Spaggiari, 2011). Essentially, the removal of unwanted fine-grained sediments enhanced the diamond concentration within the condensed gravel sequences (Spaggiari, 2011).

The economic success of a potential diamond hosting deposit primarily relies on three major factors during its assessment:

1. the availability of diamonds during the emplacement of a gravel deposit,
2. the degree to which the gravel has undergone reworking and
3. the preservation potential.

The onshore gravel beach deposits of Namdeb's MA1 are not directly supplied with diamonds from the Orange River (Bluck *et al.,* 2005) and as such, the offshore is seen as the primary diamond reservoir for the onshore beaches (Spaggiari, 2011). RSL fluctuations since at least the Eocene have reworked pre-existing diamond bearing shoreline deposits that had developed off the palaeo-Orange River mouth on raised marine cut-platforms, back into the system (Bluck *et al.,* 2005; Spaggiari, 2011). During regressions, the older submerged diamondiferous deposits were reworked, distributed by the northward longshore drift and then driven landward during the subsequent transgressions, where secondary diamondiferous deposits were allowed to accumulate once RSL stabilised (Spaggiari, 2011). A decrease in diamond size and gravel accumulation is recorded from the Orange River mouth northward, attributed to longshore sorting (e.g. Hallam, 1964; Apollus, 1995; Spaggiari *et al*., 2006; Spaggiari, 2011).

Based on the onshore analogues, the ED area spit/barrier beaches, located within the palaeo-Orange River mouth, yield considerably lower diamond grades compared to the bedrock floored linear beaches northward (Spaggiari *et al.,* 2006). This is a result of the ED barrier environment resting on an incompetent fluvial sediment footwall, which is ill-suited for forming fixed trap-sites for diamond accumulation (Spaggiari *et al.,* 2006; Jacob, 2016). The Late Proterozoic bedrock that underlies the linear beaches of MA1 commonly comprises deep potholes and gullies, and forms bedrock cliffs (Jacob, 2016). Diamond concentrations are found within gravel accumulations close to the bedrock, which suggest accumulation in depositional environments of high energy (de Decker, 1988). Under such conditions, high energy waves and a large supply of resistant quartzite clasts (primarily derived from the Nama Group) are believed to have repeatedly carved deep seated potholes and gullies into the wave-cut platforms during transgressions (Jacob *et al.,* 1999; Spaggiari, 2011). The sedimentary evolution of these potholes is considered paramount in diamond exploration in this region, because the potholes

played an integral role in the trapping of diamondiferous marine gravel comprising many generations of diamond input along the Namibian coast (Bluck *et al.,* 2007; Spaggiari, 2011). The linear beaches developed on these wave-cut platforms.

High wave energy and longshore drift facilitated the emplacement of the coast-parallel MA1 raised gravel beaches. The distribution of diamonds for the A – F linear beaches within MA1 varies, with the B and F beaches hosting the best diamond grade (Hallam, 1964; Jacob, 2001). Therefore, the potential for a high quality diamondiferous beach is dependent on the diamond pulse available during deposition of the specific beach, and the quality and quantity of fixed trapsites on the underlying bedrock platform (Jacob, 2001).

Even though the gravel beaches are ultimately not as effective in trapping diamonds as other surfaces, particularly, fixed trap sites carved into the bedrock (Hallam, 1964; Jacob, 2001), the gravel beaches are still a potential trap site for diamond accumulation. In addition to the fixed trapsites in the bedrock and avaiability of diamonds during gravel beach emplacement, the cross-beach sorting patterns of the beach sequence is equally important (Jacob, 2016). Based on the ED area, the spit/barrier beach can contribute to the trapping of diamonds, depending on its gravel fabric, mobility and preservation (Spaggiari, 2011). The seaward-facing foreshore (intertidal) deposits of the spit/barrier beach yield the highest average diamond grade within the beach sequence. The area is subjected to the highest wave energy and promotes sorting of coarse clastic material (and diamonds) through the swash and backwash process (**Figure 5.5**). The main trapping method in this area is thought to be through percolation, where diamonds filter through the coarse gravel until their size inhibits further descent. The crests and back-barrier deposits of the spit/barrier yield the lowest average stone size. This is due to the back-barrier deposits rarely being reworked, except during storms or spring tides, and comprises mainly finer sediments (e.g. clays and silts). The preservation of diamonds within the shoreface (subtidal) area is dependent on the mobility of the spit/barrier beach. Boulder clasts, which control the local turbulence, accumulate at the base of the beach during roll-over and retain diamonds washed seaward from the steep foreshore area. The largest stones are retained within this area, but invariably yield the poorest grade (Spaggiari *et al*., 2006).

The onshore analogues shed a positive light on the mineralisation potential of the gravel hosting deposits accumulated within the PTA. Gravel development in the PTA is best developed on the sampling lines associated with the unit B and D gravel beach accumulations and wave-cut platforms. The PTA beaches rest on an incompetent footwall comprising predominantly of unconsolidated Cretaceous vein

quartz rubble, which does not promote pothole and gully development. However, the wave-cut platforms within the PTA are well-preserved due to the soft nature of the underlying Cretaceous footwall, making it more susceptible to wave erosion during transgression. Seaward of the onshore cliffs in MA1 the transgressive lag deposits (comprising numerous large clasts of local bedrock/footwall) cover the platform and increase in thickness and grain size landward (Jacob, 2001). This is analogous to the build-up of coarse clastic material associated with the primary ~70 m bmsl break in slope observed in the PTA, where the ~1.5 m thick sub-unit B3 gravel beach deposits have accumulated (**Figure 4.15**). The complete to partial cross-beach sorting patterns of sub-unit B1, and sub-unit B3 and B4 respectively, therefore provide a viable diamond trap-site, especially within the foreshore beach environment where coarse clastic material predominates. Within the PTA, the gravel has the principal trapping and upgrading role where clast size and sorting controlled the emplacement and retention of diamonds. The precise economic potential of the PTA deposits will be evaluated pending a mining campaign.

CHAPTER 6 – CONCLUSIONS AND FUTURE RESEARCH

6.1 Conclusions

The study of submerged landscapes and their associated deposits is critical to the advancement of our understanding on how relative sea-level (RSL) fluctuations have influenced the development of potential diamond hosting deposits on the Namibian continental shelf. A stratigraphic framework, achieved through the integration of borehole data and high-resolution seismic profiles, now provides the foundation of the landscape evolution model for the Purple Target Area (PTA).

The PTA stratigraphy is represented by 4 seismically defined sedimentary successions (units A – D), separated by regional sequence boundaries. The most noteworthy landforms recognised in the PTA are well-preserved gravel beaches (within units B and D) that exhibit an exceptional fully preserved barrier beach succession with distinctive cross-beach shape and size sorting patterns (sub-unit B1). The vertical stacking pattern of the gravel beaches, which comprise rudaceous angular rubble at the base followed by a single layer or multiple layers of rounded meso-Orange River derived gravel, suggests a complex sea-level history with possible substantial time gaps between the phases of clastic material emplacement. However, based on palaeo-bathymetric reconstruction, the bulk of the facies making up the gravel beaches (normal regressive deposits) are linked to the last transgressive event, after the Last Glacial Maximum, which saw the shelf being sub-aerially exposed to 120 – 130 m bmsl. The formation and preservation of the PTA stratigraphy are primarily driven by the relationship between rate of sediment input and RSL fluctuations. The depth, at which the gravel beaches are emplaced, corresponds to eustatic sea-level directly prior to and including Meltwater Pulse 1B (MWP-1B). It is postulated that the form of barrier overstepping responsible for the partial to complete preservation and offshore abandonment of the gravel beaches is rapid rise in RSL, associated with MWP-1B, over an area of lower seafloor gradient (relative to the ~70 m bmsl break in slope area).

The signature of the completely preserved gravel barrier beach and back-barrier facies, sub-units B1 and B2, respectively, are comparable to the locally preserved onshore Estuarine Delta (ED) area spit/barrier beach system of Spaggiari (2011). The emplacement of the ~12 m high ED gravel spit/barrier is attributed to its proximity to the palaeo-Orange River mouth where coarse clastic material, theoretically not suitably mobile under longshore drift, accumulates close to the point source. In contrast, the emplacement of the ~3.5 m high and ≥7 km long gravel barrier in the PTA suggests a longshore drift capable of transporting coarse clastic material up to ~65 km from the point source.

Based on the onshore analogues, the Cretaceous footwall underlying the PTA gravel beaches, comparable to the ED area fluvial footwall underlying the onshore spit/barrier beaches, does not promote pothole and gully development. Therefore, the diamond potential within the PTA is exclusively controlled by the gravel fabric of the beaches and their ability to trap and retain diamonds within their pore spaces. The most economical diamond concentrations in the ED spit/barrier beaches are documented in the foreshore area, whilst the shoreface and back-barrier setting prove uneconomical and it is proposed that, likewise, this is the case in the PTA.

6.2 Future Research

Control dates would assist with quantifying the age relationship between the emplacement of the gravel beaches and the factors driving their preservation. The dating of lagoonal material (B2_CY), preserved landward of the gravel barrier (sub-unit B1), should provide a good approximation for confirmation of the timing and magnitude of the RSL changes, for comparison with the global far field database.

An additional tighter spaced high-resolution seismic survey (e.g. 100 m) in the PTA and extending southward of it, possibly as far as current Orange River mouth, would assist with tracing the magnitude of the wave-cut platforms and deducing the regional scale effect the RSL changes had on the continental shelf.

The preservation of barrier beaches within the PTA proves that the onshore and offshore settings differ with respect to the emplacement of different beach types in a down-drift direction (northwards). The onshore gravel spit/barrier beaches are confined to the palaeo-Orange River mouth only and replaced by linear beaches that trend for approximately 70 km northwards. The PTA has preserved a barrier beach complex offshore within the onshore linear beach “territory” approximately 65 km from the point source. It should therefore be investigated, with the assistance from high-resolution seismic data, whether the shoreline parallel gravel beaches of the PTA, in particular the gravel barrier, extend to the point source and if or how the dimensions of the gravel beaches modify down-drift.

REFERENCES

Abdul, N.A., Mortlock, R.A., Wright, J.D. and Fairbanks, R.G., 2016. Younger Dryas sea level and meltwater pulse 1B recorded in Barbados reef crest coral *Acropora palmata. Paleoceanography*, **31**, 330-344.

Aizawa, M., Bluck, B., Cartwright, J., Milner, S., Swart, R. and Ward, J., 2000. *Constraints on the geomorphological evolution of Namibia from the offshore stratigraphic record*. Communications of the Geological Survey of Namibia, **12**, 383-393.

Apollus, L., 1995. The distribution of diamonds on a late Cainozoic gravel beach, southwestern Namibia. M.Sc. thesis (unpublished), Department of Geology and Applied Geology, University of Glasgow, 170pp.

Bache, F., Sutherland, R. and King, P.R., 2014. Use of ancient wave-ravinement surfaces to determine palaeogeography and vertical crustal movements around New Zealand. *New Zealand Journal of Geology and Geophysics*, **57**(4), 459-467.

Barboza, E.G., 2005. *Análise Estratigráfica do Campo de Namorado (Bacia de Campos) com base na Interpretação Sísmica Tridimensional. Tese apresentada como requisite parcial para obtenção do Título de Doutor em Geociências. Universidade Federal do Rio Grande do Sul. Instituto de Geociências. Programa de Pós-graduação em Geociênci,* 220pp.

Bard, E., Hamelin, B., Arnold, M., Montaggioni, L., Cabioch, G., Faure, G. and Rougerie, F., 1996. Deglacial sea level record from Tahiti corals and the timing of the meltwater discharge. *Nature*, **382**, 241-244.

Bard, E., Hamelin, B. and Delanghe-Sabatier, D., 2010. Deglacial meltwater pulse 1B and Younger Dryas sea-levels revisited with new onshore boreholes at Tahiti. *Science*, **327**, 1235-1237.

Bard, E., Hamelin, B., Deschamps, P. and Camoin, G., 2016. Comment on "Younger Dryas sea level and meltwater pulse 1B recorded in Barbados reef crest coral *Acropora palmata*" by N.A. Abdul *et al*. *Paleoceanography*, **31**, 1603-1608.

Basei, M.A.S., Frimmel, H.E., Nutam, A.P., Preciozzi, F. and Jacob, J., 2005. A connection between the Neoproterozoic Dom Feliciano (Brazil/Uruguay) and Gariep (Namibia/South Africa) orogenic belts – evidence from a reconnaissance provenance study. *Precambrian Research*, **139**, 195-221.

Bluck, B.J., 1967. Sedimentation of beach gravels: examples from South Wales. *Journal of Sedimentary Petrology*, **37**, 128-156.

Bluck, B.J., 1999. Clast assembling, bed-forms and structure in gravel beaches. Transactions of the Royal Society of Edinburgh, Earth Sciences **89**, 291-323.

Bluck, B.J. and Ward, J.D., 2000. The Orange River – Namib Desert link: a long-lived sediment dispersal system in southern Africa. Abstract Volume, Geoluanda 2000 International Conference (15th African Colloquium on micropaleontology, 4th Colloquium on the stratigraphy and palaeogeography, on the South Atlantic, Regional Meeting on South Atlantic Mesozoic correlations (ICGP381), 4th Annual Meeting on the Kibaran Orogeny (ICGP418)). University Agostinho Neto, Department of Geology and Angolan Association of Geologists, Luanda, Angola, 30pp.

Bluck, B.J., Ward, J.D. and Spaggiari, R.I., 2001. Gravel beaches of southern Namibia. In: Packham, J.R., Randall, R.E., Barnes, R.S.K. and Neal, A. (Eds). *Ecology and Geomorphology of Coastal Shingle*. Westbury Academic and Scientific, U.K., 56-76.

Bluck, B.J., Ward, J.D. and De Wit, M.C.J., 2005. Diamond mega-placers: southern Africa and the Kaapvaal craton in a global context. *In*: McDonald, I., Boyce, A.J., Butler, I.B., Herringston, R.J. and Polya, D.A. (Eds). *Mineral Deposits and Earth Evolution*. Geological Society, London, Special Publications, **248**, 213-245.

Bluck, B.J., Ward, J.D., Cartwright, J., Swart, R., 2007. The Orange River, southern Africa: an extreme example of a wave-dominated sediment dispersal system in the South Atlantic Ocean. *Journal of the Geological Society*, London, **164**, 341-351.

Boggs, S., 2010. Principles of Sedimentology and Stratigraphy. 4th edition. Pearson Education International, U.S.A., 662pp.

Brown, R.W., Gallagher, K., Griffin, W.L., Ryan, C.G., de Wit, M.C.J., Belton, D.X. and Harmon, R., 1998. Kimberlites, accelerated erosion and evolution of the lithospheric mantle beneath the Kaapvaal Craton during the mid-Cretaceous. 7th International Kimberlite Conference, University of Cape Town, South Africa. Abstract volume, 105-107.

Brown, A., 1999. Interpretation of Three-Dimensional Seismic Data. 5th edition. AAPG Memoir 42 SEG Investigations in Geophysics 9, 355pp.

Brown, R.W., Gallagher, K., Gleadow, A.J.W. and Summerfield, M.A., 2000. Morphotectonic evolution of the South Atlantic margins of Africa and South America. *In:* Summerfield, M.A. (Ed). *Geomorphology and Global Tectonics*. Wiley, 255-281.

Burke, K., 1996. The African Plate. *South African Journal of Geology*, **99**(4), 341-409.

Burke, K. and Gunnel, Y., 2008. The African erosion surface: a continental-scale synthesis of geomorphology, tectonics, and environmental change over the past 180 million years. *Geological Society of America Memoirs*, **201**, 66pp.

Carlson, A.E. and Clark, P.U., 2012. Ice sheet sources of sea level rise and freshwater discharge during the last deglaciation. *Reviews of Geophysics*, **50**(4), 72pp.

Carter, R.W.G., Orford, J.D., Forbes, D.L. and Taylor, R.B., 1990. Morphosedimentary development of drumlin flank barriers with rapidly rising sea-level: Story Head, Nova Scotia. *Sedimentary Geology*, **69**, 117-138.

Cattaneo, A. and Steel, R.J., 2003. Transgressive deposits: a review of their variability. *Earth-Science Reviews*, **62**, 187-228.

Catuneanu, O., 2002. Sequence Stratigraphy of clastic systems: Concepts, merits and pitfalls. *Journal of African Earth Sciences*, **35**, 1-43.

Catuneanu, O., 2006. Principles of Sequence Stratigraphy. *Elsevier*, 375pp.

Catuneanu, O., Abreu, V., Bhattacharya, J.P., Blum, M.D., Dalrymple, R.W., Eriksson, P.G., Fielding, C.R., Fisher, W.L., Galloway, W.E., Gibling, M.R., Giles, K.A., Holbrook, J.M., Jordan, R., Kendall, C.G. St. C., Macurda, B., Martinsen, O.J., Miall, A.D., Neal, J.E., Nummedal, D., Pomar, L., Posamentier, H.W., Pratt, B.R., Sarg, J.F., Shanley, K.W., Steel, R.J., Strasser, A., Tucker, M.E., Winker, C., 2009. Towards the standardization of sequence stratigraphy. *Earth-Science Reviews*, **92**, 1-33.

Catuneanu, O., Galloway, W.E., Kendall, C.G. St. C., Miall, A.D., Posamentier, H.W., Strasser, A. and Tucker, M.E., 2011. Sequence Stratigraphy: Methodology and Nomenclature. *Newsletters on Stratigraphy*, **44**(3), 173-245.

Cawthra, H.C., Bateman, M.D., Carr, A.S., Compton, J.S. and Holmes, P.J., 2014. Understanding Late Quaternary change at the land ocean interface: a synthesis of the evolution of the Wilderness coastline, South Africa. *Quaternary Science Reviews*, **99**(1), 210-223.

Compton, J.S., Mulabisana, J. and McMillan, I.K., 2002. Origin and age of phosphorite from the Last Glacial Maximum to Holocene transgressive succession off the Orange River, South Africa. *Marine Geology*, **186**, 243-261.

Conradie, J., 2014. 2013 TE Drilling Depths versus 2011 Seismics. Namdeb Diamond Corporation (Pty) Ltd. Internal Report, 21pp.

Cooper, J.A.G., Green, A.N., Meireles, R.P., Klein, A.H.F., Souza, J. and Toldo, E.E., 2016. Sandy barrier overstepping and preservation linked to rapid sea level rise and geological setting. *Marine Geology*, **382**, 80-91.

Cooper, J.A.G. and Green, A.N., 2016. Geomorphology and preservation potential of coastal and submerged aeolianite: Examples from KwaZulu-Natal, South Africa. *Geomorphology*, **271**, 1-12.

Corbett, I.B., 1989. The sedimentology of the diamondiferous deflation deposits, Namibia. Ph.D. thesis (unpublished), Department of Geological Science, University of Cape Town, 430pp.

Corbett, I.B., Ward, J., Pickford, M. and McMillan, I.K., 1995. Applications of sequence stratigraphy to the high-energy arid continental margin of south-western Africa. Abstracts Centennial Geocongress (1995). Geological Society of South Africa, Rand Afrikaans Universiteit, Johannesburg, 2, 871.

Corbett, I.B., 1996. A review of the diamondiferous marine deposits of south western Africa. *African Geoscience Reviews*, **3**, 157-174.

Corbett, I. and Burrell, B., 2001. The earliest Pleistocene(?) Orange River fan-delta: an example of successful exploration delivery aided by applied Quaternary research in diamond placer sedimentology and palaeontology. *Quaternary International*, **82**, 63-73.

Corvinus, G. and Hendey, Q.B., 1978. New Miocene vertebrate locality and Arrisdrift in South West Africa. *Neues Jahrbush für Mineralogie, Geologie and Paläontologie*, **4**, 193-205.

Davis, R.A. Jr. and Clifton, H.E., 1987. Sea-level change and the preservation potential of wave dominated and tide dominated coastal sequences. *In*: Nummedal, D., Pilkey, O.H. and Howard, J.D. (Eds). *Sea-level Fluctuation and Coastal Evolution*. Society of Economic Paleontologists and Mineralogists, Special Publication, **41**, 167-178.

Davis, R.A. Jr. and Fitzgerald, D. M., 2004. Beaches and Coasts. *Blackwell Publishing*, 413pp.

De Decker, R.H., 1988. The wave regime on the inner shelf south of the Orange River and its implications for sediment transport. *South African Journal of Geology*, **91**(3), 358-372.

De Wit, M.C.J., 1999. Post-Gondwana drainage and the development of diamond placers in western South Africa. Economic Geology **94**, 721-740.

De Wit, M., 2007. The Kalahari epeirogeny and climate change: differentiating cause and effect from core to space. *South African Journal of Geology*, **110**(2-3), 367-392.

De Wit, M., Bhebhe, Z., Davidson, J., Haggerty, S.E., Hundt, P., Jacob, R.J., Lynn, M., Marshall, T.R., Skinner, C., Simithson, K., Stiefenhofer, J., Robert, M., Revitt, A., Spaggiari, R. and Ward, J., 2016. Overview of Diamond Resources in Africa. *Episodes*, **39**(2), 199-234.

Dingle, R.V., 1971b. Tertiary sedimentary history of the continental shelf off Southern Cape Province, South Africa. *South African Journal of Geology*, **74**(3), 173-186.

Dingle, R.V., Siesser, W.G. and Newton, A.R., 1983. Mesozoic and Tertiary Geology of Southern Africa. *A.A. Balkema, Rotterdam*, 375pp.

Dingle, R.V., 1993. Structural and sedimentary development of the continental margin off southwestern Africa. Communications Geological Survey of Namibia **8**, 37-46.

Einsele, G., 1992. Sedimentary Basins: Evolution, Facies and Sediment Budget. *Springer Verlag, Berlin,* 628pp.

Fairbanks, R.G., 1989. A 17,000-year glacio-eustatic sea-level record: influence of glacial melting rates on the Younger Dryas event and deep-ocean circulation. *Nature*, **342**, 637-642.

Forbes, D.L., Orford, J.D., Carter, R.W.G., Shaw, J. and Jennings, S.C., 1995. Morphodynamic evolution, self-organisation, and instability of coarse-clastic barriers on paraglacial coasts. *Marine Geology*, **126**, 63-85.

Fowler, J.A., 1976. The alluvial geology of the Lower Orange River an adjacent coastal deposit, South West Africa. M.Sc. thesis (unpublished), University of London, 285pp.

Fowler, J.A., 1982. Sedimentology and distribution of heavy minerals in the Lower Orange River valley. Ph.D. thesis (unpublished), University of London, 317pp.

Francis, J.E. and Hambrey, M., 2008. From Greenhouse to Icehouse – The Eocene/Oligocene in Antarctica. *In*: Siegert, M. and Florindo, F. (Eds). *Antarctic Climate Evolution*. Elsevier, 309-368.

Frimmel, H.E., Hartnady, C.J.H., and Koller, F., 1996. Geochemistry and tectonic setting of magmatic units in the Pan-African Gariep Belt, Namibia. *Chemical Geology*, **130**, 101-121.

Frimmel, H.E. and Frank, W., 1998. Neoproterozoic tectono-thermal evolution of the Gariep Belt and its basement, Namibia and South Africa. *Precambrian Research*, **90**, 1-28.

Frimmel, H.E., 2000. The Pan-African Gariep Belt in southwestern Namibia and western South Africa. *In*: Miller, R. McG. (Ed). *Henno Martin Commemorative Volume*. Communications of the Geological Survey of Namibia, **12**, 197-209.

Frimmel, H.E., 2008. Neoproterozoic Gariep Orogen. *In*: Miller, R.McG. (Ed). *The Geology of Namibia*. Neoproterzoic to Lower Palaeozoic, Volume 2. Ministry of Mines and Energy, Geological Survey of Namibia, 14-1 – 14-39.

Gallagher, K. and Brown, R., 1999. The Mesozoic denudational history of the Atlantic margins of southern Africa and southeast Brazil and the relationship to offshore sedimentation. *In*:

Cameron, N.R., Bate, R.H. and Clure, V.S. (Eds). *The Oil and Gas Habitats of the South Atlantic*. The Geological Society of London, Special Publications, **153**, 381-402.

Goudie, A. and Viles, V., 2014. Landscapes and landforms of Namibia. Springer, 37pp.

Green, A.N., 2009. Sediment dynamics on the narrow, canyon-incised and current-swept shelf of the northern KwaZulu-Natal continental shelf, South Africa. *Geo-Marine Letters*, **29**, 201-219.

Green, A.N. and Garlick, L., 2011. A sequence stratigraphic framework for a narrow, current-swept continental shelf: the Durban Bight, central KwaZulu-Natal, South Africa. *Journal of African Earth Sciences*, **60**, 303-314.

Green, A.N., Cooper, J.A.G., Leuci, R. and Thackeray, Z., 2013. Formation and preservation of an overstepped segmented lagoon complex on a high-energy continental shelf. *Sedimentology*, **60**(7), 1755-1768.

Green, A.N., Cooper, A.G. and Salzmann, L., 2014. Geomorphic and stratigraphic signals of postglacial meltwater pulses on a continental shelf. *Geology*, **42**, 151-154.

Green, A.N., Cooper, J.A.G. and Salzmann, L., 2017. The role of shelf morphology and antecedent setting in the preservation of palaeo-shoreline (beachrock and aeolianite) sequences: the SE African shelf. *Geo-Marine Letters*, **110**, 1-14.

Grobbelaar, G., Hirsch, M., Jacob, J. and Viviers, G., 2008. The Geology and Estimation of the 2008 Midwater Megadrill Sampling Programme Bogenfels Licence Key Target of Zones 8, 10 and 11. Namdeb Diamond Corportation (Pty) Ltd. Internal Report, 106pp.

Gurney, J.J., Levinson, A.A. and Smith, H.S., 1991. Marine mining of diamonds off the west coast of southern Africa. *Gems and Gemology*, **27**(4), 206-219.

Hallam, C.D., 1964. The Geology of the coastal diamond deposits of Southern Africa (1959). *In:* Haughton, S.H. (Ed). *The Geology of some Ore Deposits in Southern Africa*. Geological Society of South Africa, **2**, 671-728.

Hanson, E.K., Moore, J.M., Bordy, E.M., Marsh, J.S., Howarth, G. and Robey, J.V.A., 2009. Cretaceous Erosion in Central South Africa: Evidence from Upper-Crustal Xenoliths in Kimberlite Diatremes. *South African Journal of Geology*, **112**, 125-140.

Hawthorne, J.B., 1975. Model of a kimberlite pipe. *In*: Erlank, A.J. (Ed). *Physics and chemistry of the Earth*. Pergamon, Oxford, 1-15.

International Mining and Dredging Holding Ltd., 2016. THE EXPLORER. Available: http://www.imdhgroup.com/mv-explorer.php [2016, July 21].

Jacob, J., 2001. Late Proterozoic bedrock geology and its influence on Neogene littoral marine diamondiferous trapsites, MA1 – Sperrgebiet, Namibia. M.Sc. thesis (unpublished), Department of Geological Science, University of Cape Town, 140pp.

Jacob, J., Ward, J.D., Bluck, B.J., Scholz, R.A. and Frimmel, H.E., 2006. Some observations on diamondiferous bedrock gully trapsites on Late Cainozoic, marine-cute platforms of the Sperrgebiet, Namibia. *Ore Geology Reviews*, **28**, 493-506.

Jacob, J., 2016. Contextualized Risk Mitigation based on Geological Proxies in Alluvial Diamond Mining using Geostatistical Techniques. Ph.D. thesis (unpublished), Faculty of Engineering and the Built Environment, University of the Witwatersrand, 116pp.

Jacob, R.J., Bluck, B.J and Ward, J.D., 1999. Tertiary-age diamondiferous fluvial deposits of the Lower Orange River Valley, Southwestern Africa. *Economics Geology*, **94**, 749-758.

Jacob, R.J., 2005. The Erosional and Cainozoic Depositional History of the Lower Orange River, southwestern Africa. Ph.D. thesis (unpublished), Division of Earth Science, University of Glasgow, Volume 1, 178pp.

Kalbskopf, S., 1978. Bedrock gullies, their patterns, morphology and relationship to the major wave-cut shelves at CDM. The Consolidated Diamonds Mines of South West Africa (Pty) Ltd. Internal Report, 10pp.

Kennett, J.P. and Stott, L.D., 1990. Proteus and Proto-Oceanus: Ancestral Paleogene Oceans as revealed from Antarctic Stable Isotopic results; ODP Leg 113. *In*: Barker, P.F., Kennett, J.P. *et al*. (Eds). *Proc. ODP, Sci. Results, Ocean Drilling Program*, College Station, Texas, 865-880.

Lambeck, K., Rouby, H., Purcella, A., Sunc., Y. and Sambridge, M., 2014. Sea level and global ice volumes from the Last Glacial Maximum to the Holocene. *Proceedings of the National Academy of Sciences, U.S.A*, **111**(43), 15,296-15,303.

Lear, C.H., Elderfield, H. and Wilson, P.A., 2000. Cenozoic Deep-Sea Temperatures and Global Ice Volumes from Mg/Ca in Benthic Foraminiferal Calcite. *Science*, **287**, 269-272.

Liu, J.P., Milliman, J. D., Gao, S. and Cheng, P., 2004. Holocene development of the Yellow River's subaqueous delta, North Yellow Sea. *Marine Geology*, **209**, 45-67.

Liu, J.P. and Milliman, J.D., 2004. Reconsidering Melt-water Pulses 1A and 1B: Global Impacts on Rapid Sea-level Rise. *Journal of Ocean University of China*, **3**(2), 183-190.

Makhubele, M.M.H., 2014. The Role of Salt Tectonics in the Hydrocarbon Potential of the Post-Salt Deposits (Albian to Recent), Offshore Gabon. M.Sc. thesis (unpublished), University of the Western Cape, 112pp.

Mellett, C.L., Hodgson, D.M., Lang, A., Mauz, B., Selby, I. and Plater, A.J., 2012. Preservation of a drowned gravel barrier complex: A landscape evolution study from the north-eastern English Channel. *Marine Geology*, **315-318**, 115-131.

Miller, W. R., Ramsay, P. J., Leuci, R., Bosman, C., 2000. Geophysical Interpretation of the Kerbehuk Inshore Survey Block, Namibia. Council for Geoscience, South Africa. Report No. 2000-0246, 23pp.

Miller, R.McG., 2008. The Geology of Namibia, Upper Palaeozoic to Cenozoic 3, Namibian Ministry of Mines and Energy, Geological Survey of Namibia, 25-1–25-66.

Mitchum, R.M., Jr., Vail, P.R. and Sangree, J.B., 1977. Seismic Stratigraphy and Global Change of Sea-level, Part 6: Stratigraphic Interpretation of Seismic Reflection Patterns in Depositional Sequences. *In*: Payton, C. E. (Ed). *Seismic Stratigraphy – applications to Hydrocarbon exploration*. Memoir AAP, **26**, 117-132.

Murray, L.G., Joynt, R.H., O'Shea, D.O'C., Foster, R.W. and Kleinjan, J., 1970. The geological environment of some diamond deposits off the coast of South West Africa. Institute of Geological Sciences Report, **70**, 119-141.

Nichols, G., 2009. Sedimentology and Stratigraphy. 2nd Edition. *Wiley-Blackwell Publishing*, 419pp.

Oelofsen, A. 2008. Late Cenozoic Shallow Marine Diamond Placers off the Northern Sperrgebiet, Namibia. M.Sc. thesis (unpublished), Department of Geological Science, University of Cape Town, 193pp.

Orford, J.D., Carter, R.W.G. and Forbes, D.L., 1991. Gravel Barrier Migration and Sea-level Rise: Some Observations from Story Head, Nova Scotia, Canada. *Journal of Coastal Research*, **7**(2), 477-488.

Orford, J.D., Carter, R.W.G. Jennings, S.C. and Hinton, A.C., 1995. Processes and timescales by which a coastal gravel-dominated barrier responds geomorphologically to sea-level rise: Story Head barrier, Nova Scotia. *Earth Surface Processes and Landforms*, **20**(1), 21-37.

Orford, J.D. and Carter, R.W.G., 1995. Examination of mesoscale forcing of a swash-aligned, gravel barrier from Nova Scotia. *Marine Geology*, **126**, 201-211.

Partridge, T.C. and Maud, R.R., 1987. Geomorphic evolution of southern Africa since the Mesozoic. *South African Journal of Geology*, **90**, 179-208.

Paul, J.D., Roberts, G.G. and White, N., 2014. The African landscape through space and time. *Tectonics*, **33**(6), 898-935.

Pether, J., 1994. The sedimentology, palaeontology and stratigraphy of coastal-plain deposits at Hondeklip Bay, Namaqualand, South Africa. M.Sc. thesis (unpublished), Department of Geological Science, University of Cape Town, 313pp.

Pether, J., 2000. Deposits of the Namibian Coast. Chapter 3, Deposits of the West Coast, Pether, J., Roberts, D.L. and Ward, J.D. In: Partridge, T.C. and Maud, R.R. (Eds). *The Cenozoic of Southern Africa*. Oxford University Press, 41-46.

Pether, J., 2013. The Last Transgression Sequence (LTS) and Formation of the Sediment Body (draft), Namdeb Diamond Corporation (Pty) Ltd. Midwater Campaign Internal Report, 13pp.

Pether, J. and Williamson, M., 2014. 2014 mv The Explorer Sampling Campaign Midwater Sampling Report – Purple South – November 2014. Namdeb Diamond Corporation (Pty) Ltd. Midwater Campaign Internal Report, 60pp.

Pether, J. and Williamson, M., 2016. 2016 mv The Explorer Sampling Campaign Midwater Sampling Report – Purple Target – June 2016. Namdeb Diamond Corporation (Pty) Ltd. Midwater Campaign Internal Report, 112pp.

Pether, J., 2016. Context of Samples from the Midwater Zone off Southern Namibia Selected for Radiocarbon Dating. Namdeb Diamond Corporation (Pty) Ltd. Midwater Campaign Internal Report, 24pp.

Pether, J., 2017. Palaeontological Impact Assessment for proposed extension of Tormin Mine, West Coast, South Africa. Heritage Specialist Study, South African Heritage Resources Agency (SAHRA), 68pp.

Pettijohn, F.J., Potter, P.E. and Siever, R., 1987. Sand and Sandstones. 2nd Edition. *Springer-Verlage, Berlin, Germany*, 553pp.

Pickford, M., 2000. Neogene and Quaternary vertebrate biochronology of the Sperrgebiet and Otavi Mountainland, Namibia. *Communications of the Geological Survey of Namibia*, **12**, 411-419.

Posamentier, H. W., Jervey, M.T., Vail, P.R., 1988. Eustatic controls on clastic deposition. I. Conceptual framework. *In*: Wilgus, C. K., Hastings, B. S., Kendall, C. G. St. C., Posamentier, H.W., Ross, C. A., Van Wagoner, J. C. (Eds). *Sea-level Changes – An Intergrated Approach*, **42**, SEPM Special Publication, 110-124.

Posamentier, H.W. and Allen, G. P., 1999. Siliclastic sequence stratigraphy; sequence stratigraphy: concepts and applications. *SEPM Concepts in Sedimentology and Paleontology*, **7**, 204pp.

Pretorius, L., Green, A. and Cooper, A., 2016. Submerged shoreline preservation and ravinement during rapid postglacial sea-level rise and subsequent “lowstand”. *Geology Society of American Bulletin*, **128**(7-8), 1059-1069.

Pretorius, L., Green, A.N. and Cooper, J.A., 2017. Submerged beachrock preservation in the context of wave ravinement. *Geo-Marine Letters*, tbc.

Prins, C.F. and Jacob, J., 2014. Improved variography using simulated annealing to adjust sample locations to align with diamondiferous linear beach structures. *The Journal of Southern African Institute of Mining and Metallurgy*, **114**, 251-254.

Rampino, M.R. and Sanders, J.E., 1980. Holocene transgression in south-central Long Island, New York. *Journal of Sedimentary Petrology*, **50**, 1063-1080.

Rogers, J. and Bremner, J.M., 1991. The Benguela Ecosystem. Part VII. Marine geological aspects. *Oceanography and Marine Biology: An Annual Review*, **29**, 1-85.

Rogers, J. and Rau, A.J., 2006. Surficial sediments of the wave-dominated Orange River Delta and the adjacent continental margin off south-western Africa. *African Journal of Marine Science*, **28**(3-4), 511-524.

Salzmann, L., Green, A. and Cooper, J.A.G., 2013. Submerged barrier shoreline sequences on a high energy, steep and narrow shelf. *Marine Geology*, **346**, 366-374.

Sanders, J.E. and Kumar, N., 1975. Evidence of shoreface retreat and in-place “drowning” during Holocene submergence of barriers, shelf off Fire Island, New York. *Geology Society of America Bulletin*, **86**, 65-76.

Schulmeister, J., 2016. Landscape and Quaternary Environmental Change in New Zealand. *Science*, 334pp.

Séranne, M. and Anka, Z., 2005. South Atlantic continental margins of Africa: A comparison of the tectonic vs climate interplay on the evolution of equatorial West Africa and SW Africa margins. *Journal of African Earth Sciences*, **43**, 283-300.

Siddall, M., Stocker, T.F., Bluiner, T., Spahni, R., Schwander, J., Barnola, J. and Chappellaz, J., 2007. Marine Isotope Stage (MIS) 8 millennial variability stratigraphically identical to MIS 3. *Paleocenography*, **22**, 1-4.

Siesser, W.G., 1977b. Late Eocene age of marine sediments at Bogenfels, South West Africa, based on calcareous nannofossils. *South African Geological Society Bulletin*, **60**, 73-74.

Siesser, W.G. and Salmon, D. 1979. Eocene marine sediments in the Sperrgebiet, South West Africa. *Annals of the South African Museum*, **79**, 9-34.

Siesser, W.G. and Dingle, R.V., 1981. Tertiary sea-level movements around southern Africa. *Journal of Geology*, **89**, 523-536.

Sloss, C.R., Murray-Wallace, C.V. and Jones, B.G., 2007. Holocene sea-level change on the southeast coast of Australia: a review. *The Holocene*, **17**(7), 999-1014.

South African Committee for Stratigraphy (SACS), 1980. Stratigraphy of South Africa. Part 1: lithostratigraphy of the Republic of South Africa, South West Africa/Namibia and the Republics of Bophuthatswana, Transkei and Venda. Handbook 8. Geological Survey of South Africa, 690pp.

Spaggiari, R.I., Bluck, B.J., Ward, J.D., 1999. Beaches, barriers and bars: sedimentary facies of Early Pleistocene diamondiferous deposits within the Orange River mouth, Namibia. *In*: Lee-Thorp, J., and Clift, H. (Eds). Abstract Volume. *The Environmental Background to Hominid Evolution*, XV International Congress, International Union for Quaternary Research, 3–11 August 1999, Durban, South Africa, 169-170.

Spaggiari, R.I, Ward, J.D. and Bluck, B.J., 2002. Quaternary diamond bearing beaches of southern Namibia. Abstract Volume. 16th International Sedimentological Congress, RAU Johannesburg, 341.

Spaggiari, R.I., Bluck, B.J. and Ward, J.D., 2006. Characteristics of Plio-Pleistocene littoral deposits within the Palaeo-Orange River Mouth, Namibia. *In*: Els, B.G. and Eriksson, P.G. (Eds). Special Issue: *Placer Formation and Placer Minerals*, Ore Geology Reviews, **28**(4), 475-492.

Spaggiari, R.I., 2011. Sedimentology of Plio-Pleistocene Gravel Barrier Deposits in the Palaeo-Orange River Mouth, Namibia: Depositional History and Diamond Mineralisation. Ph.D. thesis (unpublished), Rhodes University, 462pp.

Stevenson, I., 1999. The Application of High Resolution Geophysical Techniques for Seismic Stratigraphic Analysis at an Outcrop Scale: A study from the Namaqualand Continental Shelf, west coast, South Africa. Ph.D. thesis (unpublished), University of Reading.

Stevenson, I.R. and McMillan, I.K., 2004. Incised valley fill stratigraphy of the Upper Cretaceous succession, proximal to the Orange Basin, Atlantic margin of southern Africa. *Journal of Geological Society, London*, **161**, 185-208.

Stocken, C.G., 1962. The diamond deposits of the Sperrgebiet, South West Africa. Field trip, 4th Annual Congress of the Geological Society of South Africa, 15pp.

Stocken, C.G., 1978. A review of the later Mesozoic and Cainozoic deposits of the Sperrgebiet. Consolidated Diamond Mines of South West Africa (Pty.). Internal Report, 38pp.

Storms, J.E.A., Weltje, G.J., van Dijke, J.J., Geel, C.R., Kroonenberg, S.B., 2002. Process-response modeling of wave-dominated coastal systems: simulating evolution and stratigraphy on geological timescales. *Journal of Sedimentary Research*, **72**(2), 226-239.

Storms, J.E.A., Weltje, G.J., Terra, G.J., Cattaneo, A. and Trincardi, F., 2008. Coastal dynamics under conditions of rapid sea-level rise: Last Pleistocene to Early Holocene evolution of barrier-lagoon systems on the northern Adriatic shelf (Italy). *Quaternary Science Reviews*, **27**(11-12), 1107-1123.

Tucker, M.E., 1988. Techniques in Sedimentology. *Blackwell Scientific Publication, Oxford, U.K.*, 394pp.

van Wyk, F.M. and Pienaar, L.F., 1986. Diamondiferous gravels of the Lower Orange River, Namaqualand. *In*: Anhaeusser, C. R. and Maske, S. (Eds). *Mineral deposits of southern Africa*, **2**, Geological Society of South Africa, 2309-2321.

Verboom, G.A., Archibald, J.K., Bakker, F.T., Bellstedt, D.U., Conrad, F., Dreyer, L.L., Forest, F., Galley, C., Goldblatt, P., Henning, J.F., Mummenhoff, K., Linder, H.P., Muasya, A.M., Oberlander, K.C., Savolainen, V., Snijman, D.A., van der Niet, T. and Nowell, T.L., 2009. Origin and diversification of the Greater Cape flora: Ancient species repository, hot-bed of recent radiation, or both? *Molecular Phylogenetics and Evolution*, **51**, 44-53.

Walker, R.G. and Noel, P.J., 1992. Facies Models Response to Sea-level Change. Geological Association of Canada, 454pp.

Ward, J.D., 1988. Eolian, fluvial and pan (playa) facies of the Tertiary Tsondab Sandstone Formation in the central Namib Desert, Namibia. *Sedimentary Geology*, **55**, 143-162.

Ward, J.D., van der Westhuizen, A., Jacob, R.J., Apollus, L. and Spaggiari, R.I., 1998. 7th International Kimberlite Conference. Excursion guide: West Coast field excursion, University of Cape Town, Cape Town, South Africa, 23pp.

Wildman, M., Brown, R., Watkins, R., Carter, A., Gleadow, A. and Summerfield, M., 2015. Post break-up tectonic inversion across the southwestern cape of South Africa: New insights from apatite and zircon fission track thermochronometry. *Tectonophysics*, **654**, 30-55.

Wildman, M., Brown, R., Persano, C., Beucher, R., Stuart, F.M., Mackintosh, V., Gallagher, K., Schwanethal, J. and Carter, A., 2017. Contrasting Mesozoic evolution across the boundary between on and off craton regions of the South African plateau inferred from apatite fission track and (U-Th-Sm)/He thermochronology. *Journal of Geophysical Research: Solid Earth*, **122**, 1517-1547.

Williams, R., 1996. King of Sea Diamonds: The saga of Sammy Collins. *W.J. Flesch and Partners*, *South Africa*, 176pp.

Wright, J.A., 1964. Gully pattern and development in wave-cut bedrock shelves north of the Orange River mouth, South West Africa. *Transactions of the Geological Society of South Africa*, **67**, 163-172.

Zecchin, M., 2007. The architectural variability of small-scale cycles in shelf and ramp clastic systems: the controlling factors. *Earth Science Review*, **84**, 21-55.

Zecchin, M., Ceramicola, S., Gordini, E., Deponte, M. and Critelli, S., 2011. Cliff overstep model and variability in the geometry of transgressive erosional surfaces in high-gradient shelves: The case of the Ionian Calabrian margin (southern Italy). *Marine Geology*, **281**, 43-58.

APPENDIX A – PRINCIPLES OF SEQUENCE STRATIGRAPHY AND SEA-LEVEL FLUCTUATIONS

A.1 Sea-level Fluctuations and Sedimentation

Sea-level can be classified into two categories depending on its scale: eustatic sea-level (sea-level fluctuations on a global scale) and relative sea-level (sea-level fluctuations on a local scale).

Eustatic sea-level (ESL) fluctuations are attributed to a range of causes: global climate (affecting changes in global sea water temperature as well as waxing and waning of continental ice sheets) and global tectonics (breakup and formation of supercontinents and changes in rates of formation of oceanic crust; **Figure A.1**). All the causes that affect ESL changes can be grouped under changes in volume of water and/or changes in the capacity of the ocean basins (Boggs, 2010).

Relative sea-level (RSL) fluctuations are relative to a datum (top of basement rock) and governed by local tectonics (local isostasy, tectonic movements through down-warping or uplift of basin floor) and eustasy (**Figure A.1**; Catuneanu, 2006). Accommodation, the space available for sediments to accumulate, is influenced by rates of RSL fluctuations and sedimentation (Catuneanu, 2006).

The interplay of three factors: tectonic subsidence or uplift, global climate change and ESL changes control the rate of sedimentation and architecture of the basin fill, which are integral to stratigraphy and sedimentology (Nichols, 2009).

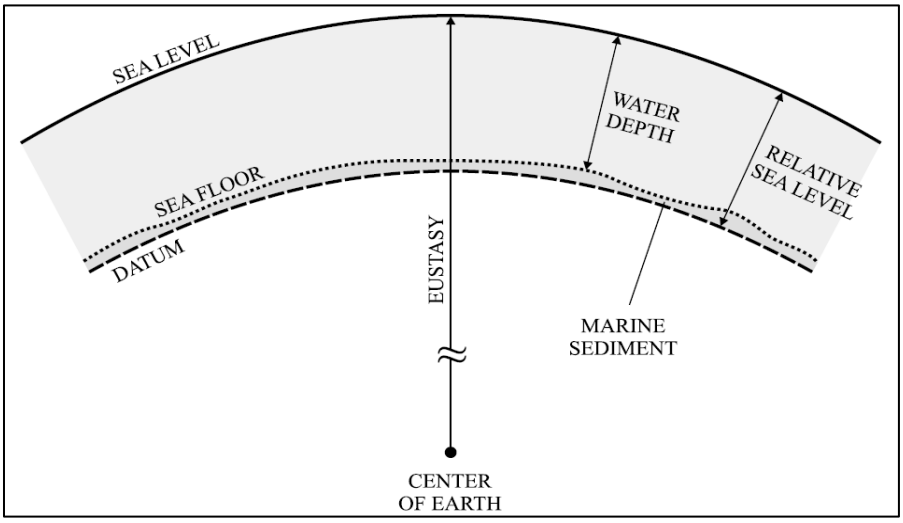

Figure A.1. Relationship between eustasy, relative sea-level (RSL), water depth and accumulated marine sediment. RSL is a function of the sea-levels position with respect to a local datum (top of basement rock) and eustasy is a function of the sea-level with respect to a fixed datum (center of Earth; Catuneanu, 2002 adapted from Posamentier *et al.,* 1988).

The types and nature of the lateral shoreline shifts is dependent on the rate of RSL rise and fall, and the rate of sedimentation at the shoreline (Catuneanu, 2006; Nichols, 2009). Changes in these rates control the vertical stratal stacking pattern (Boggs, 2010). During a transgression the facies shift landward and create a retrograding stacking pattern where fine-grained sediments overlie coarse-grained sediments or vertical build-up to create an aggradational stacking pattern (**Figure A.2**). A seaward shift of facies during a regression forms a prograding stacking pattern where coarse-grained sediments overlie fine-grained sediments (Boggs, 2010). Regression can be subdivided into normal regression and forced regression (Catuneanu, 2006). Force regression is the destruction of accommodation by RSL fall, irrespective of the sediment supply; whereas normal regression is where the rate of sedimentation, consuming accommodation space, outpaces the rate of RSL rise.

Within a succession, a maximum flooding surface (MFS) marks the boundary where a facies shift from shallower to deeper RSL occurs in the shoreline area (**Figure A.5**; Nichols, 2009; Boggs, 2010). Whereas the maximum regressive surface (MRS) also develops during RSL rise, but is interpreted at the top of coarsening upward trends in shallow-water settings (Catuneanu, 2009).

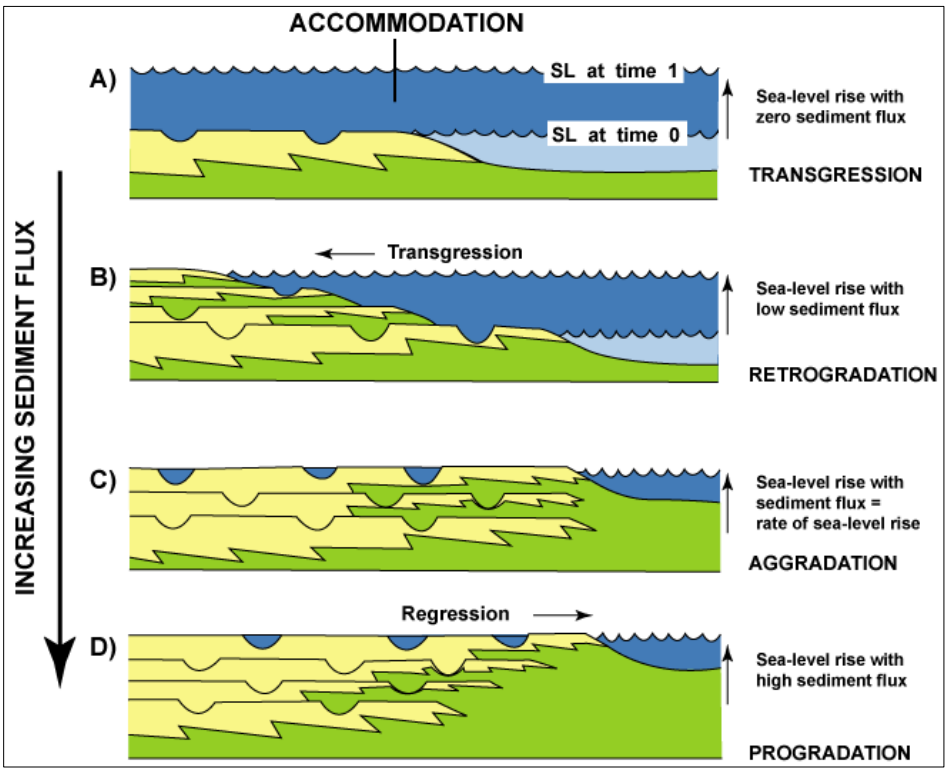

Figure A.2. The various effects of relative sea-level fluctuations and sediment input volumes on the shoreline (After Posamentier and Allen, 1999).

A.2 Seismic and Sequence Stratigraphy

Sequence Stratigraphy is a technique used for numerical modelling and mapping of genetically related strata bounded by erosional (refer to sub-section A.3) or non-depositional surfaces and their sedimentation patterns in response to available sediment supply and accommodation space through time, i.e. sequence (**Figure A.3**; Mitchum *et al*., 1977; Nichols, 2009; Catuneanu, 2011). Sequence stratigraphy gives insight into the way sedimentary basins accumulate and preserve their sediments, and determine the depositional environment through the interpretation of the architecture of the stratigraphic units (lateral and vertical variations of the strata within units and corresponding surfaces bounding the unit; Catuneanu, 2011).

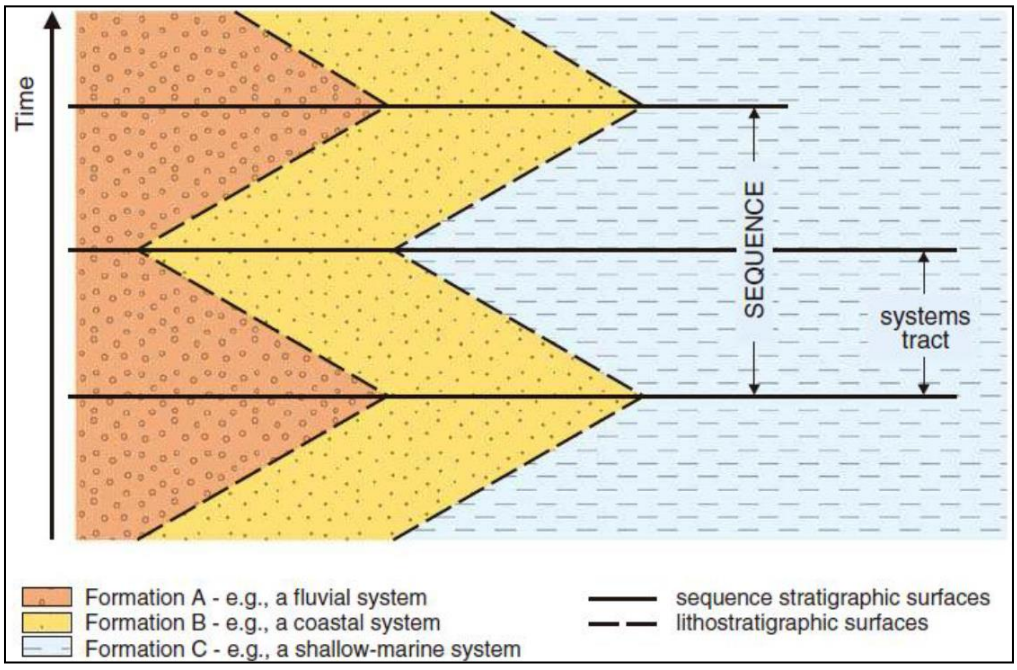

Figure A.3. Stratigraphic sequence comprising a transgressive (retrograding stacking pattern, normal grading) and regressive systems tract (prograding stacking pattern, reverse grading) in various depositional environments (fluvial, coastal and shallow-marine setting), bounded by key surfaces (Catuneanu, 2006).

A.2.1 Strata Relationships through Seismic Reflectors

A.2.1.1 Reflection Configuration on Seismic Records

The various patterns exhibited on a seismic record are referred to as reflection configuration. The characteristics of reflection configuration comprise three major patterns: parallel, prograding and divergent (Mitchum *et al.,* 1977; Boggs, 2010). Reflecting surfaces that display a disordered pattern are referred to as chaotic and are the product of soft-sediment deformation and other forms of deformation (**Table A.1**; Boggs, 2010).

Table A.1. The major stratigraphical patterns observed on seismic profiles (adapted from Mitchum *et al*., 1977; Barboza, 2005; Boggs 2010).

Reflection Pattern	Name of Feature	Interpretation
	Parallel - subparallel	Parallel to sub-parallel patterns trend toward a depositional condition where sediments were deposited at a uniform rate within a basin.
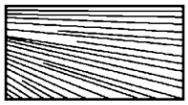	Divergent	Varying depositional rates laterally or the sedimentary surface progressively tilts during deposition.
	Parallel oblique	Gently sloping clinoforms as a result of lateral outbuilding or fast rate of progradation (relative sea-level drop).
	Oblique tangential	Accelerating rate of progradation offshore and slow rate of aggradation nearshore (during slow relative sea-level rise after transgression).
	Sigmoidal	Moderate to fast rate of progradation (during relative sea-level fall).
	Hummocky	Aggradation in shallow water setting (slow relative sea-level rise).
Chaotic-deformed  Chaotic – no stratal pattern 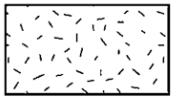	Chaotic	Disordered reflecting surface patterns which are the product of soft-sediment deformation and other forms of deformation. Seismically homogenous strata exhibit minor or no pattern.

A.2.1.2 Stratal Terminations

Stratal terminations are vital toward understanding the relationship between the strata and their corresponding termination surfaces within a basin. They assist with separating varying facies and deducing the type of shoreline shifts through time.

- Clinoforms are inclined surface that bound stratal packages (**Figure A.5**; Nichols, 2009; Mitchum *et al*., 1977).
- Continuous reflectors indicate a high variation in acoustic impedance exhibited between two different layers. Distinct contacts between continuous reflectors mark contrasting properties between the beds, i.e. a change in lithology within the sequence through a change in depositional environment (**Figure A.5**; Nichols, 2009).
- Unconformities represent a significant break or gap in the stratigraphic record and represent a period of erosion (either subaqueous or subaerial) or non-deposition. The reflector

representing the unconformity surface will only be observed where a substantial change in acoustic impedance is evident between the older underlying and younger overlying sediments, i.e. change in lithology through time. Four types of unconformities are documented: angular unconformity, disconformity, paraconformity and nonconformity (**Figure A.4**). If the erosion or non-deposition lasted for only a short duration, primarily bedding planes, then the resultant break is referred to as a diastem (Boggs, 2010; Catuneanu, 2010). Unconformities are the product of major changes in the workings of the depositional environment, whereas a diastem is the product of a short change in sedimentation without the effect on the entire depositional environment (Boggs, 2010).

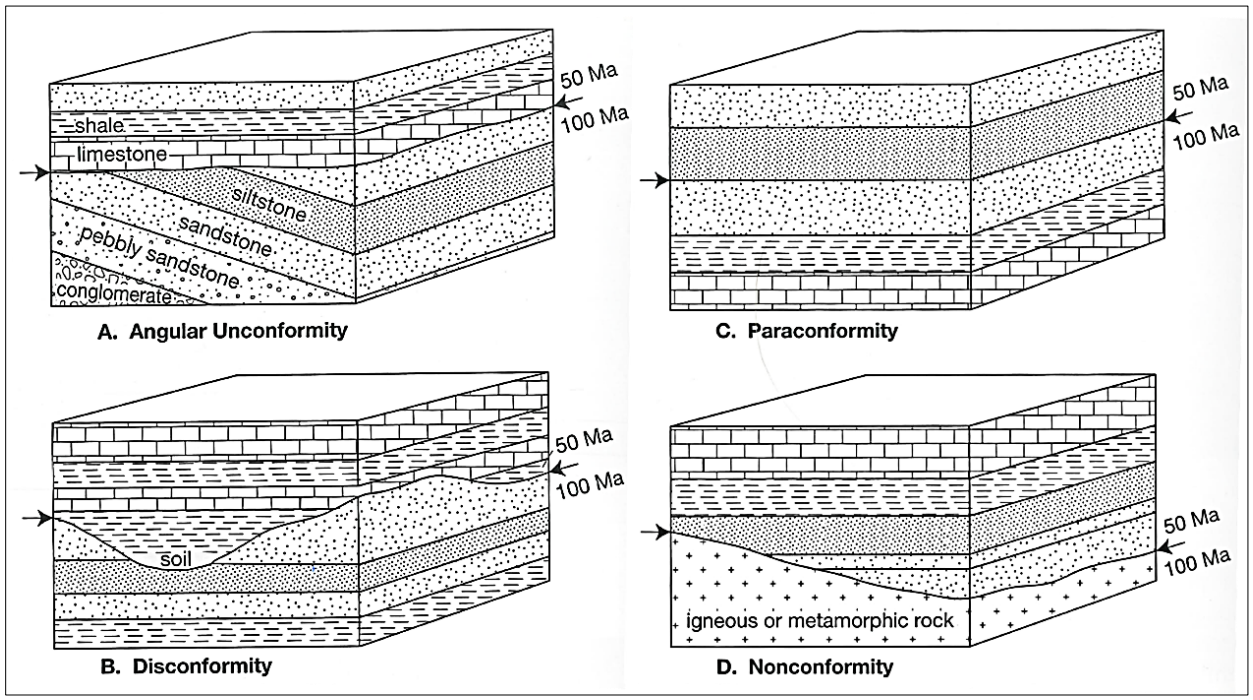

Figure A.4. A. Angular Unconformities are recognised by an angular discordance between strata. B. Disconformities are distinguished by an uneven erosional surface separating strata with the same orientation. C. Paraconformities are recognised by a disparity in age between the strata with the absence of an obvious visible surface of erosion. D. Nonconformities form between sedimentary rocks and igneous or metamorphic rocks (Boggs, 2010).

- Erosional truncation comprises reflectors that terminate against the upper boundary of a surface that has endured subaerial or submarine erosion (Catuneanu, 2006; **Figure A.5**). It may point toward forced regression.
- Inclined reflectors that terminate at the upper boundary against a horizontal surface are termed toplap (Catuneanu, 2006). Toplap points toward progradation of clinoforms, without aggradation, i.e. slow rising RSL (**Figure A.5**).

- Onlap and downlap are two types of baselaps where the termination of the strata occurs at the lower boundary of the sequence (**Figure A.5**). Onlap is where the stratal packages terminate against a boundary of greater inclination. Onlap points toward transgression. Downlap refers to originally inclined stratum that terminates down-dip against a horizontal surface. Downlapping strata are observed in shallow marine or deep marine settings and uncommon in land settings, except lacustrine environments (Catuneanu, 2006). Downlap may point toward normal or forced regressions.
- Offlap does not refer to a type of reflector termination, but rather a type of pattern the reflectors form. The pattern exhibits a building upward and seaward of the stratal packages (**Figure A.5**). Offlap points toward forced regression (Nichols, 2009; Boggs, 2010).

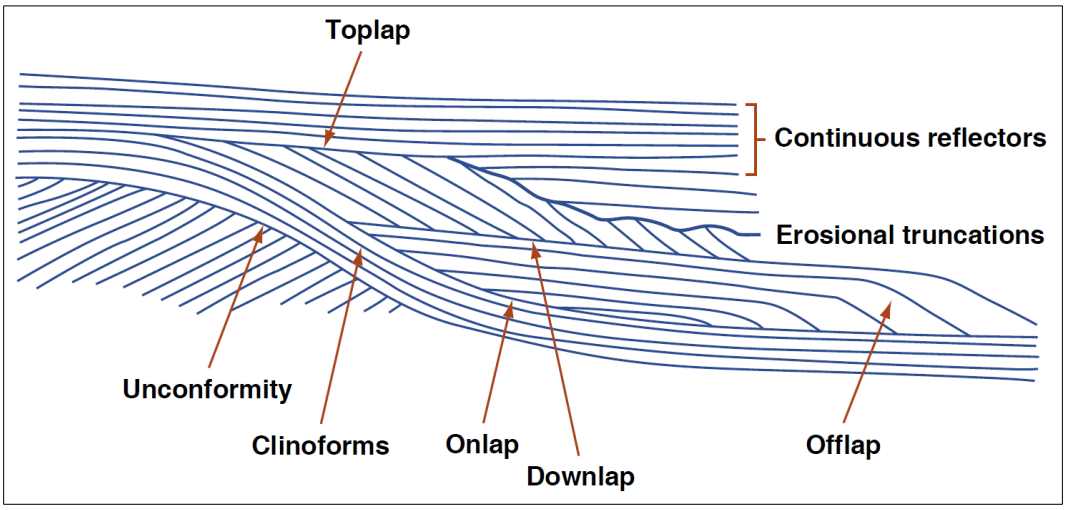

Figure A.5. Idealised cross-section profile exhibiting the various stratal terminations of a depositional sequence (Nichols, 2009).

A.2.2 Systems Tracts

A change in shoreline trajectory during high to low and back to high RSL forms a complete sea-level curve (**Table A.2** Insert) and sediments deposited at particular stages of this curve are referred to as system tracts (**Figure A.3**; Catuneanu *et al*., 2009; Boggs, 2010). The systems tracts comprise High Stand Systems Tracts (HST), Falling Stage Systems Tract (FSST), Low Stand Systems Tract (LST) and Transgressive Systems Tract (TST). The key features of each of the four system tracts in their various settings (fluvial, coastal, shallow-water and deep-water) are defined in **Table A.2**.

Table A.2. Primary characteristics, including stratal terminations and bounding surface, of the four systems tracts defined on seismic profiles. INSERT: RSL curve comprising High Stand Systems Tract (HST), Falling Stage Systems Tract (FSST), Low Stand Systems Tract (LST) and Transgressive Systems Tract (TST; Makhubele, 2014 adapted from Catuneanu, 2011).

Systems Tract	Key features	Fluvial	Coastal	Shallow-water	Deep-water
HIGHSTAND SYSTEMS TRACT	Depositional trends	Aggradation	Progradation	Progradation	Starvation
	Stratal termination	-	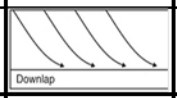	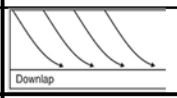	-
	Lower bounding surfaces	Maximum flooding surface	Maximum flooding surface	Maximum flooding surface	Maximum flooding surface (hard to detect)
	Upper bounding surfaces	Subaerial unconformity	Basal surface of forced regression	Regressive surface of marine erosion	Basal surface of forced regression
	Sediment budget	Aggrading system	Deltas and coastal strandplains	Gradationally based shoreface and shelf facies	-

Systems Tract	Key features	Fluvial	Coastal	Shallow-water	Deep-water
FALLING STAGE SYSTEMS TRACT	Depositional trends	-	-	Progradation	Progradation
	Stratal termination	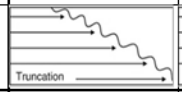	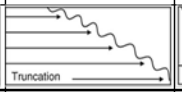	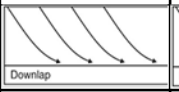	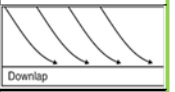
	Lower bounding Surfaces	Subaerial unconformity	Basal surface of forced regression	Regressive surface of marine erosion	Basal surface of forced regression
	Upper bounding surfaces	Subaerial unconformity	Correlative conformities	Correlative conformities	Correlative conformities
	Sediment budget	Sediment bypass	Offlapping deltas, downstepping	Sharp based shoreface and shelf facies	Debris flows deposits and turbidites

Systems Tract	Key features	Fluvial	Coastal	Shallow-water	Deep-water
LOWSTAND SYSTEMS TRACT	Depositional trends	Aggradation	Progradation	Progradation	Progradation
	Stratal termination	-	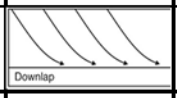	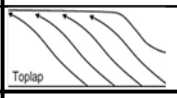	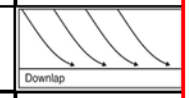
	Lower bounding surfaces	Subaerial unconformity	Subaerial unconformity	Correlative conformities	Correlative conformities
	Upper bounding surfaces	Maximum regressive surface	Maximum regressive surface	Maximum regressive surface	Maximum regressive surface
	Sediment budget	Amalgamated channel fills in incised valleys	Shelf/shelf-edge deltas, strandplains	Gradationally based shoreface and shelf facies	Low density turbidity flows

Systems Tract	Key features	Fluvial	Coastal	Shallow-water	Deep-water
TRANSGRESSIVE SYSTEMS TRACT	Depositional trends	Aggradation	Retrogradation	Retrogradation	-
	Stratal termination	-	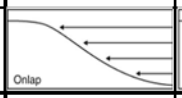	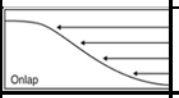	-
	Lower bounding surfaces	Maximum regressive surface	Maximum regressive surface	Maximum regressive surface	-
	Upper bounding surfaces	Maximum flooding surface	Maximum flooding surface	Maximum flooding surface	-
	Sediment budget	Rapidly aggrading systems	Estuaries, backstepping beaches	Fair amount of onlapping shoreface and shelf facies	Low density turbidity flows

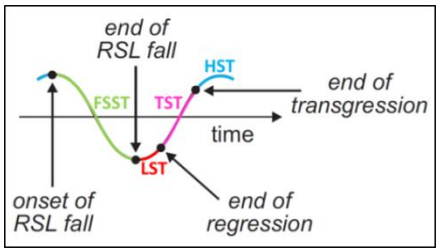

A.2.2.1 High Stand Systems Tract (HST)

High Stand System Tract (HST) refers to the beds deposited during high RSL (Nichols, 2009). Sediments are deposited in reducing accommodation space during the late stage of RSL rise, i.e. normal regression of the shoreline. Seaward migration of the shoreline across the shelf yields beds in either an aggrading or prograding pattern due to abundant sediment supply. Most of the sediment accumulation occurs on the shelf with minor sediment reaching the deeper basin (**Figure A.6**; Nichols, 2009). HST is dominated by coastal-plain and deltaic facies (Boggs, 2010). Bounded by the maximum flooding surface (MFS) at the base and by a subaerial unconformity (SU), basal surface of marine erosion (BSME) and regressive surface of marine erosion (RSME) at the top (Catuneanu *et al*., 2009; Boggs, 2010). Downlapping stratal terminations occur at the base of prograding clinoforms developed during normal regression (**Table A.2**). Sedimentation rate exceeds RSL rise and normal regression of the shoreline occurs.

A.2.2.2 Falling Stage Systems Tract (FSST)

Sediments deposited in severe reducing accommodation space, irrespective of the sedimentation rate in the shoreline area, i.e. forced regression of the shoreline are referred to as Falling Stage Systems Tract (FSST). Sediments are not preserved in settings landward of the shoreline due to reduced accommodation and sediment bypass, resulting in an aerial unconformity. FSST deposited in a marine setting are bounded at the base by a basal surface of force regression (BSFR) and RSME, with a SU and marine correlative conformity (c.c.; boundary in the basin that correlates to the lateral surface equivalent sequence boundary toward the inshore) bounding the top. Erosional truncation termination patterns will be evident at the surface of previously deposited nearshore deposits due to subaerial erosion during forced regression (**Figure A.6**). Diagnostic rapidly prograding and offlapping stratal stacking patterns will be observed in the shallow-marine setting (**Table A.2**; Catuneanu, 2006). In addition, gravity flows initiated during forced regression, due to instability of the shelf region, are characterised by slope fans, slumps and basin floor fans.

A.2.2.3 Low Stand Systems Tract (LST)

Low Stand Systems Tract refers to the sediments deposited in reducing accommodation space during the early stage of RSL rise, when the RSL is outpaced by the sedimentation rate, i.e. normal regression of the shoreline. During early rise normal regression previously incised valleys will fill up with sediments first and the sediments will feasibly continue to inundate the floodplain area and finally the deeper marine setting (**Figure A.6**). If sediments succeed in reaching the deep marine, they may initiate turbidites and gravity flows within the environment. Distinguished from the HST by its bounding surface: a SU and c.c. at the base and MRS at the top (Catuneanu, 2006). Seaward migration of the

shoreline across the shelf yields diagnostic aggrading or prograding stratal stacking patterns comprising reverse graded marine (shallow, offshore and sub-marine fan) and aggrading normal graded terrigenous (alluvial and coastal plain) sediments (**Table A.2**).

A.2.2.4 Transgressive Systems Tract (TST)

Transgressive Systems Tract (TST) is deposited in enlarged accommodation space during the stage where RSL rise outpaces sedimentation rate in the shoreline area, i.e. transgression of the shoreline. Landward migration of the shoreline across the shelf yields diagnostic retrogradational stacking patterns in the marine and non-marine setting (**Figure A.6**). During escalated rates of sea-level rise, the unconsolidated sediments deposited on the floodplains during the early rise normal regression can be eroded by wave action to form a scour surface called the ravinement surface or transgressive surface (Boggs, 2010; Catuneanu, 2006). Bounded by a MRS and MFS at the base and top, respectively (Nichols, 2009; Catuneanu *et al*., 2009; Boggs, 2010). The ravinement surface will be partially or even completely onlapped by the healing phase deposits in the upper shoreface (**Figure A.6**; Catuneanu, 2006).

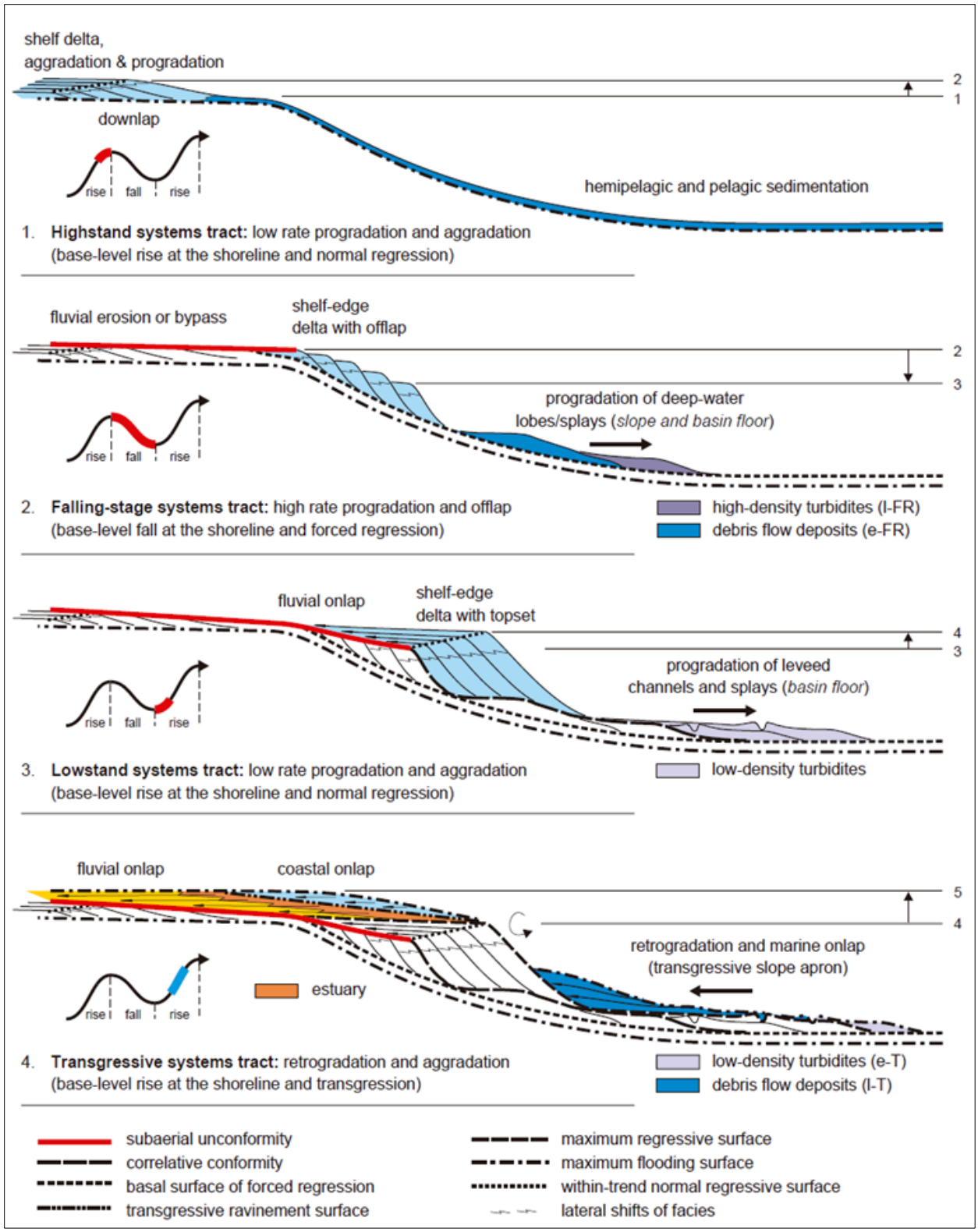

Figure A.6. Architecture of depositional sequences as defined by their respective systems tract. The systems tracts are defined by bounding surfaces and stratal stacking patterns (Catuneanu, 2006).

APPENDIX B – STRATIGRAPHY OF THE PTA

Table B.1. sp. = species, ssp. = sub-species and spp. = plural of species, e.g. *Bullia* spp. means various *Bullia* species (*digitalis, laevissima, annulata, natalensis*, etc.)

SEISMIC UNIT	SEISMIC SUB-UNIT	LITHOFACIES	ESTIMATED PERIOD/ EPOCH	DESCRIPTION	INTERPRETED DEPOSITIONAL ENVIRONMENT	FOSSILS/SHELLS	THICKNESS
D	D2	D2_Sand (**D2_SND**) and D2_Mud (**D2_MD**)	Later Holocene	Inner shelf sands with interbedded pebble stringer *tempestites* capped by a Late Holocene sediment wedge comprising sands, muddy sands and shell lags, periodically winnowed during major storms	Modern shelf regime	*Dosinia, Lucinoma, Volutocorbis, Nassarius vinctus*	<4 m
	D1	D1_Gravel (**D1_GVL**)	Early Holocene	Sub-rounded to rounded clasts comprising Orange River Suite (ORS) gravel fractions and exotics, with minor amounts of reworked Basal_SST1 and Basal_SST2 with depth	Foreshore gravel beach	Shell fragments mainly (mussel, barnacle)	~1.5 m
C	–	C_Gravel (**C_GVL**)	Early Holocene	Reworked Cretaceous footwall, Basal_SST1, Basal_SST2 and ORS derived material fining upward into marine sand	Transgressive "healing phase deposits"	–	~2 m
B	B5	B5_Sand (**B5_SND**)	Early Holocene	Inner shelf sands with interbedded pebble stringer *tempestites*	Shoreface and inner shelf	*Phaxas, Venerupis, Choromytilus, Aulacomya, Bullia laevissima, Argobuccinum, Nassarius speciosus*	<4.5 m
	B1 and B2	B1_Gravel Upper (**B1_GVL Upper**) and B2_Clay (**B2_CY**)	Late Pleistocene to Early Holocene (~14-11 ka)	Gravels comprising lower and higher proportions of reworked Basal_SST2 and ORS derived material, respectively, protecting a sand core, with preserved back-barrier lagoonal deposits	Barrier (barrier shore and back-barrier)	*Solen, Protomella, Assiminea, Choromytilus,* wood	≤1.5 m
		B1_Gravel Lower (**B1_GVL Lower**)				Shell fragments mainly (mussel, barnacle)	≤1 m
	B3	B3_Gravel (**B3_GVL**)		Gravels of multiple sub-units with increasing proportions of reworked Basal_SST1, Cretaceous footwall derived material, ORS gravels and reworked shelly Basal_SST2 with depth	Foreshore beaches destroyed during storms or rapid sea-level rise		~2 m
	B4	B4_Gravel (**B4_GVL**)					≤1.5 m
Seismically Undefined Basal Deposits	–	Basal_Sandstone 3 (**Basal_SST3**)	Late Quaternary, MIS2	*In situ* competent, very well-sorted medium sandstone lacking marine shell input	Aeolian	–	<0.1 m
		Basal_Sandstone 2 (**Basal_SST2**)	Late Quaternary, MIS 4 and 3 (~80-30 ka)	Angular to sub-rounded clasts comprising well-sorted grey medium sandstone, coquina and common pebble to rare large pebble/small cobble paraconglomerates	Shoreface and foreshore beach	Modern fauna (*Choromytilus*, *Venerupis*, *Bullia* spp.)	~0.2 m
		Basal_Clay (**Basal_CY**)	Earliest Late Quaternary, MIS5e, -c, -a (~120-80 ka)	Deeper-water grey to yellow-brown, muddy very fine-grained sand or mud shelf facies.	Deeper water shelf (~70-50 m palaeo-depths)	–	~0.5 m
		Basal_Gravel (**Basal_GVL**)	Mid Quaternary, MIS6	Mostly colourful mixture of reworked Cretaceous footwall, Basal_SST1 and ORS derived material, usually stained brown	Foreshore gravel beaches destroyed during storms or rapid sea-level rise	–	~0.5 m
		Basal_Sandstone 1 (**Basal_SST1**)	?Mid Pliocene	Sub-angular to rounded yellow-brown very hard reworked marine sandstone clasts	Shoreface and shallow shelf environments under conditions of abundant sandy sediment supply	Reworked Early Miocene *Ostrea, Mactra, Turritellas, Diplochaetetes* and contemporary *Ostrea, Perna perna,* and *Venerupis corrugata*	<0.2 m
A	–	Bedrock/Footwall	Neoproterozoic/Late Cretaceous/Palaeocene	–	–	–	–